Copyright Warning & Restrictions

The copyright law of the United States (Title 17, United States Code) governs the making of photocopies or other reproductions of copyrighted material.

Under certain conditions specified in the law, libraries and archives are authorized to furnish a photocopy or other reproduction. One of these specified conditions is that the photocopy or reproduction is not to be "used for any purpose other than private study, scholarship, or research." If a, user makes a request for, or later uses, a photocopy or reproduction for purposes in excess of "fair use" that user may be liable for copyright infringement,

This institution reserves the right to refuse to accept a copying order if, in its judgment, fulfillment of the order would involve violation of copyright law.

Please Note: The author retains the copyright while the New Jersey Institute of Technology reserves the right to distribute this thesis or dissertation

Printing note: If you do not wish to print this page, then select "Pages from: first page # to: last page #" on the print dialog screen

INFORMATION TO USERS

This reproduction was made from a copy of a manuscript sent to us for publication and microfilming. While the most advanced technology has been used to photograph and reproduce this manuscript, the quality of the reproduction is heavily dependent upon the quality of the material submitted. Pages in any manuscript may have indistinct print. In all cases the best available copy has been filmed.

The following explanation of techniques is provided to help clarify notations which may appear on this reproduction.

1. Manuscripts may not always be complete. When it is not possible to obtain missing pages, a note appears to indicate this.

2. When copyrighted materials are removed from the manuscript, a note appears to indicate this.

3. Oversize materials (maps, drawings, and charts) are photographed by sectioning the original, beginning at the upper left hand corner and continuing from left to right in equal sections with small overlaps. Each oversize page is also filmed as one exposure and is available, for an additional charge, as a standard 35mm slide or in black and white paper format.*

4. Most photographs reproduce acceptably on positive microfilm or microfiche but lack clarity on xerographic copies made from the microfilm. For an additional charge, all photographs are available in black and white standard 35mm slide format.*

***For more information about black and white slides or enlarged paper reproductions, please contact the Dissertations Customer Services Department.**

U·M·I Dissertation Information Service

University Microfilms International
A Bell & Howell Information Company
300 N. Zeeb Road, Ann Arbor, Michigan 48106

Hui, Kwok Wah

DEPOSITION OF SUSPENSIONS IN CONVERGENT CHANNELS DUE TO ELECTROSTATIC IMAGE FORCES

New Jersey Institute of Technology D.ENG.SCI. 1986

PLEASE NOTE:

In all cases this material has been filmed in the best possible way from the available copy. Problems encountered with this document have been identified here with a check mark __✓__.

1. Glossy photographs or pages _____
2. Colored illustrations, paper or print _____
3. Photographs with dark background _____
4. Illustrations are poor copy _____
5. Pages with black marks, not original copy _____
6. Print shows through as there is text on both sides of page _____
7. Indistinct, broken or small print on several pages _____
8. Print exceeds margin requirements ✓
9. Tightly bound copy with print lost in spine _____
10. Computer printout pages with indistinct print _____
11. Page(s) _____ lacking when material received, and not available from school or author.
12. Page(s) _____ seem to be missing in numbering only as text follows.
13. Two pages numbered _____. Text follows.
14. Curling and wrinkled pages _____
15. Dissertation contains pages with print at a slant, filmed as received _____
16. Other _____

_____

_____

University
Microfilms
International

DEPOSITION OF SUSPENSIONS IN CONVERGENT CHANNELS DUE TO ELECTROSTATIC IMAGE FORCES

BY

HUI, KWOK WAH

A DISSERTATION

PRESENTED IN PARTIAL FULFILLMENT OF

THE REQUIREMENTS FOR THE DEGREE

OF

DOCTOR OF ENGINEERING SCIENCE

IN

MECHANICAL ENGINEERING

AT

NEW JERSEY INSTITUTE OF TECHNOLOGY

NEWARK, NEW JERSEY, U.S.A.
1986

To my parents, my beloved wife and my 2 daughters,
for their patience and encouragement these years

ABSTRACT

The deposition of suspensions for uniform flow in convergent channels under the combined influences of inertia, viscous and electrostatic image forces was studied theorectically. The fluid phase was assumed to be two-dimensional, steady, uniform, incompressible and laminar while the particle phase was assumed to be uniform, steady, dilute and with negligible gravity effects.

Since the image force equations for convergent channels have not been derived, it becomes one of the main purposes of this study to perform the derivation of the image force equations. The lengths of the channels were chosen in a way that the exit area is only 20% of the inlet.

The governing equations were solved numerically (with Runge-Kutta fourth order algorithm) using the trajectory method to calculate the deposition of the solid particles.

Derivation and analysis of the image force equations for convergent channels revealed that the images are confined on an Image Circle and that both X and Y components of image forces are experienced. For zero angle of convergence ($\theta = 0°$), the image force equations reduce to that of the parallel-plate channel.

It was found that, for a given St (100 => St => 0) and Q (100 => Q => 0), the particle deposition is higher for higher convergent angles. At a fixed convergent angle (7.5° => θ => 0°), particle deposition increases with both St and Q. When St and Q are both = 0, no deposition occurs. When St <= 0.01 and Q < 1, the inertia effects may be neglected.

It was also observed that, for a constant convergent angle and St, particle deposition increased with increasing Q. For high Q (Q => 10) even with moderate St (10 > St => 0.01), more than 80% of the deposition rate takes place within X < 2. For small St and small Q (St < 1 and Q < 0.01) the fraction of deposition near the entrance of the channel (X < 0.3) increased from 0 to about 0.1 and then remained relatively constant.

APPROVAL OF DISSERTATION

DEPOSITION OF SUSPENSIONS IN CONVERGENT CHANNELS DUE TO ELECTROSTATIC IMAGE FORCES

BY

HUI, KWOK WAH

FOR

DEPARTMENT OF MECHANICAL ENGINEERING

NEW JERSEY INSTITUTE OF TECHNOLOGY

BY

FACULTY COMMITTEE

APPROVED: _____ Chairman

_____

_____

_____

_____

NEWARK, NEW JERSEY

APRIL, 1986

ACKNOWLEDGEMENTS

The author would like to express his sincere gratitute to his advisor, Dr. Rong-Yaw Chen, who provided many valuable suggestions, magnificient guidance and continuous encouragement throughout the course of the entire investigation.

The author wishes also to express his sincere gratitude to Dr. J. S. Hsieh, Dr. R. P. Kirchner, Dr. H. E. Pawel and Dr. R. Andrushkiw I, who have kindly read through the original manuscript and provided valuable suggestions.

Further acknowledgement is given to the Mechanical Engineering Department of the New Jersey Institute of Technology for the teaching fellowship appointment during the summer of 1983, and the research assistantship during the 1982-1983, 1983-1984 academic years.

The author is also grateful to Borg-Warner Air-conditioning, Inc., York, Pennsylvania, for using their computer and other accessaries.

TABLE OF CONTENTS

CHAPTER			PAGE NUMBER
ABSTRACT			iii
APPROVAL PAGE			v
ACKNOWLEDGEMENTS			vi
TABLE OF CONTENTS			vii
LIST OF TABLES			x
LIST OF FIGURES			xiii
NOMENCLATURE			xix
1.	INTRODUCTION		1
2.	LITERATURE SURVEY ON THE DEPOSITION OF PARTICLES IN CHANNELS		6
3.	THEORECTICAL ANALYSIS OF IMAGE FORCE EQUATIONS		22
	3.1	IMAGE FORCE EQUATION FOR PARALLEL-PLATE CHANNELS	24
	3.2	MODIFICATION OF THE IMAGE FORCE EQUATION	25
	3.3	THE IMAGE CIRCLE	28
	3.4	IMAGE FORCE EQUATIONS IN CONVERGENT CHANNELS	32
4.	FLOW OF SUSPENSIONS IN CONVERGENT CHANNELS WITH INERTIA, ELECTROSTATIC IMAGE FORCES AND VISCOUS EFFECTS		40
	4.1	GOVERNING EQUATIONS	42
	4.2	BOUNDARY CONDITIONS	50

4.3 METHOD OF SOLUTION 53

5. RESULTS AND DISCUSSION 59

5.1 FLUID PHASE 59

5.2 PARTICLE PHASE 60

5.2.1 PARTICLE TRAJECTORY 61

5.2.2 PARTICLE VELOCITY DISTRIBUTION . . 62

5.3 ELECTROSTATIC IMAGE FORCE DISTRIBUTION . . 63

5.4 ANGLE OF CONVERGENCE EFFECT ON PARTICLE DEPOSITION 65

5.5 DEPOSITION DUE TO VISCOUS AND ELECTROSTATIC IMAGE FORCES 67

5.6 DEPOSITION DUE TO VISCOUS AND INERTIA FORCES 69

5.7 DEPOSITION DUE TO VISCOUS, INERTIA, AND ELECTROSTATIC IMAGE FORCES 71

6. CONCLUSIONS 75

7. RECOMMENDATIONS 78

REFERENCES 80

APPENDICES 85

A APPLICATION OF THE RUNGE-KUTTA SOLUTION IN PARTICLE DEPOSITION ANALYSIS 85

B DIMENSIONLESS QUANTITIES AND PARAMETERS-PHYSICAL MEANING AND ORDER OF MAGNITUDE 89

C COMPUTER PROGRAM FOR PARTICLE CHARGE PARAMETERS CALCULATION 95

D COMPUTER PROGRAM FOR PARTICLE FLOW CHARACTERISTIC ANALYSIS 97

TABLES 110

FIGURES 127

VITA 176

LIST OF TABLES

Table		Page Number
4.1	Comparison of the Infinite Terms of Image Force ($n \rightarrow \infty$) and the result from the Modified Formula; θ = 0°, L = 12.5, Q = 1, St = 0 . . .	110
5.1	Particle Trajectory along a Convergent Channel; Yo = 0.9, θ = 7.5°, L = 6.07, Q = 10, St = 10 .	111
5.2	Particle Trajectory along a Convergent Channel; Yo = 0.5, θ = 7.5°, L = 6.07, Q = 10, St = 10 .	112
5.3	Particle Trajectory along a Convergent Channel; Yo = 0.1, θ = 7.5°, L = 6.07, Q = 10, St = 10 .	113
5.4	Image Charge Distribution at various Particle Vertical Positions; (a) θ = 7.5°, (b) θ = 5°, (c) θ = 2.5°	114
5.5	Particle Deposition along a Convergent Channel for various Charge Parameter Q; θ = 7.5°, L = 6.07, St = 100	117
5.6	Particle Deposition along a Convergent Channel for various Charge Parameter Q; θ = 7.5°, L = 6.07, St = 10	117
5.7	Particle Deposition along a Convergent Channel for various Charge Parameter Q; θ = 7.5°, L = 6.07, St = 1	118

5.8 Particle Deposition along a Convergent Channel for various Charge Parameter Q; θ = 7.5°, L = 6.07, St = 0.1 118

5.9 Particle Deposition along a Convergent Channel for various Charge Parameter Q; θ = 7.5°, L = 6.07, St = 0.01 119

5.10 Particle Deposition along a Convergent Channel for various Charge Parameter Q; θ = 7.5°, L = 6.07, St = 0 119

5.11 Particle Deposition along a Convergent Channel for various Charge Parameter Q; θ = 5°, L = 9.14, St = 100 120

5.12 Particle Deposition along a Convergent Channel for various Charge Parameter Q; θ = 5°, L = 9.14, St = 10 120

5.13 Particle Deposition along a Convergent Channel for various Charge Parameter Q; θ = 5°, L = 9.14, St = 1 121

5.14 Particle Deposition along a Convergent Channel for various Charge Parameter Q; θ = 5°, L = 9.14, St = 0.1 121

5.15 Particle Deposition along a Convergent Channel for various Charge Parameter Q; θ = 5°, L = 9.14, St = 0.01 122

5.16 Particle Deposition along a Convergent Channel for various Charge Parameter Q; θ = 5°, L = 9.14, St = 0 122

5.17 Particle Deposition along a Convergent Channel for various Charge Parameter Q; θ = 2.5°, L = 18.3, St = 100 123

5.18 Particle Deposition along a Convergent Channel for various Charge Parameter Q; θ = 2.5°, L = 18.3, St = 10 123

5.19 Particle Deposition along a Convergent Channel for various Charge Parameter Q; θ = 2.5°, L = 18.3, St = 1 124

5.20 Particle Deposition along a Convergent Channel for various Charge Parameter Q; θ = 2.5°, L = 18.3, St = 0.1 124

5.21 Particle Deposition along a Convergent Channel for various Charge Parameter Q; θ = 2.5°, L = 18.3, St = 0.01 125

5.22 Particle Deposition along a Convergent Channel for various Charge Parameter Q; θ = 2.5°, L = 18.3, St = 0 125

5.23 Particle Deposition along a Parallel Plate Channel for various Charge Parameter Q; θ = 0°, L = 12.5, St = 0 126

LIST OF FIGURES

Figure		Page Number
3.1	Coordinate System in a Parallel Plate Channel with Charged Particle and Image Pairs	127
3.2	Coordinate System in a Convergent Channel with Charged Particle and Image Pairs	128
3.3	Distribution of Image Pairs on Image Circle of a Convergent Channel of 90 Degrees	129
3.4	Distribution of Image Pairs on Image Circle of a Convergent Channel of 60 Degrees	130
3.5	Distribution of Image Pairs on Image Circle of a Convergent Channel of 45 Degrees	131
3.6	Distribution of Image Pairs on Image Circle of a Convergent Channel of 42 Degrees	132
3.7	Distribution of Image Pairs on Image Circle of a Convergent Channel of 30 Degrees	133
3.8	Limiting Case of a Convergent Channel of 180 Degrees	134
3.9	Distribution of Image Pairs on Image Circle of a Convergent Channel of 15 Degrees	135

3.10 Distribution of Image Pairs on Image Circle of a Convergent Channel of 10 Degrees 136

3.11 Distribution of Image Pairs on Image Circle of a Convergent Channel of 5 Degrees 137

3.12 Scheme of Images Pairs on Image Circle of a Convergent Channel of 45 Degrees 138

5.1 Axial Velocity of Fluid along a Convergent Channel; θ = 7.5°, L = 6.07, Q = 10, St = 10 . 139

5.2 Vertical Velocity of Fluid along a Convergent Channel; θ = 7.5°, L = 6.07, Q = 10, St = 10 . 140

5.3 Particle Trajectory along a Convergent Channel; θ = 7.5°, L = 6.07, Q = 10, St = 10 141

5.4 Particle Axial Velocity along a Convergent Channel; θ = 7.5°, L = 6.07, Q = 10, St = 10 . 142

5.5 Particle Vertical Velocity along a Convergent Channel; θ = 7.5°, L = 6.07, Q = 10, St = 10 . 143

5.6 Effect of Charge Parameter Q on Deposition for Uniform Flow in a Convergent Channel; θ = 7.5°, L = 6.07, St = 100 144

5.7 Effect of Charge Parameter Q on Deposition for Uniform Flow in a Convergent Channel; θ = 7.5°, L = 6.07, St = 10 145

5.8 Effect of Charge Parameter Q on Deposition for Uniform Flow in a Convergent Channel; θ = 7.5°, L = 6.07, St = 1 146

5.9 Effect of Charge Parameter Q on Deposition for Uniform Flow in a Convergent Channel; θ = 7.5°, L = 6.07, St = 0.1 147

5.10 Effect of Charge Parameter Q on Deposition for Uniform Flow in a Convergent Channel; θ = 7.5°, L = 6.07, St = 0.01 148

5.11 Effect of Charge Parameter Q on Deposition for Uniform Flow in a Convergent Channel; θ = 7.5°, L = 6.07, St = 0 149

5.12 Effect of Charge Parameter Q on Deposition for Uniform Flow in a Convergent Channel; θ = 5°, L = 9.14, St = 100 150

5.13 Effect of Charge Parameter Q on Deposition for Uniform Flow in a Convergent Channel; θ = 5°, L = 9.14, St = 10 151

5.14 Effect of Charge Parameter Q on Deposition for Uniform Flow in a Convergent Channel; θ = 5°, L = 9.14, St = 1 152

5.15 Effect of Charge Parameter Q on Deposition for Uniform Flow in a Convergent Channel; θ = 5°, L = 9.14, St = 0.1 153

5.16 Effect of Charge Parameter Q on Deposition for Uniform Flow in a Convergent Channel; θ = 5°, L = 9.14, St = 0.01 154

5.17 Effect of Charge Parameter Q on Deposition for Uniform Flow in a Convergent Channel; θ = 5°, L = 9.14, St = 0 155

5.18 Effect of Charge Parameter Q on Deposition for Uniform Flow in a Convergent Channel; θ = 5°, L = 9.14, St = 100 156

5.19 Effect of Charge Parameter Q on Deposition for Uniform Flow in a Convergent Channel; θ = 5°, L = 9.14, St = 10 157

5.20 Effect of Charge Parameter Q on Deposition for Uniform Flow in a Convergent Channel; θ = 5°, L = 9.14, St = 1 158

5.21 Effect of Charge Parameter Q on Deposition for Uniform Flow in a Convergent Channel; θ = 5°, L = 9.14, St = 0.1 159

5.22 Effect of Charge Parameter Q on Deposition for Uniform Flow in a Convergent Channel; θ = 5°, L = 9.14, St = 0.01 160

5.23 Effect of Charge Parameter Q on Deposition for Uniform Flow in a Convergent Channel; θ = 5°, L = 9.14, St = 0 161

5.24 Effect of Charge Parameter Q on Deposition for Uniform Flow in a Convergent Channel; θ = 2.5°, L = 18.3, St = 100 162

5.25 Effect of Charge Parameter Q on Deposition for Uniform Flow in a Convergent Channel; θ = 2.5°, L = 18.3, St = 10 163

5.26 Effect of Charge Parameter Q on Deposition for Uniform Flow in a Convergent Channel; θ = 2.5°, L = 18.3, St = 1 164

5.27 Effect of Charge Parameter Q on Deposition for Uniform Flow in a Convergent Channel; θ = 2.5°, L = 18.3, St = 0.1 165

5.28 Effect of Charge Parameter Q on Deposition for Uniform Flow in a Convergent Channel; θ = 2.5°, L = 18.3, St = 0.01 166

5.29 Effect of Charge Parameter Q on Deposition for Uniform Flow in a Convergent Channel; θ = 2.5°, L = 18.3, St = 0 167

5.30 Effect of Charge Parameter Q on Deposition for Uniform Flow in a Convergent Channel; θ = 2.5°, L = 18.3, St = 100 168

5.31 Effect of Charge Parameter Q on Deposition for Uniform Flow in a Convergent Channel; θ = 2.5°, L = 18.3, St = 10 169

5.32 Effect of Charge Parameter Q on Deposition for Uniform flow in a Convergent Channel; θ = 2.5°, L = 18.3, St = 1 170

5.33 Effect of Charge Parameter Q on Deposition for Uniform Flow in a Convergent Channel; θ = 2.5°, L = 18.3, St = 0.1 171

5.34 Effect of Charge Parameter Q on Deposition for Uniform Flow in a Convergent Channel; θ = 2.5°, L = 18.3, St = 0.01 172

5.35 Effect of Charge Parameter Q on Deposition for Uniform Flow in a Convergent Channel; θ = 2.5°, L = 18.3, St = 0 173

5.36 Effect of Charge Parameter Q on Deposition for Uniform Flow in a Parallel Plate Channel; θ = 0°, L = 12.5, St = 0 174

5.37 Comparison of Deposition in a Parallel Plate Channel with Yu and Chandra's Result; θ = 0°, St = 0 175

NOMENCLATURE

Symbol	
a	particle radius
D	Brownian diffusion coefficient
Dp	particle diameter
f	Stoke's drag force
Fx,Fy	image force per particle in the axial and vertical components
Fx',Fy'	dimensionless image force per particle in the axial and vertical components
ho	half the convergent channel inlet width
h	half the convergent channel width
hn	h value at location of the nth image (n=1,2....)
hn'	h value at location of the n'th image (n=1,2....)
H	ratio of the local convergent channel width to the channel inlet width
k	Boltzmann's constant
Kn	Knudsen number
L	mean free path of gas given in Chapter two
L	dimensionless convergent channel length
m	mass of a particle
n	charge-inertia parameter defined in chapter 2
N	total number of image pairs
q	electric charge per particle
q"	penetration parameter defined in chapter 2
qn	distance between the particle and the nth image above the upper channel wall (n = 1,2....)

qn'	distance between the particle and the n'th image below the lower channel wall (n = 1,2....)
Q	dimensionless electrostatic charge parameter
Qn	dimensionless distance between the particle and the nth image above the upper channel wall
Qn'	dimensionless distance between the particle and the n'th image below the lower channel wall
qnx,qny	axial and vertical components of qn (n = 1,2....)
qn'x,qn'y	axial and vertical components of qn' (n = 1,2...)
QnX,QnY	dimensionless axial and vertical components of Qn (n = 1,2....)
Qn'X,Qn'Y	dimensionless axial and vertical components of Qn' (n = 1,2....)
Re	Reynolds number based on half convergent channel inlet width
St	Stoke's number or particle inertia parameter
t	time variable
T	dimensionless time variable
u,v	axial and vertical component of fluid velocity
up,vp	axial and vertical component of particle velocity
uo	inlet velocity of fluid (uniform)
upo	inlet velocity of particle
U,V	dimensionless axial and vertical component of fluid velocity
Up,Vp	dimensionless axial and vertical component of particle velocity
Uo	dimensionless inlet velocity of fluid (uniform)

Upo	dimensionless inlet velocity of particle
Vg	settling velocity of particle
Vs	terminal settling velocity
x,y	axial and vertical coordinates
X,Y	dimensionless axial and vertical coordinates
$\bar{Y}$	dimensionless vertical coordinate = Y/H (always unity at convergent channel wall)
yu,yl	critical values of y defined in equation (4-7)
Yu	dimensionless critical values of Y defined in equation (4-21)

Greek Letters

ϵ_o	permittivity of free space
θ	half the convergent channel angle
θ_n	angle between qn and the vertical axis
$\theta_{n'}$	angle between qn' and the vertical axis
μ	viscosity of the fluid of suspension
ν	kinematic viscosity of the fluid of suspension
π	3.14159.....
ρ	density of the fluid phase
ρ_p	density of the particle cloud (concentration)
σ	sticking probability
σ_w	sticking probability at wall

Superscripts

'	dimensionless quantities as defined

Subscripts

n	for the nth image (n = 1,2....)
n'	for the n'th image (n = 1,2....)
o	initial or inlet condition
p	for particle phase
w	for wall condition
x,y	axial and vertical components
X,Y	dimensionless axial and vertical components

1. INTRODUCTION

The flow of a two-phase fluid-solid particle suspension in conduits is of extreme importance because it is closely related to a variety of practical situations and many engineering and scientific applications. Examples of such technological problems are turbomachines --- compressors and turbines, dust collectors, furnace exhausts, fluid scrubbers, pneumatic conveyors, aerosol and paint sprays, blood flow, respiratory tracts, and rocket and missile exhaust systems. The primary cause of fluidic contamination and air pollution is the flow of suspensions which results in deposition. Therefore, reliable prediction is based on thorough understanding of the contamination process itself whereby changes in plugging characteristics and performance can be expected for better fluidic control.

Recently, investigation has concentrated on the significance of parameters that affect the deposition process in laminar flow in symmetrical channels. Since the flow was assumed to be perfectly symmetric, gravitational effects were neglected. In a variety of cases of practical importance, the particle cloud with a high concentration of particles was treated as a continuum so that the flow of suspensions can be regarded, at least for the purposes of analysis, as a mixture of two interpenetrating continuous

fluids. Thus it was found that an appreciable amount of particle deposition can result because of the electrostatic charge effect on the particles. However, most of the investigators in this field of particle depositions concentrated only on fully developed laminar flows, turbulent flows, or symmetrical laminar entrance flows in a constant area horizontal or vertical channel. Although the convergent channels and/or diffusers had also been investigated, they were restricted to a high particle concentration flow in the entrance regions of the channels.

The electrostatic force due to the charges fall into two categories: (1) caused by the mutual electrostatic repulsion between particles, the so called field force, and (2) caused by the image force exerted on the particles induced on the electrostatic. Investigations have shown that when the particle number density is sufficiently low, i.e. less than ten to the minus five power (1.0E-5) per cubic centimeter, the predominant effect is mainly due to the image force. Many practical problems involving suspension of particles are relatively low particle number density and fall into the image force domain. Thus, in this study, it is assumed that the particle mass density or the particle concentration in the channels is low enough that the image force becomes the dominant effect on deposition.

The image force acting on a particle in a conduit is a

function of its position with respect to the conduit wall and the shape of the conduit. The image force equation for constant area parallel-plate and cylindrical channels have been given, but not for convergent channels and diffusers. It thus becomes an important but essential objective of this study to derive and analyze the image force equations for convergent channels. The consequence of this theorectical analysis leads to utilizing the image force equations derived in investigating numerically the symmetrical uniform flow of suspensions in convergent channels under the influences of inertia force of the particle, electrostatic image force due to charges on the particle, and viscous force of the fluid.

The characteristics of the deposition curve for different flow parameters like the inertia parameter and image forces will be considered. In particular, the effect of the angle of convergence (θ) together with the inertia force and image force on the fraction of deposition of the solid particles will be fully investigated. Since no gravitational influences are considered, a symmetrical fraction of deposition of particles on both the top and bottom walls of the convergent channels (or diffuser) is expected. Thus the particle phase together with the fluid phase, and the convergent channel, will follow a symmetrical pattern, and consequently only one half of the convergent channels need be considered.

The fluid phase is assumed to be two-dimension, steady, uniform, incompressible, and viscous throughout the entire flow field. Based on Newton's Second Law of Motion, which states that the product of mass and acceleration of a particle in any direction is proportional to the force acting on the particle in that direction, a mathematical model is developed for the motion of the particle. The resulting governing equations and boundary conditions are solved numerically using the Runge-Kutta (of fourth order) algorithm. A brief description on the application of the Runge-Kutta solution in particle deposition analysis is contained in Appendix A.

In chapter two, a concise literature survey on the deposition of particles in multiphase flow is reported. Analysis and derivation of the image force equation in convergent channels is studied in chapter three. The flow of suspensions in convergent channels under the influence of the inertia force, the electrostatic image force, and the viscous force is included in chapter four. As described in Appendix B, dimensionless parameters Q (Electrostatic image charge parameter; of values 100, 10, 1, 0.1, 0.01, and 0), and St (Stoke's number or inertia parameter; of values 100, 10, 1, 0.1, 0.01, and 0) will be investigated. The Reynold's number Re considered is around 400. Consequences of investigation are given and fully discussed in chapter five while the numerical results are tabulated in Tables

4.1, 5.1 to 5.23 and plotted in Figures 5.1 to 5.37. All of the numerical work was carried out on an IBM 370 computer, while most of the analytical results were plotted with a Nicolet ZETA 1453SX plotter. Computer programs for particle charge parameters calculation and for particle flow characteristic analysis are included in Appendices C and D, respectively. Conclusions and recommendations for further investigation are given in chapters six and seven, respectively.

2. LITERATURE SURVEY ON THE DEPOSITION OF PARTICLES IN CHANNELS

The main purpose of our investigation is to derive the image force equations for convergent channels so as to study the flow of suspensions in such channels under the influence of the electrostatic image force in addition to the inertia force of the particle and the viscous force of the fluid. In order to have some theoretical background and understanding on the investigation results thus far obtained, a literature survey on previous research of this topic is required. The survey will mainly focus on the particle deposition in two-dimensional parallel-plate channel due to image force.

Many scholars have studied and investigated the internal flow of suspensions and deposition of suspended particles from laminar and turbulent flows. As early as 1938, the transport of suspended particles by turbulent streams of water was studied by Kalinske and Van Driest {1}*. In 1953, Longwell and Weiss {2}, studied the mixing and distribution of liquid droplets in high velocity gas streams.

* { } : Numbers in brackets designate References used

It is important to understand the behavior of particles in flows in order to control it. Theoretically, particles as small as several molecules can exist; however, the practical lower limit for control is about 0.01 micrometer. Therefore, it is important to recognize the diameter and size of particles since they may be affected by diffusion, gravity, electrostatic charge, inertia, acoustic, phoretic, magnetic and other forces {3}. In situations where gravitational or inertia forces act on a particle proportional to its mass, a "pseudo" particle size called aerodynamic diameter specifies its motion. This aerodynamic diameter is defined by Stober {4} as the diameter of a sphere of unit density (1 gm/cc) that attains the same terminal settling velocity (Vs) at low Reynolds number in still air as the actual particle under consideration. In this way, not only particles of circular or spherical shape, but also of irregular geometry can be defined as long as they are of unit density.

Particle behavior often depends on the ratio of particle size to some other characteristic length. The mechanisms of heat, mass, and momentum transfer between particle and carrier gas depend on the Knudsen number, Kn = 2L/Dp, where L is the mean free path of the gas. This mean free path or mean distance traveled by a molecule between successive collisions can be calculated from the kinetic theory of gases. As a good approximation for a gas composed

of molecules that act like rigid elastic spheres, Friedlander {5} uses the following expression:

$$L = \nu \left(\frac{\pi * m}{2kT} \right)^{1/2}$$

In the expression above, ν is the kinematic viscosity of the gas, m is the molecular mass, k is the Boltzmann's constant, and T is the absolute temperature. At standard temperatures and pressures, the mean free path in air is about 0.065 micrometer.

The particle size of interest in aerosol behavior range from molecular clusters of 10 Å to as large as 100 micrometer for droplets and dust particles. Because it is difficult to define terms exactly and because many real systems composed of mixtures of particles are so complex, only some common classifications for the clouds of particles are specified by the following categories {3}.

MIST - represents fine particles that have diameters of 5 micrometer and larger

DUST - consists dispersion aerosols of solid particulate matter up to several hundred micrometer in diameter

AEROSOLS - implies particles less than 50 micrometer in diameter

Stukel and Soo (6) studied and investigated experimentally the hydrodynamics of a suspension with particles suspended in turbulent flow over the inlet of a channel formed by two parallel-plates made for various flow velocities, plate gap widths, and mass flow ratios of solids in air. Their purpose was to further the understanding of the aerodynamics of air pollution control equipment.

Testing was performed in a 12 inch by 12 inch subsonic wind tunnel with maximum tunnel speed of up to 120 ft/sec. Mass flow ratios of particles to air varied from 0.01 to 0.1 pound particles per pound air and with plate gap widths of 1/4, 1, and 2 inches. They determined the particle and air velocities, the particulate mass flow and density distributions, and the particle size distribution as affected by the flow response.

Observations were obtained on the nature of the developing turbulent boundary layer for dilute suspensions that the density of particles is higher at the wall than at the core because of the presence of charge on the particles induced by surface contacts. Furthermore, as analogous to rarefied gas motions, a particle slip velocity brought about by the lack of particle-to-particle collisions in the suspension at the wall was also observed. They thus concluded that similarity laws for the scaling of equipment for air pollution control should include the momentum

transfer parameter and the electroviscous parameter in addition to the Reynolds number. The electroviscous number is especially important when the particles possess large charge-to-mass ratios.

Friedlander and Johnstone (7) discovered that when a stream of gas carrying suspended particles flows in turbulent motion past a surface, the particles are deposited due to the radial fluctuating component of velocity. By performing an experimental study of the deposition of dust particles on the walls of tubes with an analysis of the mechanics of transport of particles in a turbulent stream, they found that the net rate of deposition depends on both the rate of transport of the particles to the wall and the rate of re-entrainment. The latter effect can be reduced to a minimum if they allow only a single layer of particles to accumulate on the surface and taking precautions to ensure adherence of all particles that struck the wall.

The occurrence of particle deposition due to field forces was studied by Soo and Rodgers (8). They defined a sticking probability, σ, which depends on the material properties and also relates to the force of adhesion of particles to a surface. When all particles drifting to the wall stick to or settle at the wall $\sigma = 1$; and $\sigma = 0$ for complete re-entrainment.

Corn {9} showed that adhesive forces are either electrical or liquid (viscosity and surface tension) in origin. Contact potential and dipole effect, space charge and electronic structure are included in the electrical forces. He also found that the effect of gravity alone produces settling, but the fact that a particle may again become re-entrained gives $\sigma < 1$. There is another sticking probability σ_w which concerns adhesion of particles at the immediate vicinity of the wall. Opposite to settling is the lifting of a particle in the shear flow of a fluid. This leads to a redistribution of density of particle clouds and erosion of a bed of deposited particles.

In 1971, a continuum theory of solid-fluid suspensions including solid-phase viscosity was discussed by Yang and Peddieson {10}. They applied this theory to the solution of uni-directional, plane, parallel-flow problems. Their assumptions included: (1) no-slip condition for the dispersing phase, (2) slip condition for the dispersed phase at a solid surface, (3) Stokes drag formula that governed the interphase force, and (4) both components obeyed Newton's law of viscosity. The resulting equations were used to solve three steady state flow problems: (1) plane Poiseuille flow, (2) plane Couette flow, and (3) vertical film flow. They further assumed an incompressibl Newtonian fluid with indeterminate pressure, whereas the solid phase contributed nothing to the pressure of the mixture.

Closed-form solutions were obtained for these problems and were used to evaluate the velocity profiles, skin friction coefficients, and flow rates of both phases for a variety of numerical values of the parameters arising in the problem.

Their results showed that the inclusion of solid-phase viscosity and the amount of particle slip allowed at the channel walls have important consequences in the problems solved. Some preliminary results for an unsteady parallel-flow problem of the boundary layer type (Stokes' first problem) were also included. Since they treated the particle cloud in their analysis as a continuum, the suspension can be regarded as a mixture of two interpenetrating continuous fluids.

Thomas {11} has determined the mininum transport velocity for flocculated thorium oxide and kaolin suspensions flowing in glass pipes. The minimum transport velocity was defined as the mean stream velocity required to prevent the accumulation of a layer of stationary or sliding particles on the bottom of a horizontal conduit. As the pipes ranged from 1 to 4 inches in diameter and the concentration varied from 0.01 to 0.17 volume fraction solids, two flow regimes were observed depending on the concentration of the suspension. In the first case, the suspension was sufficiently concentrated to be in the

compaction zone and hence had an extremely low settling rate. The second regime was observed with more dilute suspensions which were in the hindered-settling zone and settled ten to one-hundred times faster than slurries which were in the compaction.

The concentration for transition from one regime to the other was dependent on both the tube diameter and the degree of flocculation; and when the suspension particles were smaller than the thickness of the laminar sublayer, they settled according to Stokes' drag law. Under these circumstances the relation obtained for dilute suspensions was found to be consistent with particle transfer in the radial direction according to Bernoulli forces on the particle and the action of turbulent fluctuations which penetrate the laminar sublayer. For the case of a concentrated suspension in compaction, the minimum transport velocity was given by a characteristic critical Reynolds number.

The general case of a fully developed turbulent flow in a pipe with electrically charged particles or with significant gravity effect, or both, and for any inclination of the pipe was fully analyzed by Soo and Tung {12}. The influencing parameters that defined the state of motion include: pipe flow Reynolds number, Froude number, diffusion-response number, electro-diffusion number, momentum-transfer number and particle Knudson number.

Comparison with experimental results was made for both gas-solid and liquid-solid suspensions. The result showed that the gravity effect becomes significant in the case of large pipe diameters and large particle concentrations.

Soo and Tung {13} further included the effect of sedimentation into their previous studies of fully developed turbulent flow. particles in a turbulent fluid. Additional considerations from their previous studies were the diffusion and settling under field forces, the sticking probability of a particle at the wall, and that to a bed of similar particles. The rate of deposit build-up at the wall was also studied.

Robinson {14}, Van Deemter and Van Der Laan {15}, Hinze {16}, Marble {17}, Murray {18}, Pigford and Baron {19}, Anderson and Jackson {20}, and Soo {21} have significantly contributed to this field of study by proposing their own sets of hydromechanical equations for the analysis of two-phase solid-fluid flows. Among them, Soo's work seems to be the most general in that he begins with the equations of the general theory of mixtures discussed by Truesdell and Toupin {22}, and Truesdell and Noll {23}. The equations given by these authors have similar forms but are not in complete agreement. However, one of the best understood situations appears to be the case of negligible volume concentration of particles (i.e., a

dilute suspension). Marble {24}, in his review article, has discussed equations that are appropriate to this typical condition.

The motion of a two-phase (dust-carrier gas) suspension in the vicinity of a sphere or a circular cylinder was studied by Peddieson {25}. The problem of analyzing the flow of a fluid containing solid particles or droplets past such bodies has been of interest for a long time because such flows exist in several situations of engineering interest. These include the formation of ice on airplane wings, the erosion of missile surfaces due to high-speed raindrop impacts, and the collection and sampling of dust for the purposes of monitoring and controlling air pollution.

Comparin et al. {26} and Eldighidy et al. {27} performed some thoretical analysis and investigations on deposition in the entrance of a channel and in a diffuser. In these analyses, effects of diffusion, electrostatic charge repulsive force and adhesive force were considered and the results showed that the electrostatic charge effect played an important role in the deposition of particles. Eldighidy et al. {27} further found that the surface adhesion has a smaller effect on the rate of deposition than the electric charge. Moreover, it was found that the rate of deposition was greatly affected by the divergence angle

in a diffuser flow. The pressure gradient as well as the rate of deposition increases as the diffuser angles increase. However, because the separation occurs earlier at larger diffuser angles, the rate of deposition increases rapidly in the presence of electric charge. In the limiting case of the absence of electric charge, the rate of deposition decreases rapidly with increasing diffuser angle. The effect of electrostatic image force was not investigated in these analyses.

Ingham {28,29} investigated theoretically the simultaneous diffusion and sedimentation of aerosol particles in two dimensional channels. Both plug (uniform) and fully developed (Poisoulle) flow were considered with the emphasis on the case when diffusion effects are larger than or are of the same order of magnitude as sedimentation effects due to gravity.

A similar investigation for both slug and Poisouille flow was conducted by Taulbee and Yu {30}. They found that the fractional penetration depends on a parameter q" = h*Vg/D where h is the channel half height, Vg is the settling velocity of a particle and D is the Brownian diffusion coefficient. The result shown that for q" < 0.1, the particle loss was practically due to diffusion alone while for q" > 200, the deposition was mainly due to settling. The deposition due to the combined mechanism in

the range $0.1 < q'' < 200$ was significantly smaller than the algebric sum of deposition due to two independent mechanism.

A new approach based on the concepts of the particle trajectory function and the limiting trajectory is developed by Wang {31} for calculating the precipitation efficiency of channels of different cross-section. The trajectory function he used is equivalent to the stream function of a virtual flow field where the motion of particles are considered. His analyses was limited to two-dimensional motions of small particles and solutions were derived for gravitational deposition of particles from laminar flows in inclined flat channels and circular tubes. According to Wang, the use of the trajectory function provides a simple way for calculating the flow rate of particles through any area. This is particularly useful in the analysis of the deposition in the inclined channels of which the inlet and outlet cross-sections are not verticle.

Precipitation of charged particles under the influence of image force from laminar flows in rectangular and cylindrical channels was investigated theoretically by Yu and Chandra {32}. They neglected the gravity, inertial and diffusion (Brownian motion) effects of particles and studied the effect of electrostatic image force on the deposition of particles from laminar flows in a rectangular (parallel-plate) channel and that in a circular tube. The equation of

image force for rectangular channel is introduced in the following chapter on which the derivation of the equation of image force for a convergent channel is based.

Yu and Chandra's numerical calculations were based on the analysis of limiting trajectories of particles that enabled the determination of the precipitation efficiency for channels of different dimensions. The results for cylindrical tubes are applicable to the deposition of charged particles in human lung airways.

Yu {33} further analyzed the precipitation of unipolarly charged particles of uniform size in cylindrical and spherical vessels by their own space charge. When the particle number density is high and particle-to-particle interaction is important, particle loss to the wall is due to mutual electrical repulsion. On the other hand, if the particle number is low, the image force acting on the particle due to the presence of the wall is the principal force responsible for particle deposition. Yu derived expressions for the fractional deposition of particles to the wall in both cases in order to calculate charged particle deposition in the lung airways.

Chen {34} studied the deposition of aerosols in a long channel due to diffusive and electrostatic charge effects. The diffusion equation and the Poisson equation for flow of

aerosol particles with electrostatic charge field force were solved with integral method based on flow of liquid with a uniform or parabolic velocity profile. He found that the inverse of the centerline particle density increased linearly with the product of the electrostatic parameter and the axial distance for the flow near the channel inlet. The centerline particle density, the penetration and the electric field force decreased exponentially with the axial distance for flow far from the channel inlet.

Ingham {35} considered the deposition of a steady flow of suspensions due to electrostatic charge field force near the entrance of a cylindrical tube. Neglecting axial diffusion and with zero radial velocity, his governing equations included the steady state transport equation and Poisson's equation for electrostatic field. He solved these equations analytically.

Laminar flow of particle in a parallel-plate channel with electrostatic charge field force, diffusion, and gravitational effects was studied by Chen and Gelber {36}. Variations in deposition were determined using a dimensionless parameter (charge-diffusion parameter) which is a ratio of the space electrostatic charge effect to the diffusion effect. They found that when this parameter was greater than 50, the diffusion effect may be neglected. When gravity acting in the direction of flow was considered,

a velocity ratio (terminal velocity of the particle to the mean velocity of the fluid flow) was introduced. The space electrostatic charge field force effect and the gravity effect were considered in this case, and the velocity profile was either uniform or fully-developed.

In the theoretical investigations on deposition in channels carried out by Yu {33}, Chen {34}, Ingham {35} and Chen and Gelber {37}, the axial diffusive term in the continuity equation was neglected in the analyses and, thus, the axial velocity of the fluid was considered to be the same as that of the particle. In other words, the inertia of the particle was totally neglected.

Chen et al {38} extended the study to include the effect of particle inertia on the deposition of aerosol in a parallel-plate channel. Highly charged fine particles of sizes less than 20 micrometer had been analyzed numerically for both uniform and fully-developed flows using a trajectory method. They considered the deposition to be primarily due to space charge alone and the image and gravity forces were not included in the analysis. They also defined a charge-inertia parameter n (ranging from 0 to 1) to characterize the flow deposition phenomena. They found that for n less than 0.1, the effect of inertia forces may be neglected and that the fraction of deposition near the entrance of the channel deviated substantially from the result that neglected the inertia effect.

The following analysis will investigate the electro-hydrodynamic flow system of diluted suspensions of charged solid particles of constant mass and electrostatic charge penetrating between convergent channel plates. Viscous effect will be encountered in addition to the two dimensional subsonic flow field. Thus, the electrostatic force that attracts the particle towards the wall are solely due to the image charge forces of the conducting walls. Inertia effect will also be considered and dimensionless parameters will be introduced in the analysis.

3. THEORECTICAL ANALYSIS OF IMAGE FORCE EQUATIONS

The problem of internal flow of suspensions and deposition of suspended particles in two-dimensional parallel-plate channels have been extensively studied theoretically by many investigators as mentioned in the previous chapter. The interest in such studies stems from the fact that aerosol deposition experiments often yield higher deposition than could be accounted for by normal mechanisms such as gravitational settling, Brownian diffusion and impaction; the increased precipitation could be due to the particle charge.

As stated in Chapter one, the force due to charge may arise in two ways: (1) by the mutual electrostatic repulsion between particles, the so-called field force, and (2) by the charge induced on the walls, the so-called image force. It has been demonstrated by Yu {33} that when the particle number density is sufficiently low, the predominant effect is due to the image force.

The image force equation have been given by Yu and Chandra {32} and Yu {33} in parallel-plate and cylindrical channels. Yu and Chandra {32} used this equation in studying the precipitation from aerosol flows due to the image force alone neglecting sedimentation and concluded

that the charge could significantly affect the particle deposition in the farthest human airways.

Later, Thiagarajan and Yu {39} utilized the image equation in the study of precipitations from aerosol flows in parallel-plate and cylindrical channels due to the simultaneous effect of gravitational and electrostatic image forces. They found that the penetration efficiencies are a function of several non-dimensional parameters.

Although the image force equation has been extensively used in particle deposition analysis in additional to the influences of inertia, viscous and gravitational forces, it is restricted to constant area parallel-plate {40} and cylindrical channels {41} studies only. Image force equations in convergent channels and diffusers have not been derived for further analysis yet. In this chapter, a detailed study on the image force equation for constant area parallel-plate channels is presented first. Then, an in-depth derivation and analysis of the image force equations for convergent channels together with the theorectical analysis on the Image Circle are given.

The derivation of the image force equations for convergent channels is based on that given for parallel-plate channels with the assumption that both channel plates are conducting and grounded.

3.1 IMAGE FORCE EQUATION FOR PARALLEL-PLATE CHANNELS

In this section, the original image force equation for parallel-plate channels is given. In order that the derivation of the image force equations for convergent channels can be easily based on, the original equation is modified to be expressed in a way that all the images above the upper channel wall and below the lower channel wall are grouped together separately.

The coordinate system for parallel-plate channels is shown in Figure 3.1. The flow is along the x-direction. Let 2ho be the width of the long parallel-plate channel where y = ho and -ho correspond to the upper and lower walls of the channel, respectively. Based on Coulomb's Law {43} of Electromagnetic Theory and with the assumption that the walls are conducting and grounded, the image force equation for a charged particle between two parallel-plates is given by Yu and Chandra {32} as:

$$Fx = 0$$

$$Fy = \frac{q^2 ho\, y}{4\pi\epsilon o}\left\{\underbrace{\frac{1}{(ho - y)^2}}_{\text{1st pair}} + \underbrace{\sum_{n=1}^{\infty} \frac{2n+1}{((2n+1)\, ho - y)^2}}_{\text{2nd pair on}}\right\} \qquad (3\text{-}1)$$

where

q: particle charge

ho: half channel width

ϵ_o: free space permittivity

The first term in Equation (3-1) represents the image force on the particle due to the first pair of images. The second term is a summation of the image force due to the second pair up to infinite pair of images; i.e. n = 1 represents the second pair, n = 2 represents the third pair and so on. The image pairs in Figure 3.1 are indicated by 1 and 1' for the first pair, 2 and 2' for the second pair and so on, where 1, 2, 3..... are images located above the upper channel wall and 1', 2', 3'.... are images located below the lower channel wall. It is noticed that the images are all along the y-direction, no image force contributes in the x-direction.

3.2 MODIFICATION OF THE IMAGE FORCE EQUATION

The image force terms in Equation (3-1) are summed up in pairs. It can be expressed out to be summation of individual pair of images as,

$$Fx = 0$$

$$Fy = \frac{q^2}{4\pi\epsilon_o}\left\{\underbrace{\frac{ho\ y}{(ho^2 - y^2)^2}}_{\text{1st pair}} + \underbrace{\frac{3ho\ y}{\{(3ho)^2 - y^2\}^2}}_{\text{2nd pair(n=1)}}\right.$$

$$+\frac{5ho\ y}{\{(5ho)^2 - y^2\}^2} + \frac{7ho\ y}{\{(7ho)^2 - y^2\}^2}$$

3rd pair(n=2) 4th pair(n=3)

$$+ \ldots\ldots\ldots\ldots\ldots\ldots \Bigg\} \qquad (3\text{-}2)$$

5th pair on(n=4,...)

where the first, second, third, ... terms represent image force due to the first, second, third, ... pair of images, respectively.

Equation (3-2) can be further expressed out as summation of image force due to individual single particle images as,

$$Fx = 0$$

$$Fy = \frac{q^2}{4\pi\epsilon_o}\left\{\frac{1}{\{2(ho - y)\}^2} + \frac{-1}{\{2(ho + y)\}^2}\right.$$

upper side lower side
1st pair(n=0)

$$\left. + \frac{1}{\{2(3ho - y)\}^2} + \frac{-1}{\{2(3ho + y)\}^2}\right.$$

lower side upper side
2nd pair(n=1)

$$+ \frac{1}{\{2(5ho - y)\}^2} + \frac{-1}{\{2(5ho + y)\}^2}$$

upper side lower side
3rd pair(n=2)

$$+ \ldots\ldots\ldots\ldots\ldots\ldots \Bigg\} \qquad (3\text{-}3)$$

4th pair on(n=3,...)

where the first term on each pair of images represents the particle image which produces a positive force to the particle (particle will thus be moving in the positive y-direction towards the upper channel wall); and the second term represents the particle image which produces a negative attraction force to the particle (particle will thus be moving in the negative y-direction towards the lower channel wall).

If all the images that produce positive force to the particle, and all the images that produce negative force to the particle are grouped together separately, Equation (3-3) becomes,

$$Fx = 0$$

$$Fy = \frac{q^2}{4\pi\epsilon_o} \sum_{n=0}^{\infty} \left\{ \frac{1}{(2\{(2n+1)ho - y\})^2} \right.$$

due to positive force
production images

$$+ \frac{-1}{(2\{(2n+1)ho + y\})^2} \Bigg\} \qquad (3\text{-}4)$$

due to negative force production images

where the first term is a summation force due to all the images that produce positive force to the particle and the second term is a summation force due to all the images that produce negative force to the particle.

It can be easily obtained, as a cross check by setting n = 0 in Equation (3-4), the image force Equation (3-1) which due only to the first pair of images as,

$$Fx = 0$$

$$Fy = \frac{q^2}{4\pi\epsilon_o} \left\{ \frac{1}{\{2(ho - y)\}^2} + \frac{-1}{\{2(ho + y)\}^2} \right\}$$

upper side lower side
1st pair

$$= \frac{q^2}{4\pi\epsilon_o} \left\{ \frac{ho\ y}{(ho - y)^2\ 2^2\ 2} \right\} \qquad (3\text{-}1)$$

1st pair

3.3 THE IMAGE CIRCLE

Before the derivation of the image force equation for

convergent channels, it is necessary to understand the characteristics of the system of images due to conducting and grounded walls of convergent channels; so that appropriate assumptions may be applied in the derivations.

The coordinate system for convergent channels is shown in Figure 3.2. The flow is along the x-direction. Let 2ho be the entrance width of the convergent channel where y = ho and -ho refer to the upper and lower walls of the channel at entrance, respectively. When x > 0, the channel half width h (< ho) is not a constant but a function of x. The channel walls are also assumed to be conducting and grounded.

A convergent channel can be thought of as a parallel-plate channel with its lower and upper walls tilted at an angle θ and $-\theta$ with respect to the x-axis, respectively, as shown in Figure 3.2.

It is because of this tilted angle of the channel walls, that the images to a point particle between this convergent channel walls which are conducting and grounded are no longer two infinite sequences as that shown in Figure 3.1. The first pair of images (1 and 1' in Figure 3.2) of the particle are shifted ahead of the point particle through an angle θ. The second pair of images (2 and 2'), which are actually resulted from the first pair, are now shifted

further ahead of the first pair of images also through an angle θ. The third and fourth pair of images (3 and 3', 4 and 4') and so on can then be obtained in a similar manner until the nth pair of images is reached.

From basic electromagnetic theory {42,43,44}, it is noted that for two conducting planes intersect at an angle 2θ, the system of images of a point charge (particle) is finite and confined on a circle --- THE IMAGE CIRCLE. This image circle is defined by having its center at the intersecting point of the two conducting planes, and the distance from this intersecting point to the point charge as radius.

The total number of pair of images, N, confined on the image circle is related to the intersecting angle of the two conducting planes --- the convergent channel angle, by the following equation {42,43,44},

$$N = \frac{\pi}{2\theta} \qquad (3\text{-}5)$$

Obviously N in the above equation is inversely proportional to the convergent channel angle. Examples of image pairs confined on an image circle is given in Figures 3.3 to 3.7 for convergent angles of 90, 60, 45, 42, and 30 degrees, respectively. For instance, in Figure 3.4, there are a total number of 3 pairs of images confined on the image circle of a convergent channel of 60 degrees.

Based on Equation (3-5) and graphical analysis of these figures, the following assumptions are made in the present investigation.

1. For a particle with positive charge q within a convergent channel, its immediate (first) pair of images are of negative charge -q; and positive charge q for the second pair, negative charge -q for the third pair and so forth.

2. If N in Equation (3-5) is an integer, there will be a total number of N pairs of images confined on the image circle. If N happens to be real, there will be a total number of the integer part of N plus one pairs of images on the image circle. For example, as shown in Figure 3.6, N = 4.28 for a convergent channel of 42 degrees, there is a total number of 4 plus 1 equals 5 pairs of images confined on the image circle.

3. Assumed that the two images of the last pair are coincide for simplicity.

4. For the limiting case of zero convergent channel angle, N becomes infinite. Actually, this becomes the case of a parallel-plate channel.

5. On the other hand, when the convergent channel angle is 180 degrees, N = 1 as seen in Figure 3.8. The channel becomes a plane mirror and is out of application in our channel flow analysis.

The image force under investigation in the present analysis are the cases with convergent channel angles 15, 10, and 5 degrees. The image circles together with the exact number of pairs of images correspond to these channel angles are shown in Figures 3.9 to 3.11 for reference.

3.4 IMAGE FORCE EQUATIONS IN CONVERGENT CHANNELS

In the previous section, the image force equation (3-3) for parallel-plate channels is given in a form of summation of forces due to individual images as,

$$Fx = 0$$

$$Fy = \frac{q^2}{4\pi\epsilon_o}\left\{\underbrace{\frac{1}{\{2(ho-y)\}^2}+\frac{-1}{\{2(ho+y)\}^2}}_{\text{image 1 and image 1' — 1st pair (n=0)}}+\underbrace{\frac{1}{\{2(3ho-y)\}^2}+\frac{-1}{\{2(3ho+y)\}^2}}_{\text{image 2' and image 2 — 2nd pair (n=1)}}\right.$$

$$+\frac{1}{\{2(5ho - y)\}^2}+\frac{-1}{\{2(5ho + y)\}^2}$$

image 3 image 3'
3rd pair(n=2)

$$+ \ldots\ldots\ldots\ldots\ldots\ldots \Big\} \qquad (3\text{-}6)$$

4th pair on(n=3,...)

It is worth noticing that for the first two terms, the value inside the bracket of the denominators in Equation (3-6) represent the distances between the point charge (particle) and the first pair of images of the point charge. For example, 2(ho - y) in the first term is the distance between the point charge and the image 1 (first image of the point charge locating above the upper channel wall). For the nth pair of images, the value inside the bracket of the denominators represent the distance between the corresponding (n-1)th and n'th (or the (n-1)'th and nth) images, respectively. For instance, 2(5ho + y) in the sixth term is the distance between the images 2 and 3' (n = 2).

For convergent channels, the same approach is applied to obtain the governing image force equations. As stated in the previous section, it is shown that the images of a point charge between a convergent channel confines on an image circle rather than two infinite sequences of images as for the case of a parallel-plate channel. In order to

apply Equation (3-6) onto a convergent channel, the following terms are geometrically defined as shown in Figure 3.12. For the first pair of images,

$q1$ = distance between the point charge and image 1

$= 2(ho - y)\cos\theta$

$q1x$ = x-component of distance q1

$= 2(ho - y)\cos\theta\sin\theta$

$= (ho - y)\sin(2\theta)$

$q1y$ = y-component of distance q1

$= 2(ho - y)\cos\theta\cos\theta$

$= (ho - y)2\cos^{2}\theta$

$q1'$ = distance between the point charge and image 1'

$= 2(ho + y)\cos\theta$

$q1'x$ = x-component of distance q1'

$= 2(ho + y)\cos\theta\sin\theta$

$= (ho + y)\sin(2\theta)$

$q1'y$ = y-component of distance q1'

$= 2(ho + y)\cos\theta\cos\theta$

$= (ho + y)2\cos^{2}\theta$

and in a similar manner, for the second pair of images,

$q2$ = distance between the point charge and image 2

$= \sqrt{q2x^{2} + q2y^{2}}$

$q2x$ = x-component of distance q2

$= (h1' - y + q1'y)\sin(2\theta) + q1'x$

$q2y$ = y-component of distance q2

$= (h1' - y + q1'y)2\cos^2\theta - q1'y$

$q2'$ = distance between the point charge and image 2'

$= \sqrt{q2'x^2 + q2'y^2}$

$q2'x$ = x-component of distance q2'

$= (h1' - y + q1'y)\sin(2\theta) + q1'x$

$q2'y$ = y-component of distance q2'

$= (h1 + y + q1y)2\cos^2\theta - q1y$

and so on until the nth pair of images,

qn = distance between the point charge and image n

$= \sqrt{qnx^2 + qny^2}$

qnx = x-component of distance qn

$= \{h(n-1)' - y + q(n-1)'y\}\sin(2\theta) + q(n-1)'x$

qny = y-component of distance qn

$= \{h(n-1)' - y + q(n-1)'y\}2\cos^2\theta - q(n-1)'y$

qn' = distance between the point charge and image n'

$= \sqrt{qn'x^2 + qn'y^2}$

$qn'x$ = x-component of distance qn'

$= \{h(n-1) + y + q(n-1)y\}\sin(2\theta) + q(n-1)x$

$qn'y$ = y-component of distance qn'

$= \{h(n-1) + y + q(n-1)y\}2\cos^2\theta - q(n-1)y$

Since h (< ho) is now a function of x, hr or hr' (r = 1,2.....n) in the above expressions represents the local half channel width at the location of image r or r', which are at a distance qrx or qr'x away from the point charge horizontally.

Substituting the proper distances into Equation (3-6) will deduce the prototype image force equation for convergent channels as,

$$Fx = 0$$

$$Fy_{local} = \frac{q^2}{4\pi\epsilon_o}\left\{ \underbrace{\frac{1}{(q1)^2} + \frac{-1}{(q1')^2}}_{\substack{\text{image 1} \quad \text{image 1'} \\ \text{1st pair}}} + \underbrace{\frac{1}{(q2)^2} + \frac{-1}{(q2')^2}}_{\substack{\text{image 2} \quad \text{image 2'} \\ \text{2nd pair}}} + \ldots\ldots\ldots\ldots\ldots \text{ 3rd pair on} \right.$$

$$\left. + \underbrace{\frac{1}{(qn)^2} + \frac{-1}{(qn')^2}}_{\substack{\text{image n} \quad \text{image n'} \\ \text{nth pair}}} \right\} \qquad (3\text{-}7)$$

Noticed that the y-component image force in Equation (3-7) is a local value since the attraction or repulsion

forces acting between the point charge and its images are all in the direction of their distances q1, q1', q2, q2', ... qn, and qn', respectively. All these forces have to be resolved into the global x and y coordinates of the two phase flow field for analysis. From Figure 3.12, it can be deduced that the distances q1, q1', q2, q2', ... qn, and qn' are inclined with the y-axis through an angle θ_1, θ_2, $\theta_{1'}$, $\theta_{2'}$, ... θ_n, and $\theta_{n'}$, respectively where these angles are defined as,

$$\theta_1 = \tan^{-1}\left(\frac{q1x}{q1y}\right)$$

$$\theta_{1'} = \tan^{-1}\left(\frac{q1'x}{q1'y}\right)$$

$$\vdots$$

$$\theta_n = \tan^{-1}\left(\frac{qnx}{qny}\right)$$

$$\theta_{n'} = \tan^{-1}\left(\frac{qn'x}{qn'y}\right)$$

From vector analysis, all the forces due to the images above the upper channel wall have to multiply by the corresponding sin θ_n and cos θ_n to be resolved into the global fluid flow coordinates. Similarly, the forces due to the images below the lower channel wall have to multiply by -sin $\theta_{n'}$ and cos $\theta_{n'}$ to transfer to the global coordinates.

Inserting these factors into Equation (3-7) and rearranging them in the x and y components separately yields,

$$Fx = \frac{q^2}{4\pi\epsilon_o}\left\{ \underbrace{\frac{\sin\theta_1}{(q1)^2} + \frac{\sin\theta_{1'}}{(q1')^2}}_{\substack{\text{image 1} \quad \text{image 1'} \\ \text{1st pair}}} + \underbrace{\frac{\sin\theta_2}{(q2)^2} + \frac{\sin\theta_{2'}}{(q2')^2} + \cdots\cdots\cdots\cdots\cdots}_{\substack{\text{image 2} \quad \text{image 2'} \\ \text{2nd pair} \qquad\qquad \text{3rd pair on}}} + \underbrace{\frac{\sin\theta_n}{(qn)^2} + \frac{\sin\theta_{n'}}{(qn')^2}}_{\substack{\text{image n} \quad \text{image n'} \\ \text{nth pair}}} \right\} \qquad (3\text{-}8a)$$

$$Fy = \frac{q^2}{4\pi\epsilon_o}\left\{ \underbrace{\frac{\cos\theta_1}{(q1)^2} - \frac{\cos\theta_{1'}}{(q1')^2}}_{\substack{\text{image 1} \quad \text{image 1'} \\ \text{1st pair}}} + \underbrace{\frac{\cos\theta_2}{(q2)^2} - \frac{\cos\theta_{2'}}{(q2')^2} + \cdots\cdots\cdots\cdots\cdots}_{\substack{\text{image 2} \quad \text{image 2'} \\ \text{2nd pair} \qquad\qquad \text{3rd pair on}}} \right\}$$

$$+\left.\frac{\cos\theta_n}{(qn)^2}-\frac{\cos\theta_{n'}}{(qn')^2}\right\} \qquad \text{(3-8b)}$$

image n image n'
nth pair

Equations (3-8a) and (3-8b) are the final image force equations for convergent channels. It is interested to know that θ_1 and $\theta_{1'}$ happen to be the half convergent channel angle θ. Also, for the limiting case of convergent channel angle equals 180 degrees, it becomes the case of a parallel-plate channel. The image force in the x-component will then be zero because of the sine function, and the image circle reduces to the two infinite image sequences.

4. FLOW OF SUSPENSIONS IN CONVERGENT CHANNELS WITH INERTIA, ELECTROSTATIC IMAGE FORCES AND VISCOUS EFFECTS

In this chapter, a numerical scheme is presented to study the uniform flow of suspensions in a two dimensional convergent channel including the fraction of deposition of solid particles on the channel walls due to the inertia force of the particle, electrostatic charge image force on the particle, and viscous force of the fluid. Due to dilute suspension assumption and since the solid particle are very small (size of order 2 micrometer diameter), the effect of gravity can be neglected. Furthermore, it is also assumed that the thickness of the layer of deposit is much smaller than the channel width, so that the effective reduction in channel width is not enough to change appreciably the fluid velocity distribution.

It is assumed that the suspension flow is uniform and incompressible, which is a good approximation for compressible flow at very low Mach numbers (i.e. $M < 0.1$). Moreover, the case of low particle concentration (i.e. dilute suspension) will be considered such that the particles have relatively no effect on the fluid phase.

As a result, assumptions are made as follows:

1. Incompressible, steady flow

2. Two-dimensional, uniform flow
3. Negligible gravitational effect
4. Fluid-particle interaction is negligible
5. Particle-particle interaction is negligible
6. Negligible diffusion force in comparison to image force
7. Convergent conducting channel walls are assumed to be grounded and may be extended to intersect at one point
8. Thickness of the layer of deposit is much smaller than the channel width
9. Negligible lift force on the particle
10. Material density of the fluid phase in comparison to that of the solid particles is negligible
11. No chemical reactions considered
12. Particle number density sufficiently low that mutual electrostatic repulsion (i.e. field force) between particles negligible
13. Electrostatic charge (intensity) is uniformly distributed on surface of particle only
14. Particles behave like a uniform sphere of radius a

Rectangular Cartesian coordinates will be applied in this analysis in a way that the positive x-axis will be placed in the streamwise direction along the centerline of the convergent channel and the positive y-axis in the vertical upward direction as shown in Figure (3.1).

4.1 GOVERNING EQUATIONS

Treating the fluid as a continuum and employing a field representation of fluid properties, we may express the principle of coservation of mass in rectangular coordinates for the fluid phase and particle phase under steady state as follows:

(a) Fluid Phase

$$\frac{\partial u}{\partial x} + \frac{\partial v}{\partial y} = 0 \tag{4-1}$$

$$uo = \frac{1}{2ho} \int_{-h}^{h} u \, dy \tag{4-2}$$

$$vo = v = 0 \tag{4-3}$$

where uo, vo are the uniform fluid flow at the entrance of the convergent channel. Here, we have considered the case of connecting the convergent channel at the inlet to a constant area channel of width of 2ho where the uniform flow is from.

(b) Particle Phase

$$\frac{\partial (\rho_p \, up)}{\partial x} + \frac{\partial (\rho_p \, vp)}{\partial y} = 0 \tag{4-4}$$

This continuity equation of the particle phase can be expanded in the form,

$$\rho_p \frac{\partial up}{\partial x} + up \frac{\partial \rho_p}{\partial x} + \rho_p \frac{\partial vp}{\partial y} + vp \frac{\partial \rho_p}{\partial y} = 0$$

which contains partial derivatives of the same order for up, vp and ρ_p.

Based on Newton's Second Law of motion, which states that the product of mass and acceleration of a particle in any direction is proportional to the force acting on the particle in that direction, a mathematical model is developed for the particle deposition analysis.

In rectangular cartesian coordinate system and imposing the assumptions made above, the equations of motion for a particle in a uniform flow of a convergent channel under the influence of image charge, and viscosity based on results from Yu {32} and Chen {38} and also derived in the previous Chapter are:

$$m \frac{d\,up}{dt} = f(u-up) + Fx \qquad (4-5)$$

$$m \frac{d\,vp}{dt} = -f(v-vp) + Fy \qquad (4-6)$$

where

Fx = image force per particle in x-direction

Fy = image force per particle in y-direction

$f = 6\pi\mu a$: Stoke's drag force

m = mass of particle

t = time unit

u = velocity of fluid in x-direction

v = velocity of fluid in y-direction

up = velocity of particle in x-direction (=dx/dt)

vp = velocity of particle in y-direction (=dy/dt)

a = radius of particle

μ = dynamic viscosity of air

In Equation (4-5), the inertia term on the left hand side is the product of the particle mass and acceleration. On the right hand side is the sum of the viscous force which based on Stoke's law and valid at low Reynolds number, and the x-component image force which acts on the given charge q and is induced by its interaction with the conducting channel planes. In a similar fashion, the left hand side in Equation (4-6) is the inertia term while the right hand side is the sum of the viscous force and the y-component image force on the particle.

It is interesting to note that, when the convergent channel angle θ is zero, it conforms to a parallel-plate channel and has no x-component image force. It should also be noted that the solid particles, although under the inertia effect, do not have to follow the streamline of the fluid, i.e. the particle lines (path lines) and streamlines of the fluid do not necessarily coincide.

The main purpose of solving these equations is to determine the fraction of deposition of the particles on the convergent channel wall due to electric image force (mainly) which can be obtained from equation of conservation of mass of the particle phase as follows:

Fraction of Deposition

$$= \frac{\int_{-ho}^{yl} \rho_p \, up \, dy + \int_{yu}^{ho} \rho_p \, up \, dy}{\int_{-ho}^{ho} \rho_p \, up \, dy} \qquad (4\text{-}7)$$

Following the concept of limiting trajectories by Pich {45}, yl and yu in Equation (4-7) are two critical values of y at the channel entrance x = 0, such that the particles entering the channel between y = -ho and yl will deposit on the lower channel wall; those entering between y = yu and ho will deposit on the upper channel wall; and those entering between y = yl and yu will penetrate the convergent channel.

Since the particle density ρ_p is assumed to be constant and that the flow follows a symmetrical pattern because of the negligible of gravitational force, only one half of the convergent channel need be considered. With upo represents the particle velocity in the x-direction at the channel inlet, equation (4-7) thus becomes,

Fraction of Deposition

$$= \frac{2\int_{yu}^{ho} upo\ dy}{\int_{-ho}^{ho} upo\ dy} \tag{4-8}$$

Equations (4-1) to (4-4) can be nondimensionalized as given in Appendix B as follows:

$$\frac{\partial U}{\partial X} + \frac{\partial V}{\partial Y} = 0 \tag{4-9}$$

$$\int_{-1}^{1} U\ dy = 2.0 \tag{4-10}$$

$$Vo = V = 0 \tag{4-11}$$

$$\frac{\partial (\rho_p\ Up)}{\partial X} + \frac{\partial (\rho_p\ Vp)}{\partial Y} = 0 \tag{4-12}$$

Substituting the dimensionless quantities into Equation (4-5), we have

$$\frac{uo}{ho} m \frac{d^2 X}{dT^2} = f\ uo\left(U - \frac{dX}{dT}\right) + \frac{q^2}{4\pi \epsilon o} \sum_{n=1}^{N} \left\{ \frac{\sin\theta n}{ho^2 (QnX^2 + QnY^2)} + \frac{\sin\theta n'}{ho^2 (Qn'X^2 + Qn'Y^2)} \right\} \tag{4-13}$$

if the whole equation is divided by fuo, it becomes

$$\frac{m\,uo}{f\,ho}\frac{d^2X}{dT^2} = U - \frac{dX}{dT} + \frac{q^2}{4\pi\epsilon_o\, f\, uo}\sum_{n=1}^{N}\left\{\frac{\sin\theta n}{ho^2\,(QnX^2 + QnY^2)} + \frac{\sin\theta n'}{ho^2\,(Qn'X^2 + Qn'Y^2)}\right\} \tag{4-14}$$

or

$$\frac{m\,uo}{f\,ho}\frac{d^2X}{dT^2} = U - \frac{dX}{dT} + \frac{q^2}{4\pi\epsilon_o\, f\, uo\, ho^2}\sum_{n=1}^{N}\left\{\frac{\sin\theta n}{QnX^2 + QnY^2} + \frac{\sin\theta n'}{Qn'X^2 + Qn'Y^2}\right\} \tag{4-15}$$

so that

$$St\,\frac{d^2X}{dT^2} = U - \frac{dX}{dT} + Q\,Fx' \tag{4-16}$$

In a similar way, when substituting the dimensionless quantities into Equation (4-6) yields

$$\frac{uo}{ho}\, m \frac{d^2 Y}{dT^2} = f\, uo\left(V - \frac{dY}{dT}\right) + \frac{q^2}{4\pi\epsilon_o} \sum_{n=1}^{N} \left\{ \frac{\cos\theta n}{ho^2 (QnX^2 + QnY^2)} + \frac{\cos\theta n'}{ho^2 (Qn'X^2 + Qn'Y^2)} \right\} \tag{4-17}$$

further reduction leads to

$$\frac{uo}{ho}\, m \frac{d^2 Y}{dT^2} = f\, uo\left(V - \frac{dY}{dT}\right) + \frac{q^2}{4\pi\epsilon_o\, ho^2} \sum_{n=1}^{N} \left\{ \frac{\cos\theta n}{QnX^2 + QnY^2} - \frac{\cos\theta n'}{Qn'X^2 + Qn'Y^2} \right\} \tag{4-18}$$

again, divided the whole equation by f uo, we have

$$\frac{m\, uo}{f\, ho} \frac{d^2 Y}{dT^2} = V - \frac{dY}{dT} + Q \sum_{n=1}^{N} \left\{ \frac{\cos\theta n}{QnX^2 + QnY^2} - \frac{\cos\theta n'}{Qn'X^2 + Qn'Y^2} \right\} \tag{4-19}$$

or

$$St \frac{d^2 Y}{dT^2} = V - \frac{dY}{dT} + Q\, Fy' \qquad (4\text{-}20)$$

Equation (4-8) can also be nondimensionalized as:

Fraction of Deposition

$$= \frac{2\int_{Yu}^{1} Upo\, dY}{\int_{-1}^{1} Upo\, dY} \qquad (4\text{-}21)$$

where Upo = upo/uo = particle entrance velocity/fluid entrance velocity, and is assumed that Upo = U = 1, for uniform flow, at the channel entrance (x = 0). So that, after integration, Equation (4-21) becomes,

Fraction of Deposition

$$= 1.0 - Yo \qquad (4\text{-}22)$$

where Yo is the positive y-location of the particle at the convergent channel inlet.

The physical meaning and order of magnitude of the dimensionless quantities and parameters are explained in Appendix B.

Note that from the above equations, the solution depends on the electrostatic charge parameter Q, Stoke's number St, convergent channel angle 2θ, and the boundary conditions.

4.2 BOUNDARY CONDITIONS

In our analysis, we have considered the convergent channel to be connected at its inlet to a constant area channel of width 2ho.

Referring to Figure 3.2, the width of the convergent channel at entrance (x = 0) is 2ho, the centerline is located at y = 0, so that the upper channel wall at entrance is at y = ho and the lower channel wall at entrance is at y = -ho. At further downstream (x > 0), the convergent channel half width h is less than ho and is a function of x. Considering symmetrical flow through the convergent channel with uniform inlet conditions, the boundary conditions are:

At x = 0 (at convergent channel inlet) and for 0 <= y <= ho

u = up = uo (uniform flow)

v = -(uo ho y tanθ)/(ho - x tanθ)**2

vp = 0 (no vertical particle velocity) (4-23)

$h = ho$

$\rho_p = \rho_{po}$ (constant particle density)

At y = 0 (at centerline of the convergent channel) and for x > 0 (at further downstream)

$$\frac{\partial u}{\partial y} = \frac{\partial up}{\partial y} = 0 \qquad \text{(symmetry)}$$

$$v = vp = 0 \qquad (4\text{-}24)$$

$$\frac{\partial \rho_p}{\partial y} = 0 \qquad \text{(symmetry)}$$

At y = h (at upper wall of the convergent channel) and for x > 0 (at further downstream)

$u = v = 0$ (no slip condition)

$$h = ho - x \tan\theta \qquad (4\text{-}25)$$

At x > 0 and for 0 <= y <= ho

$u = uo\ ho/(ho - x \tan\theta)$

$$v = -(uo\ ho\ y \tan\theta)/(ho - x \tan\theta)^{**2} \qquad (4\text{-}26)$$

here, the y-direction component of fluid velocity v is a function of u, y, and the convergent angle θ to the x-axis.

It is worth noticing that since no gravity force is

considered, the y-component velocity at the centerline of the channel is equal to zero. Hence, a particle on the centerline will stay on the same horizontal level and, theoretically, will deposit at an infinite channel distance.

The above equations of the boundary conditions can be nondimensionalized as follows:

At X = 0 and 0 <= Y <= 1

$$U = Up = 1 \quad \text{(uniform flow)}$$

$$V = Vp = 0 \quad \text{(no y-component velocity)}$$

$$H = 1 \tag{4-27}$$

$$\rho_p = \rho_{po} \quad \text{(constant particle density)}$$

At Y = 0 and X > 0

$$\frac{\partial U}{\partial Y} = \frac{\partial Up}{\partial Y} = 0 \qquad \text{(symmetry)}$$

$$V = Vp = 0 \tag{4-28}$$

$$\frac{\partial \rho_p}{\partial Y} = 0 \qquad \text{(symmetry)}$$

At Y = 1 and X > 0

$$U = V = 0 \qquad \text{(no slip condition)}$$

$$H = 1 - X \tan\theta \tag{4-29}$$

At $X > 0$ and $0 <= Y <= 1$

$$U = 1/H = 1/(1 - X \tan\theta)$$

$$V = -U * \bar{Y} * \tan\theta \tag{4-30}$$

where $\bar{Y} = Y/H = (y/ho)/(h/ho)$; i.e. at $\bar{Y} = 0$, $V = 0$, and at $\bar{Y} = 1$, $V = -U * \tan\theta$.

4.3 METHOD OF SOLUTION

The governing equations (4-16) and (4-20) and boundary conditions (4-27) to (4-30) are integrated and solved with Runge-Kutta method. A description on the application of the Runge-Kutta solution in particle deposition analysis is given in Appendix A.

The second-order differential equations (4-16) and (4-20) can be rewritten in the form of two equivalent first-order differential equations as follows:

Let

$$A = \frac{dX}{dT} \tag{4-31}$$

be the particle velocity in the X-direction, so that

$$\frac{dA}{dT} = \frac{d}{dT}\left(\frac{dX}{dT}\right) = \frac{d^2X}{dT^2} \tag{4-32}$$

is the particle acceleration in the X-direction. Substituting these expressions into equation (4-16) yields,

$$St\,\frac{dA}{dT} = U - A + Q\,Fx' \tag{4-33}$$

or,

$$\frac{dA}{dT} = \frac{U - A + Q\,Fx'}{St} \tag{4-34}$$

In a similar manner, let

$$B = \frac{dY}{dT} \tag{4-35}$$

be the particle velocity in the Y-direction, so that

$$\frac{dB}{dT} = \frac{d}{dT}\left(\frac{dY}{dT}\right) = \frac{d^2Y}{dT^2} \tag{4-36}$$

is the particle acceleration in the Y-direction. Substituting these expressions into equation (4-20) yields,

$$St\,\frac{dB}{dT} = V - B + Q\,Fy' \tag{4-37}$$

or,

$$\frac{dB}{dT} = \frac{V - B + Q\,Fy'}{St} \qquad (4\text{-}38)$$

The initial conditions are:

1. $A = dX/dT = 1$ at $X = 0$, $T = 0$, for uniform particle flow.

2. $U = Uo = 1$ at $X = 0$, $T = 0$, for uniform inlet fluid flow.

3. $B = dY/dT = 0$ at $X = 0$, $T = 0$.

This implies that the convergent channel is connected to a constant area channel in a way that an incoming uniform flow can be assumed at the channel inlet. Moreover, it is also assumed that the particle has not exposed itself to the image force field yet prior to the entrance of the convergent channel.

The four modified equations (4-31), (4-34), (4-35), and (4-38) together with the initial conditions are solved by Runge-Kutta method. A Fortran computer program for this particular two-phase analysis is written and listed in Appendix D.

In the Runge-Kutta computer program, it is assumed that the particle has deposited on the channel wall when they reach a distance $Y = 0.998$. Initial particle positions

of 0.98, 0.94, 0.9, 0.86, 0.8, 0.7, 0.6, 0.5, 0.4, 0.3, 0.2, 0.1, 0.05, 0.01, and 0.001 were originally set at X = 0, and T = 0 between $0 < Y < 1$ to analyze the particle deposition distribution. Later, because of the wide scattering deposition distribution of the particle at certain particular conditions, more initial particle positions were added to complete and fill the fraction of deposition curve. The convergent channel angle 2θ is taken from 15, 10, and 5 degrees and later at zero degree (which is the case of a parallel-plate channel; and for St = 0 only) for comparison with previous investigation results. The electrostatic charge parameter Q as well as the Stoke's number (St) are both taken from 100 to 0.

Although an IBM 370 system was used throughout the investigation, the computational time could be very lengthy depending on the time step value used and the total number of image pairs considered. Thus, a time step dT from 10 to 0.000001 is specially selected in the program depending upon the magnitude of the Stoke's number. Normally, the time step value is positively proportional to the Stoke's number.

When the convergent channel angle equals zero, it becomes a parallel-plate channel flow, and the particle charge forms two infinite sequences of images. It can be noted that the infinite terms is a divergent series. To modify this, the total number of image pairs N in

equations (4-15) and (4-19), would be summed up to seven pairs only and a factor of 2.5 is then added. The result from this approximation is very close to the infinite terms of image force, so that the image force equations can be modified as follows: At $\theta = 0$, the force terms in equations (4-15) and (4-19) reduce to,

$$Fx = 0 \tag{4-39}$$

$$Fy = \frac{q^2}{4\pi\epsilon_o f u_o h_o^2} \sum_{n=1}^{\infty} \left\{ \frac{2n+1}{\{(2n+1)^2 - Y^2\}^2} \right\} \tag{4-40}$$

or

$$= \frac{q^2}{4\pi\epsilon_o f u_o h_o^2} \left\{ \sum_{n=1}^{7} \left[\frac{2n+1}{\{(2n+1)^2 - Y^2\}^2} \right] + 2.5 \frac{2m+1}{\{(2m+1)^2 - Y^2\}^2} \right\} \tag{4-41}$$

where m = 7, such that the last term in Equation (4-40) is

$$2.5 \frac{15}{(15^2 - Y^2)^2} < 2.5 \frac{15}{(15^2 - 1)^2}$$

$$= 0.000747 .$$

It is observed that the terms for n > 7 are very small. The comparisons between the 2 different types of expression for image forces are shown in Table 4.1. Since the results are very closed, the approximate expression equation (4-40) can then be justified.

5. RESULTS AND DISCUSSION

In this chapter, uniform flow of suspensions in convergent channels under the influences of the inertia, viscous, and electrostatic image forces will be discussed. The uniform velocity profile for the fluid phase in the convergent channel is examined briefly and then the particle trajectories for the particle phase are studied extensively to determine the effects of inertia, image force and viscous forces on the particle trajectories. As was mentioned in Chapter 1, the range of dimensionless parameters investigated in this analysis are 100, 10, 1, 0.1, 0.01, and 0 for both St (Stoke's number or inertia parameter) and Q (image charge parameter). Miller (46) states that a 7 degrees convergent nozzle has good performance since its discharge coefficient is approximately 0.96. Thus, the converging angles investigated in this study are 7.5, 5, 2.5 and 0 (for St = 0 only) degree(s). In this analysis, the flow characteristics for the suspensions in the convergent channels is analyzed from the inlet of the channel to the exit of the channel where the channel width is 20% of the width at the inlet.

5.1 Fluid Phase

Figures 5.1 to 5.2, and Tables 5.1 through 5.3 show the axial (U) and vertical (V) velocity distributions of the fluid phase at half convergent channel angle of 7.5 degrees and at initial particle positions of X = 0., Yo = 0.9, 0.5, and 0.1, respectively. The initial dimensionless fluid velocity is unity.

From the continuity requirement for the fluid phase, U = 1 and H = 1 at X = 0, and $H = 1 - X * \tan\theta$ at X > 0, the axial velocity at X > 0 is given by $U = 1/H = 1/(1 - X * \tan\theta)$. This is shown in Figure 5.1.

Again, from the continuity requirement, the vertical velocity of fluid is derived to be $V = -U * \bar{Y} * \tan\theta$, as discussed in the previous chapter.

Figure 5.2 and Tables 5.1 to 5.3 also show this vertical velocity distribution. Here, the values of V are negative, which designates that the direction of motion of the fluid elements in the vertical direction is away from the channel wall.

5.2 Particle Phase

The objective of this section is to study the particle trajectory under the influences of viscous, inertia, and electrostatic image forces. The case of particle flow in a

convergent channel of 7.5 degrees at St = 10 and Q = 10 is discussed below as an typical example.

5.2.1 Particle Trajectory

Figure 5.3 illustrates the particle trajectory at St = Q = 10, convergent angle of 7.5 degrees, and at initial particle positions of X = 0, Yo = 0.9, 0.5, and 0.1, respectively. The numerical values of this particle trajectories --- the X and Y displacements are also shown in Tables 5.1 to 5.3 for reference. It is obvious to understand that, the closer the initial particle position is to the channel wall, i.e. at Yo = 0.9, the faster the particle will be attracted and moved to the channel wall due to inertia force and image force. At initial particle positions of Yo = 0.9, 0.5, and 0.1, the particles reach the wall at X = 5.226, 1.232, and 0.108, respectively.

It is noted that the channel wall itself is a streamline. For particles near the channel wall, the vertical component of the fluid phase has a tendency to apply viscous forces on the particles and push them away from the wall; resulting in less deposition. If there is no inertia and electrostatic image charge, the particles will simply move along with the fluid and exit the channel without hitting the channel wall.

Theoretically, for a particle starting at a centerline position, the particle will move horizontally along the centerline since there is no viscous force or image force to alter its flow direction. This is due to the fact that the gravitational force is not considered in this analysis.

5.2.2 Particle Velocity Distribution

Figures 5.4 to 5.5 and Tables 5.1 to 5.3 show the X and Y components of the particle velocity in the horizontal (Up) and vertical (Vp) directions. The initial axial velocity of the particle is assumed to be the same as the fluid velocity at the channel entrance while its initial vertical velocity is assumed to be zero. In general, as a particle moves from its initial position, its velocity components in both the X and Y directions will increase gradually due to the combined forces of inertia, viscous, and image charge on the particle.

It can be seen from Figures 5.4 and 5.5 as well as Tables 5.1 to 5.3 that the particle velocities are increased more at initial positions close to the channel wall than at initial positions away from it. For instance, at Yo = 0.9, the particle axial velocity component increases from its initial value of unity to its terminal value (X = 0.108) of 2.987, while the vertical component increases from zero to 2.485. At Yo = 0.1, the particle axial and vertical

velocities increases to its terminal values (at X = 5.154) of Up = 2.388 and Vp = 0.056, respectively. This is due to the zero initial vertical velocity and the higher axial acceleration near the wall.

At smaller convergent angles, which implies a longer convergent channel, the particle will have to travel a longer distance before it reaches the channel wall. In such cases, the trajectory as well as the velocities may be different, but the flow pattern would be similar to the one discussed above.

5.3 Electrostatic Image Force Distribution

Table 5.4 gives the electrostatic image forces in the X and Y directions as well as its resultant values acting on particles at vertical positions from 0.1 (farest from the channel wall) to 0.999 (closest to the channel wall) at half convergent channel angles of 7.5, 5, and 2.5 degrees, respectively. The total number of image pairs is also shown for reference.

As stated in Chapter 3, for a flow of particle in a convergent channel, the images confined on the Image Circle are all located ahead of the particle in the X-direction; and the total number of pair of images is related to the convergent channel angle as given in Equation (3-5). Hence,

depends on the convergent channel angle as well as the vertical position (Y) of the particle, the total number of image pairs and the magnitude of the image forces in X and Y directions are defined.

As is listed in Table 5.4, the total number of image pairs are 12, 18, and 36 for half convergent channel angles of 7.5, 5, and 2.5 degrees, respectively. At a constant convergent angle, the image force increases with increasing Y, that is, the closer the particle is to the channel wall, the larger the image force it will experience. The X and Y component image forces are of 1.0E06 to 1.0E07 times larger at Y = 0.999 than that at Y = 0.1.

It is also noted that, the X component image force is slightly greater than the Y component at Y = 0.1 and 0.2 when the convergent angle is 7.5 degrees, and at Y = 0.1 when the convergent angle is 5 degrees. For all cases investigated, force in Y direction is much greater than that in X direction for all particles located at Y > 0.3.

Furthermore, at a constant Y, results reveal that the larger the convergent angle is, the larger the image force the particle will experience. However, the order of this increment is moderate for the Y component force which implies that the change in Y component image force is less sensitive to convergent angles than that in X component.

It can thus be concluded that for a particle under the influence of an electrostatic image force, regardless of the convergent channel angle and at a certain vertical position, the particle will experience almost the same amount of image force in the Y direction. With increasing convergent channel angles, because of the corresponding larger increase in the X component image force, the particle will have a higher acceleration in the horizontal direction.

5.4 Angle of Convergence effect on Particle Deposition

As described in Chapter 4 the main purpose of this investigation is to determine the fraction of deposition of particles on the convergent channel wall at various convergent angles due to viscous, inertia, and electrostatic image forces. Results of this analysis on particle depositions are given in Figures 5.6 to 5.35 and Tables 5.5 through 5.22.

For each of these figures and tables, the fraction of deposition of a particle is shown for various axial displacements in the convergent channel which is at a constant convergent angle of 7.5°, 5°, or 2.5°, a Stoke's number St of 100, 10, 1, 0.1, 0.01, or 0 and six different electrostatic image charge parameters (Q) ranging from 100, 10, 1, 0.1, 0.01, to 0, respectively. The channel exit plane is located at an area that is 20% of the inlet area.

The lengths of the channel L are given in all figure titles. Theorectically all particles would have deposited on the wall at the convergent point where the upper wall and the lower wall meet together. Calculations were not carried out beyond L, but dashed lines were used to extend each curve to the point of channel convergent.

Figures 5.6 to 5.11 and Tables 5.5 to 5.10 are results at constant half convergent channel angle of 7.5 degrees and St of 100, 10, 1, 0.1, 0.01, and 0. Figures 5.12 to 5.17 and 5.24 to 5.29 together with Tables 5.11 to 5.16 and 5.17 to 5.22 are results at constant half convergent channel angle of 5 and 2.5 degrees, respectively, also for St ranges from 100 to 0. Figures 5.18 to 5.23 and 5.30 to 5.35 are just repeated plots of Figures 5.12 to 5.17 and 5.24 to 5.29, respectively, for X = 0 to X = 8 for comparison with the results from Figures 5.6 to 5.11.

It is observed that in all cases, the particle deposition increases with increasing X-displacement.

It is also observed from these figures and tables that, in general, for a fixed Stoke's number and electrostatic image charge parameter, the particle deposition is higher for larger half convergent channel angles. This is true for (1) all Q when St = 100, (2) Q = 10 or less when St = 10, and (3) Q = 1 or less when St = 1

or less. However, for the cases when (1) St = 10 and Q = 100, and (2) St = 1 or less and Q = 100 as well as 10, the particle deposition is less for larger half convergent channel angles.

All of these cases are the result of the combination of forces considered. In general increase in convergent angle increases the axial image force (force in X-direction) and also increases the transverse (or Y-direction) viscous force which forces particles away from the wall. For example, when St = 10 and Q = 100, because of an increase in X component of acceleration for a smaller particle (i.e. smaller St), the particle may travel further downstream before it deposits on the wall. Results and effects of these combination of forces on particle depositions will be discussed more in the following sections.

5.5 Deposition due to Viscous and Electrostatic Image Forces

In this section the results on particle depositions due to viscous and electrostatic image forces alone will be discussed. This means that the Stoke's number is set to zero. Figures 5.11, 5.17 and 5.23, as well as 5.29 and 5.35 together with Tables 5.10, 5.16, and 5.22, show such results for half convergent channel angles of 7.5, 5 and 2.5 degrees, respectively.

It is revealed from these figures and tables that, at a constant convergent angle, the fraction of deposition of particle is increased with increasing electrostatic image charge Q. The deposition reaches its 80% within X = 1.5 (i.e. 1.5 times the half channel inlet width of its X direction displacement) for Q = 100 and 10 regardless of the convergent angles. For Q equals unity, the deposition also reaches its 50% within X = 1.7 and then increases moderately with increasing axial displacement. For Q = 0.1 and 0.01, 14% and 6%, respectively, are obtained within X = 0.25 but only 36% and 14% more depositions are obtained up to the end of the channel (80% of the total channel length). It is also obvious that with larger image force, the particle will be attracted to the channel wall easily.

It is observed from these figures and tables that no deposition is obtained in the channel for various convergent angles when there is no image force (Q = 0). This is true since no gravitational force is considered in this analysis.

The special case when the convergent angle equals zero, i.e. a horizontal channel of constant area, is also studied and the results are shown in Figure 5.36 and Table 5.23. Again, the fraction of deposition is increased with increasing electrostatic image charge Q. At Q = 100 and 10, particles (θ = 0°, St = 0) are so much attracted to the channel wall that essentially all particles are deposited on

the wall at X = 0.059 and 0.59, respectively. When Q is equal to unity, all particles deposit on the wall at X = 5.877. However less than 90% and 50% deposition in the parallel-plate channel exit (X = 12.5) are observed for Q = 0.1 and 0.01, respectively. No particle deposition is obtained when there is no image charge (Q = 0).

These results are also compared with that given by Yu and Chandra's {32} as given in Figure 5.37 where the abscissa is QX and is 4 times the parameter QL used by Yu and Chandra. It is revealed that all the deposition curves in this study fall into one single curve and agree with that obtained by Yu and Chandra's. However, small discrepancies up to a maximum of about 2% are observed and the reasons may be arised from (1) different numerical method are used to solve the flow problem which results in different accuracies, and (2) figure in Yu's paper was directly interpreted to obtain the data for deposition calculations.

5.6 Deposition due to Viscous and Inertia Forces

The results on particle depositions due to viscous and inertia forces alone can be seen on all the figures and tables with Q = 0.

It is noticed from these results that at a fixed convergent angle, the particle deposition is increased with

increasing inertia forces, i.e. higher St values. Since the viscous force actually pushes the particle towards the channel centerline, a larger particle will have a tendency to move straight line and results in hitting the convergent wall. Thus in a convergent channel, higher inertia force will result in a higher deposition.

At half convergent channel angle of 7.5 degrees and for St = 100 and 10, the fraction of deposition increases monotonically with the particle X-displacement from zero to about 77% and 71%, respectively, at the channel exit (L = 6.07). When St = 1 and 0.1, only 40% and 6% of the particle are deposited on the wall at the channel exit. At lower St, i.e. St = 0.01, the inertia forces are so small that no particle deposition is observed. It is therefore felt that for St < 0.01, the inertia effect may be neglected.

At half convergent channel angle of 5 degrees, a similar trend as that of 7.5 degrees is observed except that at St = 1, 30% deposition in the channel of L = 9.14 is obtained (40% in 7.5 degrees).

For the cases of 2.5 degrees convergent angles and at St = 100, again, the fraction of deposition of the particle is increased monotonically with increasing X-displacement and reaches about 75% at its channel exit (L = 18.3). Only

about 62% and 20% depositions are obtained at the channel exit for St = 10 and 1, respectively. For St < 0.1, no deposition is observed.

5.7 Deposition due to Viscous, Inertia, and Electrostatic Image Forces

The objective of this section is to discuss the results on the particle deposition due to all three forces --- viscous, inertia, and electrostatic image charge forces. The results are shown in Figures 5.6 to 5.30 and Tables 5.5 to 5.22.

It should be again noted here that the forces displayed in Tables 5.1 to 5.3 are summation forces of the viscous, inertia, as well as electrostatic image charge acting on the particle; while Table 5.4 contains the electrostatic image force only.

It is observed from the results that, at a constant convergent channel angle and a fixed Stoke's number, the particle depositions are increased with increasing Q. At high St values, i.e. St = 100 as shown in Figure 5.6 and 5.12, because of the large inertia force particles tend to move straight forward and hit the wall thus result in a higher deposition at small Q (< 0.1). However at larger electrostatic image charge, i.e. Q > 1, the particle will be

attracted and moved to the channel wall even faster and results in a even higher fraction of deposition. In such cases, the deposition increases very rapidly near the inlet of the channel.

At small St values and with small or even no Q, that is, the inertia as well as the image forces acting on the particle are both small, the particle deposition will be decreased, and the deposition curves are relatively flat along the axial distance of the channel. On the contrary, if Q is high in this case, the image force dominats and will pull the particle further towards the channel wall, resulting in deposition curves with steeper slope near the inlet of the channel.

For example, as shown in Figures 5.6 to 5.11 at half convergent channel angle of 7.5 degrees and for St = 100, the particle depositions are increased almost linearly with the X-displacement at Q = 0.01 and 0 and have a terminal deposition of about 77% at the channel exit. As St decreases, the particle terminal depositions at Q = 0.01 and 0 also decrease and eventually reach the rates of 20% and 2%, respectively, for both St = 0.01 and 0. On the other hand, the particle deposition for Q = 100 reaches 90% at X = 4.967 for St = 100. As St decreases from 10, 1, 0.1, down to 0.01, the particle deposition for Q = 100 reaches 90% even at X = 2.762, 1.719, 1.383, and 1.283, respectively.

This trend of decreasing St results in (1) decreasing the particle deposition for small Q (0.1 and lower), and (2) increasing the particle deposition for large Q (1 and higher) is also observed for constant convergent angles of 5 and 2.5 degrees.

It should be noted that if all particles were to move in a horizontal direction as was in the given inlet condition, 80% deposition would have taken place at the exit of the channel. That is to say that if the viscous effects were to be neglected, 80% deposition would have taken place at the exit of the channel without any image force effects. In Figures 5.6, 5.12, and 5.24, the deposition at the channel exit , where L = 6.07, 9.14, and 18.32, for convergent angles of 7.5, 5, and 2.5 degrees, respectively, and St = 100 are only 77%. Clearly the viscous force exerted on the particle in the Y-direction does force the particle to move toward the centerline and thus reduces the fraction of deposition.

As discussed in Section 5.4, for a fixed value of St and Q, the general trend of increasing the convergent channel angle will result in increasing the particle deposition does not applied to cases when (1) St = 10 and Q = 100, and (2) St = 1 or less and Q = 100 or 10 up to a length of the convergent channel of about 3 to 4 times the half channel inlet width. This is because the viscous

effect on the particle close to the channel wall is greater in the negative Y direction for higher convergent angles. As a result, part of the inertia and/or the electrostatic image forces will be balanced out, causing a comparatively lower deposition when the convergent angle is higher.

This phenomenon may also be demonstated by the particle velocity distributions shown in Figures 5.4 to 5.5 and the numerical values listed in Tables 5.1 to 5.3. First, it is noticed in Table 5.1 that a particle starting at Y = 0.9 has both the X and Y summation forces increasing with increasing time until Y = 0.951. Thereafter, the Y force starts decreasing, and so does the X force when Y = 0.978. In Tables 5.2, for a particle starting at Y = 0.5, the Y and X force starts decreasing at Y = 0.533 and 0.687, respectively. These are due to the fact that the vertical velocity V = -U * $\bar{Y}$ * tanθ for a uniform flow and therefore the vertical viscous force increases with increasing Y.

In Table 5.3 (Yo = 0.1, θ = 7.5°, L = 6.07, Q = 10, St = 10), the X force increases with time until Y = 0.176 and X = 1.615, but the Y force decreases once the particle movement begins. Notice that the particle starts at Y = 0.1 in this case is very far away from the channel wall as shown in Figure 5.5. Both the viscous and the image forces are small here (compare with that close to the channel wall), and thus the negative Y component viscous force dominates.

6. CONCLUSIONS

The characteristics of a two-phase fluid-solid particle flow in convergent channels are investigated and the conclusions reached are summarized as follows:

(1) The image force equations for convergent channels are derived and given as equation (3-8) in Chapter 3. For zero convergent angle, the equations reduce to that of the parallel-plate channel and is identical to that given by Yu and Chandra {32}.

(2) From the continuity requirement for the fluid phase, the dimensionless fluid velocity U = 1 at X = 0. At X > 0, the fluid velocity components are $U = 1/(1 - X \tan\theta)$, and $V = -U * \bar{Y} * \tan\theta$, respectively.

(3) It is revealed from the results that the closer the initial particle position is to the channel wall, the faster the particle will be attracted to the channel wall due to image forces and move horizontally to the convergent wall due to inertia effects of the particle.

(4) Since no gravitational force is considered in this analysis, a particle starting at a channel centerline position will move on horizontally because there is no viscous or image forces to change its motion.

(5) For all convergent angles investigated, it is observed that the image forces, induced by the particle images confined on an Image Circle, are much greater in the Y direction than the X direction for all particles located at $Y > 0.3$.

(6) Although the particle deposition increases with increasing X-displacement, at a constant St and Q, the particle deposition is, in general, higher for larger convergent angles.

(7) When $St = 0$ and at a constant convergent angle, the particle deposition increases with increasing Q. However, no deposition is obtained when $Q = 0$.

(8) When $Q = 0$ and at a fixed convergent angle, the particle deposition increases with increasing St. Furthermore, it is shown that for all convergent angles considered, no particle deposition is

observed for St < 0.01. It is thus believed that the inertia effect may be neglected for St < 0.01.

(9) Results on particle deposition due to viscous, inertia, and image charge forces revealed that, at a constant convergent angle as well as a fixed St, particle deposition increases with increasing Q. For high Q (Q => 10) and moderate St (10 > St => 0.01) values, particles are quickly attracted and moved to the channel wall which results in more than 0.8 fraction of deposition near the entrance of the channel (X < 2) as shown in Figure 5.8. When both St and Q are small (St < 1 and Q < 0.01), particle deposition increased from 0 to about 10% close to the channel entrance (i.e. X < 0.3) and then remained relatively constant along the axial distance of the convergent channel.

(10) The special case of a parallel-plate channel, i.e. convergent angle = 0°, when St = 0 is also studied. Results agree with that of Yu and Chandra's {32} on flow in a horizontal channel of constant area.

7. RECOMMENDATIONS

The deposition of solid particles in a convergent channel due to inertia, viscous, and image charge effects was investigated under uniform steady flow in an incompressible fluid. Parabolic as well as other type of flows may be added for further understanding.

Since gravity is of great significance in various problems, the gravitational force parameter may be included for further studies. In such case, the whole channel has to be studied due to non-symmetric flow.

When solid particles are considerably small, the diffusion force effect may be significant and therefore, may be involved in the future analysis. The individual of these two forces --- gravity and diffusion, as well as their combined effect may be investigated to check their influences on solid particles.

Even for hermetic centrifugal chillers, dirts or particles may still exit within the circulation system. The vaneless diffuser as well as the diffusion system of a centrifugal compressor consist of diffuser type flow paths. Thus, all the investigations performed for a convergent channel may be modified to that of a divergent channel.

In this investigation, the situation of two phase flow in a convergent channel was considered whereby all configurations were assumed horizontal. However, in actual practice, i.e. a Venturi tube, the radial vaned diffuser of a centrifugal compressor etc. are all vertically oriented. Attempts should therefore be made to extend this study for any inclination of the channel with the direction of gravity.

Although many studies have been concerned with two-phase flow, a matter of further interest would be to investigate systems concerned with three, four, or more phase flow for cases such as a centrifugal compressor whereby, refrigerant, air, oil, and solid particles would constitute the four phases.

With the advent of the human material civilization and the space age, increased problems of air, water, and/or near sea pollution as well as interest of space shuttle external tank nozzle exhausts of solid-liquid propellants lead further analysis to even more multi-phase flow situations.

REFERENCES

1. Kalinske, A. A. and Van Driest, E. R., Proceedings of Fifth International Congress on Applied Mechanics, Mechanics, Cambridge, Mass., 1938, p. 416.

2. Longwell, J. P. and Weiss, M. A., "Mixing and Distribution of Liquids in High Velocity Air Streams", Ind. Eng. Chem., Vol. 45, 1953, p. 667.

3. Hesketh, H. E., Fine Particles in Gaseous Media, Michigan, Ann Arbor Science Publishers Inc., 1977.

4. Stober, W., "A Note on the Aerodynamic Diameter and Mobility of Nonspherical Aerosol Particles", J. of Aerosol Sci., Vol. 2, 1971, pp. 453-456.

5. Friedlander S. K., Smoke, Dust and Haze, Fundamentals of Aerosol Behavior, John Wiley and Sons, Inc., 1977, p. 6.

6. Stukel, J. J. and Soo, S. L., "Turbulent Flow of a Suspension into a Channel", Powder Technology, Vol. 2, 1968/1969, pp. 278-289.

7. Friedlander, S. K. and Johnstone, H. F., "Deposition of Suspended Particles from Turbulent Gas Streams", Ind. and Eng. Chem., Vol. 49, No. 7, 1957, pp. 1151-1156.

8. Soo, S. L. and Rodgers, L. W., "Further Studies on the Electro-Aerodynamic Precipitator", Powder Technology, Vol. 5, 1971, pp. 43-50.

9. Corn, M., "The Adhesion of Solid Particles to Solid Surfaces", J. Air Pollution Control Assoc., Vol. 11(1), 1961, pp. 523-528 and Vol. 11(12), 1961, pp. 566-575, 584.

10. Yang, Y. C. and Peddieson, J., Jr., "Some Parallel Flows of Solid-Fluid Suspension", - presented at Ninth Annual Meeting of Society of Engineering Science, 1971.

11. Thomas, D. G., "Transport Characteristics of Suspensions: II, Minimum Transport Velocity for Flocculated Suspensions in Horizontal Pipes", A.I.Ch.E. Journal, Vol. 7, No. 3, 1961, pp. 423-430.

12. Soo, S. L. and Tung, S. K., "Pipe Flow of Suspensions in Turbulent Fluid, Electrostatic and Gravity Effects", Appl. Sci. Res., Vol. 24, 1971, pp. 83-97.

13. Soo, S. L. and Tung, S. K., "Deposition and Entrainment in Pipe Flow of a Suspension", Powder Technology, Vol. 6, 1972, pp. 283-294.

14. Robinson, A., "On the Motion of Small Particles in a Potential Field of Flow", Comm. Pure Appl. Math., Vol. 9, 1956, p.69.

15. Van Deemter, J. J. and Van Der Laan, E. T., "Momentum and Energy Balances for Dispersed Two -Phase Flow", Appl. Sci. Res., A10, 1961, p. 102.

16. Hinze, J. O., "Momentum and Mechanical-Energy Balance Equations for a Flowing Homogeneous Suspension with Slip between the Two Phases", Appl. Sci. Res., A11, 1962, p. 33.

17. Marble, F. E., "Dynamics of a Gas Containing Small Solid Particles", Proc. 5th AGARD Colloq., Combust. Propul., Pergamon Press, 1963, p. 175.

18. Murray, J. D., "On the Mathematics of Fluidization", J. Fluid Mech., Vol. 21, 1965, p. 465, Vol. 22, 1965, p. 57.

19. Pigford, R. L. and Baron, T., "Hydrodynamic Stability of a Fluidized Bed", Ind. Eng. Chem. Fundam., Vol. 4, 1965, p. 81.

20. Anderson, T. B. and Jackson, R., "A Fluid Mechanical Description of Fluidized Beds", Ind. Eng. Chem. Fundam., Vol 6, 1967, p.527.

21. Soo, S. L., Fluid Dynamics of Multiphase Systems, Blaisdell Publishing Co., 1967, Chapters 6 and 8.

22. Truesdell, C. and Toupin, R., "The Classical Field Theories", Handbuch der Physic III/1 (S. Flugge, ed.), 1960, p. 469.

23. Truesdell, C. and Noll, W., "The Nonlinear Field Theories of Mechanics", Handbuch der Physic III/3 (S. Flugge, ed.), 1965, p. 537.

24. Marble, F. E., "Dynamics of Dusty Gases", Annual Review of Fluid Mechanics, Vol. 3 (M. Van Dyke, W. Vincenti and J. Wehausen, eds), 1970, p. 397.

25. Peddieson, J., Jr., "Dust Collection at Moderate Void Fractions",-Proceedings of the Annual Technical Meeting of the Institute of Environmental Sciences, 1973.

26. Comparin, R. A., Moses, H. L. and Powell, E. E., III, "Contamination Effects in a Laminar Proportional Amplifier", Fluidics, State of-the -art Symposium, Sept. 30-Oct. 3, Vol. 1, 1974, pp. 247-259, U. S. Army (H.D.L.) Material Command.

27. Eldighidy, S. M., Chen, R. Y., and Comparin, R. A., "Deposition of Suspensions in the Entrance of a Channel", Presented at ASME Winter Annual Meeting, New York, 1976. 76-WA/F 1 Cs-13, J. of Fluids Engrg., Trans. ASME Vol. 99, 6/1977, pp. 365-370.

28. Ingham, D. B., "Diffusion and Sedimentation of Aerosol Particles from Poiseuille Flow in Rectangular Tubes," J. of Aerosol Sci., Vol. 7, 1976, pp. 13-20.

29. Ingham, D. B., "Simultaneous Diffusion and Sedimentation of Aerosol Particles in Rectangular Tubes", J. of Aerosol Sci., Vol. 7, 1976, pp.373-380.

30. Taulbee, D. B. and Yu, C. P., "Simultaneous Diffusion and Sedimentation of Aerosols in Channel Flows", J. of Aerosol Sci., Vol. 6, 1975, pp. 433-438.

31. Wang, C. S., "Gravitational Deposition of Particles from Laminar Flows in Onclined Channels", J. of Aerosol Science, Vol. 6, 1975, pp. 191-204.

32. Yu, C. P. and Chandra, K., "Deposition of Charged Particles from Laminar Flows in Rectangular and Cylindrical Channels by Image Force", J. Aerosol Sci., Vol. 9, 1978, pp. 175-180.

33. Yu, C. P., "Precipitation of Unipolarly Charged Particles in Cylindrical and Spherical Vessels", J. of Aerosol Sci., Vol. 8, 1977, pp. 237-241.

34. Chen, R. Y., "Deposition of Aerosol Particles in a Channel due to Diffusion and Electric Charge", J. of Aerosol Sci., Vol. 9, 1978, pp. 253-260.

35. Ingham, D. B., "Deposition of Charged Particles Near the entrance of a Cylindrical Tube", J. of Aerosol Sci., Vol. 11, 1979, pp. 47-52.

36. Chen, R. Y. and Gelber, M. W., "Deposition of Particles in a Parallel-Plate Channel due to Electrostatic Charge, Diffusion and Gravitational Effects", Powder Tech., Vol. 28, 1981, pp.229-234.

37. Chen, R. Y. and Gelber, M. W., "Deposition of Suspensions in the Entrance of a Verticle Tube", Powder Tech., Vol. 28, 1981, pp. 43-48.

38. Chen, R. Y., Pawel H. E. and Chen, W. C. "Inertia Effect on Deposition of Charged Particles in a Parallel-Plate Channel", Powder Tech., Vol. 38, No. 2, March 1983, pp. 249-253.

39. Thiagarajan V. and Yu, C. P., "Sedimentation from Charged of Aerosol Flow in Parallel-Plate and Cylindrical Channel", J. of Aerosol Sci., Vol. 10, 1978, pp. 405-410.

40. Chu, C. Y., "Deposition of Particles in Horizontal Parallel Plate Channel due to Image Charge, Inertia, Viscosity and Gravity", Master Thesis, Dept. of Mech. Eng., NJIT, New Jersey, 1983.

41. Shah, M. J., "Deposition of Charged Particles in Cylindrical Chamber under the Influence of Image, Inertia, Viscous and Gravitational Forces", Master Thesis, Dept. of Mech. Eng., NJIT, New Jersey, 1984.

42. Paris, D. T. and Hurd, F. K., Basic Electromagnetic Theory, 1969.

43. Griffiths, D. J., Introduction to Electrodynamics, Prentice-Hall, Inc., Englewood Cliffs, New Jersey, 1981.

44. Ferraro, V. C. A., Electromagnetic Theory, The Athlone Press, University of London, 1962.

45. Pich, J., "Theory of Gravitational Deposition of Particles from Laminar Flows in Channels", J. of Aerosol Sci., Vol.3, 1972, pp. 351-361.

46. Miller, D. S., Internal Flow Systems, British Hydromechanics Research Association Fluid Engineering, 1978.

47. Runge, C., "Mathematisch Annalen", Vol. 46, 1895, pp. 167-178.

48. Kutta, W., "Zeitschrift fur Math. und Phys.", Vol. 46, 1901, pp. 435-453.

49. Cheng, L. and Soo, S. L., "Charging of Dust Particles by Impart", J. of Applied Physics, Vol 41, No. 2, February 1970, pp. 585-591.

50. Cheng, L., Tung, S. K. and Soo, S. L., "Electrical Measurement of Flow Rate of Pulverized coal suspension", J. of Eng. for Power, Trans. of ASME, April 1970, pp. 135-149.

51. Torre, Edward D., and Longo, Charles V., The Electromagnetic Field, Allyn and Bacon, Inc., Boston, 1969.

APPENDIX A

APPLICATION OF THE RUNGE-KUTTA SOLUTION IN PARTICLE DEPOSITION ANALYSIS

(1) THE RUNGE-KUTTA METHOD

This method was devised by Runge {47} about the year 1894 and extended by Kutta {48} a few years later. The chief advantage of this method is that the successive increments in the functions are computed with a high degree of accuracy from a definite set of formulas, the same set of formulas being used for computing all the increments. It is particlarly suitable in case when the computation of higher derivatives is complicated. The method used in this analysis is of order four. The calculations for the first increment, for example, are exactly the same as for any other increment.

Let $$y' = f(x,y)$$
$$y(xo) = yo$$

denote any first order differential equation connecting the variables x and y, and let h denote any increment Δx in the independent variable x. Then if the initial values of the variables are xo and yo, the first increment in y is computed from the formulars

$$k1 = f(xo,yo)h,$$
$$k2 = f(xo+h/2,\ yo+k1/2)h,$$
$$k3 = f(xo+h/2,\ yo+k2/2)h,$$
$$k4 = f(xo+h,\ yo+k3)h,$$
$$\Delta y = (k1 + 2*k2 + 2*k3 + k4)/6,$$

taken in the order given. Then

$$x1 = xo + h,$$
$$y1 = yo + \Delta y.$$

The increment in y for the second interval is computed in a similar manner by means of the formulas

$$k1 = f(x1,y1)h,$$
$$k2 = f(x1+h/2,\ y1+k1/2)h,$$
$$k3 = f(x1+h/2,\ y1+k2/2)h,$$
$$k4 = f(x1+h,\ y1+k3)h,$$
$$\Delta y = (k1 + 2*k2 + 2*k3 + k4)/6,$$

and so on for the succeeding intervals.

It will be noticed that the only change in the formulas for the different intervals is in the values of x and y to be substituted. Thus, to find Δy in the nth interval, one should have to substitute x(n-1), y(n-1) in the expressions for k1, k2, etc.

This process may be described in geometric terms. At the point (xn, yn) we compute the slope k1/h and using it, then go one-half step forward and examine the slope there. Using this new slope (k2/h), we again start at (xn, yn), go one-half step forward, and again sample the slope. Using this latest slope k3/h, we again start at (xn, yn), but this time we go a full step forward where we examine the slope k4/h. The four slopes are averaged, using weights 1/6, 2/6, 2/6, 1/6, and using this average slope, we make the final step from xn, yn to x(n+1), y(n+1). However, this method has an error term proportional to h**5.

(2) APPLICATION OF THE FOURTH-ORDER RUNGE-KUTTA SOLUTION

The Runge-Kutta solution can be applied to the initial value problem of our present particle deposition analysis. First, for our simultaneous governing equations

$$x'' = f(x',x,t),$$
$$y'' = g(y',y,t)$$

we set $x' = A$, $y' = B$ and obtain the following system of simulataneous first-order equations,

$$x' = A(x,t),$$
$$y' = B(y,t),$$
$$A' = f(A,x,t), \text{ and}$$
$$B' = g(B,y,t)$$

where x and y are function of t.

Then, to integrate it, we compute the increments in x and y for the first interval by means of the formulas

$$k1 = f(xo,yo,to)\ \Delta t,$$
$$k2 = f(xo+k1/2,\ yo+l1/2,\ to+\Delta t/2)\ \Delta t,$$
$$k3 = f(xo+k2/2,\ yo+l2/2,\ to+\Delta t/2)\ \Delta t,$$
$$k4 = f(xo+k3,\ yo+l3,\ to+\Delta t)\ \Delta t,$$
$$\Delta x = (k1 + 2*k2 + 2*k3 + k4)/6,$$

and

$$l1 = g(xo,yo,to)\ \Delta t,$$
$$l2 = g(xo+k1/2,\ yo+l1/2,\ to+\Delta t/2)\ \Delta t,$$
$$l3 = g(xo+k2/2,\ yo+l2/2,\ to+\Delta t/2)\ \Delta t,$$
$$l4 = g(xo+k3,\ yo+l3,\ to+\Delta t)\ \Delta t,$$
$$\Delta y = (l1 + 2*l2 + 2*l3 + l4)/6.$$

The increments for the succeeding intervals are computed in exactly the same way except that xo, yo, to are replaced by x1, y1, t1 etc. as the computation proceed, until xn, yn, tn are achieved.

APPENDIX B

DIMENSIONLESS QUANTITIES AND PARAMETERS

PHYSICAL MEANING AND ORDER OF MAGNITUDE

(1) DIMENSIONLESS QUANTITIES AND PARAMETERS

$$H = \frac{h}{ho} = 1 - X \tan\theta$$

$$T = \frac{t\ uo}{ho}$$

$$X = \frac{x}{ho}$$

$$Y = \frac{y}{ho}$$

$$\bar{Y} = \frac{y}{h} = \frac{Y}{1 - X \tan\theta} = \frac{Y}{H}$$

$$U = \frac{u}{uo}$$

$$V = \frac{v}{uo}$$

$$Up = \frac{up}{uo}$$

$$Vp = \frac{vp}{uo}$$

$$Q = \frac{q^2}{4\pi \epsilon o \; ho^2 \; f \; uo}$$

$$St = \frac{m \; uo}{ho \; f}$$

$$Qn = \frac{qn}{ho}$$

$$QnX = \frac{qnx}{ho}$$

$$QnY = \frac{qny}{ho}$$

$$Qn' = \frac{qn'}{ho}$$

$$Qn'X = \frac{qn'x}{ho}$$

$$Qn'Y = \frac{qn'y}{ho}$$

$$Fx' = \sum_{n=1}^{N} \left\{ \frac{\sin \theta n}{QnX^2 + QnY^2} + \frac{\sin \theta n'}{Qn'X^2 + Qn'Y^2} \right\}$$

$$Fy' = \sum_{n=1}^{N} \left\{ \frac{\cos\theta n}{QnX^2 + QnY^2} - \frac{\cos\theta n'}{Qn'X^2 + Qn'Y^2} \right\}$$

(2) PHYSICAL MEANING

$$Q = \frac{q^2}{4\pi\epsilon_o\, ho^2\, f\, uo}$$ Electrostatic Charge Parameter

$$= \frac{q^2}{4\pi\epsilon_o\, ho^2} * \frac{1}{f\, uo}$$

which is the ratio of the electrostatic charge of the solid particle to the viscous force.

$$St = \frac{m\, uo}{ho\, f}$$ Stoke's Number

which is an inertia parameter and sometimes can be expressed as the ratio of stopping distance of a particle to the distance a particle must travel to be captured.(= 2Xs/D)

$$Re = \frac{uo\, ho}{\nu}$$ Reynolds Number

which is the ratio of inertia forces to viscous forces and based on half channel width.

$$H = \frac{h}{ho} = 1 - X \tan\theta$$

which is the ratio of convergent channel width to the entrance value and is also equal to the ratio of the local half channel width h to the entrance half channel width ho.

$$Qn = \frac{qn}{ho}$$

which is the ratio of distance between the point charge and the nth image above the upper convergent channel wall to the channel entrance width; QnX and QnY are the X and Y components of Qn, respectively.

$$Qn' = \frac{qn'}{ho}$$

which is the ratio of distance between the point charge and the n'th image below the lower convergent channel wall to the channel entrance width; Qn'X and Qn'Y are the X and Y components of Qn', respectively.

(3) ORDER OF MAGNITUDE

Most of the parameters and dimensionless quantities can be calculated, while the others can be estimated and taken from previous experimental results (49,50).

For an actual fluidic device, a half entrance channel width can be of ho = 0.05 cm. Assume ho = 2 cm as was used in {38}, and with air as a fluid phase with a pressure of 1 atm. and a temperature of 20 degrees C. Based on the half entrance channel width and assuming a uniform inlet velocity of uo = 30 cm/sec, the Reynolds number can be estimated to be,

$$Re = 400.$$

Considering solid particle of diameters

$2a = 0.33$ micrometer,
$2a = 2$ micrometer,
$2a = 6$ micrometer,
$2a = 10$ micrometer, and
$2a = 20$ micrometer.

As is given in {35}, consider a particle concentration of 1.0E06 particles per cubic centimeter and a charge electron density of 1 electron per 1.18E-10 square centimeter, i.e. 29 electrons on a 0.33 micrometer particle.

Thus, for a $2a = 10$ micrometer diameter size solid particle, the mass can be calculated as

$$m(10 \text{ micrometer}) = 5.2589 * 10^{-10} \text{ gram}$$

so that its electrostatic charge per unit mass is

$$\frac{q}{m} = 8.1 * 10^{-6} \text{ Coulomb/gram}$$

and is of the same order of magnitude as those measured by Cheng and Soo {49}.

With the Stoke's drag force estimated to be

$$f = 6\pi\mu a$$

$$= 3.43816 * 10^{-10} \text{ Newton-Second}$$

and free space permittivity

$$\epsilon_o = 8.85434 * 10^{-12} \text{ Coulomb}^2/\text{Newton-Meter}^2$$

we have

$$Q = \frac{q^2}{4\pi\epsilon_o \, ho^2 \, f \, uo} = 7.90586 * 10^{-7}$$

$$St = \frac{m \, uo}{ho \, f} = 4.589 * 10^{-3} \quad .$$

A Fortran computer program for these particle charge parameters calculation is written and displayed in Appendix C for reference.

APPENDIX C

COMPUTER PROGRAM FOR PARTICLE CHARGE PARAMETERS CALCULATION

```
C.....................................................
C
C     PROGRAM TO CALCULATE THE PARTICLE CHARGE PARAMETERS
C     BY  K. W. HUI
C.....................................................
      DIMENSION DIA(20),AMASS(20),Q(20),STOKE(20)
C
C     NO : NO OF PARTICLES TO BE CALCULATED
C
      NO=18
      DO 5 J=1,NO
      DIA(J)=0.
C      AMASS: MASS OF SOLID PARTICLES (KG)
      AMASS(J)=0.
5     CONTINUE
C      DIA: DIAMETER OF SOLID PARTICLES (METER)
      DIA(1)=3.3E-07
      DIA(2)=2.E-06
      DIA(3)=6.E-06
      DIA(4)=1.E-05
      DIA(5)=2.E-05
      DIA(6)=5.E-05
      DIA(7)=7.E-05
      DIA(8)=8.E-05
      DIA(9)=8.1E-05
      DIA(10)=8.2E-05
      DIA(11)=8.3E-05
      DIA(12)=8.4E-05
      DIA(13)=1.0E-04
      DIA(14)=1.6E-04
      DIA(15)=1.605E-04
      DIA(16)=1.606E-04
      DIA(17)=1.607E-04
      DIA(18)=1.608E-04
C     AMASS(1)=1.8899E-17
C     AMASS(2)=4.2071E-15
C     AMASS(3)=1.1359E-13
C     AMASS(4)=5.2589E-13
C     AMASS(5)=4.2071E-12
      PI=3.1415926536
C      U0: INLET VELOCITY (METER/SEC)
      U0=.3
C      H(OR HO): HALF CHANNEL WIDTH AT INLET (METER)
```

```
      H=.02
C     EPSLON: FREE SPACE PERMITTIVITY
C           {COULOMB**2/(NEWTON*METER**2)}
      EPSLON=8.854E-12
C     AMU: DYNAMIC VISCOSITY OF AIR {(NEWTON*SEC)/METER**2}
      AMU=1.824E-05
C     RHO: CHARGE PER UNIT MASS {COULOMB/KG}
      RHO1=8.1E-03
C     RHO=RHO1
C      TRY A DOUBLE CHARGE DENSITY PARTICLE CASE
      RHO=RHO1*RHO1
C
C      29 ELECTRONS ON A 0.33 {MICROMETER} PARTICLE EQUALS
C      1  ELECTRON PER 1.18E-14 {METER**2}
C
      AMASS(4)=PI*DIA(4)**2*1.6E-19/(RHO*1.18E-14)
C
      DO 10 I=1,NO
      IF(I.EQ.4) GO TO 9
      AMASS(I)=AMASS(4)*(DIA(I)/DIA(4))**3
9     CHARGE=AMASS(I)*RHO
      DRAG=3.*PI*AMU*DIA(I)
      Q4PI=CHARGE*CHARGE/(4.*PI*EPSLON)
      Q(I)=Q4PI/(H*H*DRAG*U0)
      STOKE(I)=AMASS(I)*U0/(H*DRAG)
10    CONTINUE
C
C     WRITE(6,20)
20    FORMAT(/2X,'DIA(METER)  MASS(KG)     Q     STOKES NO.'/)
      WRITE(6,30)
30    FORMAT(/2X,'DIA(METER)  MASS(KG)    Q*Q    STOKES NO.'/)
C
      DO 50 I=1,NO
50    WRITE(6,60) DIA(I),AMASS(I),Q(I),STOKE(I)
60    FORMAT(2X,6E13.6)
      STOP
      END
```

APPENDIX D

COMPUTER PROGRAM FOR PARTICLE FLOW CHARACTERISTIC ANALYSIS

```
C.....................................................
C
C       PROGRAM FOR CALCULATING FLOW CHARACTERISTIC OF
C       A CHARGED PARTICLE ALONG A CONVERGING CHANNEL
C.....................................................
C
      COMMON G,Q,Q1,TIME,RAD
      COMMON N,NO,NCHAN
      DIMENSION XX(200),YY(200),ZZ(200),AYY(200),PY(200)
      DIMENSION TT(200),INN(200),DEPO(200)
      DIMENSION UPAR(200),VPAR(200),WALL(200)
      DIMENSION ACX(200),ACY(200),FOX(200),FOY(200)
      DIMENSION QX(100),QY(100),QXP(100),QYP(100)
      DIMENSION THE(100),THEP(100),HQX(100),HQXP(100)
C
C.....................................................
C
C          INPUT DATA
C
C          THETA: CONVERGENT ANGLE (<= 7.5 DEGREE)
C          N    : FLOW TYPE (UNIFORM FLOW)
C          TIME : PARTICLE FLOW TIME STEP
C          Q    : PARTICLE CHARGE PARAMETER
C          ST   : STOKE'S NUMBER
C.....................................................
C
      NCHAN=0
      THETA=0.0
      N=0
      G=0.0
      Q=1.0
      ST=0.00
C
C          DEGREE TO RADIAN
C
      IF(THETA.EQ.0.) GO TO 980
      RAD=THETA*3.14159/180.0
      RAD2=RAD*2.
      XMAX=1./TAN(RAD)
      XMAX2=XMAX*2.
      XMAX8=XMAX*0.8
C
C          CALCULATION OF NO. OF IMAGE PAIRS
C
```

```
      VALUE=180.0/(2.0*THETA)
C
C          CHECK IF "VALUE" IS AN INTEGER AND MAKE
C          ADJUSTMENT ON "NO"
C
      NO=IFIX(VALUE)
      VALUE1=FLOAT(NO)
      IF((VALUE-VALUE1).NE.0.) NO=NO+1
C
      GO TO 981
C980   XMAX=1249.9875
980   XMAX=12.5
      XMAX2=XMAX*2.
      XMAX8=XMAX*0.8
      RAD=0.0
      RAD2=RAD*2.
      NO=9999
981   CONTINUE
C
      NTOT=NO
      IF(THETA .EQ. 0. .AND. NO .GT. 7) NTOT=7
      S2T=SIN(RAD2)
      S2T2=S2T*S2T
      CT2=COS(RAD)*COS(RAD)
C
      WRITE(9,110) G,ST,THETA,XMAX8
110   FORMAT(////1X,'UNIFORM FLOW IN CONVERGENT CHANNEL:'/
     1'     G=',E12.5,2X,'ST=',E12.5,2X,/
     23X,' THETA=',F8.2,2X,'MAX X=',F8.4////)
C
C       JQTO : TOTAL NO. OF DIFFERENT CHARGE VALUE Q
C
      JQTO=6
      WRITE(10,*) XMAX8,JQTO,THETA
      DO 3000 JQ1=1,JQTO
      DO 696 K=1,200
      XX(K)=0.
      YY(K)=0.
      ZZ(K)=0.
      AYY(K)=0.
      PY(K)=0.
      TT(K)=0.
      INN(K)=0.
      DEPO(K)=0.
      UPAR(K)=0.
      VPAR(K)=0.
      WALL(K)=0.
      ACX(K)=0.
      ACY(K)=0.
      FOX(K)=0.
      FOY(K)=0.
696   CONTINUE
C
```

```
      GO TO (701,702,703,704,705,706) JQ1
701   Q1=100.
      GO TO 720
C
702   Q1=10.
      GO TO 720
C
703   Q1=1.0
      GO TO 720
C
704   Q1=0.10
      GO TO 720
C
705   Q1=0.01
      GO TO 720
C
706   Q1=0.00
      GO TO 720
C
720   CONTINUE
      L=0
C
C     YO : INITIAL PARTICLE POSITION
C          => -1.0 (LOWER CHANNEL WALL)
C          <=  1.0 (UPPER CHANNEL WALL)
C
      DO 1000 I=1,15
      GO TO (1,2,3,4,5,6,7,8,9,10,11,12,13,14,15), I
1     YO=0.98
      GO TO 25
C
2     YO=0.94
      GO TO 25
C
3     YO=0.90
      GO TO 25
C
4     YO=0.86
      GO TO 25
C
5     YO=0.80
      GO TO 25
C
6     YO=0.70
      GO TO 25
C
7     YO=0.60
      GO TO 25
C
8     YO=0.50
      GO TO 25
C
9     YO=0.40
```

```
      GO TO 25
C
10    YO=0.30
      GO TO 25
C
11    YO=0.20
      GO TO 25
C
12    YO=0.10
      GO TO 25
C
13    YO=0.05
      GO TO 25
C
14    YO=0.01
      GO TO 25
C
15    YO=0.001
      GO TO 25
C
C     FI=FLOAT(I)
25    YOO=YO
      IF(ST.EQ.0.) GO TO 26
      STDT=ST
      IF(ST.GT.10.) STDT=10.
C     IF(ST.LT.0.01) STDT=0.01
      DT=(1.-YO)*0.02*STDT
      IF(ST.LT.0.01) DT=0.000001
      GO TO 6226
26    DT=0.002
C26    DT=0.000001
6226  XDUM=0.
C
C.....................................................
C
C         CHECK FOR TIME STEP VALUE
C
C.....................................................
C
      IF(ABS(YO) .GT. 0.96) DT=DT/10.0
      IF(YO .LT. (-0.8)) DT=DT/4.0
      Z=1.0
      IN=0
C
C         SET UP PARTICLE INITIAL CONDITIONS AT T=0 & X=0
C
      X=0.0
      XP=X
      Y=YO
      YP=Y
      H=1.0
      YB=Y/H
C
```

```
C.....................................................
C
C         A=DX/DT : PARTICLE VELOCITY IN X-DIRECTION
C         B=DY/DT : PARTICLE VELOCITY IN Y-DIRECTION
C         AP      : PREVIOUS PARTICLE VELOCITY OF A
C         BP      : PREVIOUS PARTICLE VELOCITY OF B
C
C.....................................................
C
C         PARTICLE INITIAL VELOCITY ( A=0.0 OR =1.0)
C
      A=1.0
      YSQ=Y*Y
      AP=A
      PAP=AP
      B=0.0
      BP=B
      T=0.0
C
C         FLOW FIELD VELOCITY (ORIGINAL INLET VELOCITY)
C         FOR UNIFORM FLOW
C
      U1=1.0/H
C
C     U, V : X, Y-COMPT. OF FLOW VELOCITY
C
      U=U1
      IF(THETA.EQ.0.) GO TO 480
      V=U*YB*TAN(RAD)
      IF(YO.GT.0.) V=-V
      GO TO 481
480   V=0.
481   DADT=0.
      DBDT=0.
      FX=0.
      FY=0.
C
C.....................................................
C
C         CALCULATION OF THE COEFFICIENTS OF THE 4TH ORDER
C         RUNGE-KUTTA METHOD
C.....................................................
C
      WRITE(9,492) THETA, NO
492   FORMAT(/6X,'CONVERGENT ANGLE=',F8.4,4X,'NO. OF IMAGE
     1PAIRS=',I6/)
495   WRITE(9,496)
496   FORMAT('|   TIME',2X,'TIME STEP',2X,'   X  ',4X,
     1'   Y  ', 5X,' UP  ',4X,' VP  ',5X,'APX  ',5X,
     2'APY  ',2X,'X-FORCE', 3X,'Y-FORCE',3X,' U ',5X,
     3' V ',3X,'  H   ',2X,'X/Q1  |'/)
500   INDEX=0
      WRITE(9,497) T,DT,X,Y,A,B,DADT,DBDT,FX,FY,U,V,H,X/Q1
```

```
497   FORMAT('|',F8.4,E10.2,F8.3,F10.3,2F9.3,4F10.3,
     1F7.3,F8.3,2F7.3,' |')
C
      GO TO 2000
C
510   X1=A*DT
      Y1=B*DT
      A1=DADT*DT
      B1=DBDT*DT
C
      X=XP+0.5*X1
      Y=YP+0.5*Y1
      A=AP+0.5*A1
      B=BP+0.5*B1
C
      GO TO 2000
C
520   X2=A*DT
      Y2=B*DT
      A2=DADT*DT
      B2=DBDT*DT
C
      X=XP+0.5*X2
      Y=YP+0.5*Y2
      A=AP+0.5*A2
      B=BP+0.5*B2
C
      GO TO 2000
C
530   X3=A*DT
      Y3=B*DT
      A3=DADT*DT
      B3=DBDT*DT
C
      X=XP+0.5*X3
      Y=YP+0.5*Y3
      A=AP+0.5*A3
      B=BP+0.5*B3
C
      GO TO 2000
C
540   X4=A*DT
      Y4=B*DT
      A4=DADT*DT
      B4=DBDT*DT
C
C         SUMMING UP OF THE 4 COEFFICIENTS
C
      DX=(X1 + 2.*X2 + 2.*X3 + X4)/6.
      DY=(Y1 + 2.*Y2 + 2.*Y3 + Y4)/6.
      DA=(A1 + 2.*A2 + 2.*A3 + A4)/6.
      DB=(B1 + 2.*B2 + 2.*B3 + B4)/6.
C
```

```
      XP=XP+DX
      X=XP
      YP=YP+DY
      Y=YP
      AP=AP+DA
      A=AP
      BP=BP+DB
      B=BP
      T=T+DT
C
      GO TO 600
C
C   ALTERNATE LOOP FOR ST = 0
C   (SINCE G.E. BECOMES 1ST ORDER D.E.)
C
5100  X1=A*DT
      Y1=B*DT
C
      X=XP+0.5*X1
      Y=YP+0.5*Y1
      A=FX+U
      B=FY+V-G
C
      GO TO 2000
C
5200  X2=A*DT
      Y2=B*DT
C
      X=XP+0.5*X2
      Y=YP+0.5*Y2
      A=FX+U
      B=FY+V-G
C
      GO TO 2000
C
5300  X3=A*DT
      Y3=B*DT
C
      X=XP+0.5*X3
      Y=YP+0.5*Y3
      A=FX+U
      B=FY+V-G
C
      GO TO 2000
C
5400  X4=A*DT
      Y4=B*DT
C
C         SUMMING UP OF THE 4 COEFFICIENTS
C
      DX=(X1 + 2.*X2 + 2.*X3 + X4)/6.
      DY=(Y1 + 2.*Y2 + 2.*Y3 + Y4)/6.
C
```

```
      XP=XP+DX
      X=XP
      YP=YP+DY
      Y=YP
      A=FX+U
      B=FY+V-G
      T=T+DT
C
      GO TO 600
C
C.....................................................
C
C          FUNCTIONAL FORCES OF THE GOVERNING EQUATIONS
C
C.....................................................
C
2000  INDEX=INDEX+1
      IF(THETA.EQ.0.) GO TO 550
C
C          CONTINUITY REQUIREMENT
C          H: RATIO OF CHANNEL LOCAL AREA TO INLET AREA
C             = 1.0 - X * TAN(THETA)
C
      XTAN=X*TAN(RAD)
      GO TO 551
550   XTAN=0.
551   H=1.0-XTAN
      YB=Y/H
      U=U1/H
      IF(THETA.EQ.0.) GO TO 552
      V=U*YB*TAN(RAD)
      IF(YO.GT.0.) V=-V
      GO TO 553
552   V=0.
553   CONTINUE
C
C.....................................................
C
C          SUMMATION OF THE IMAGE FORCES
C          FX: IMAGE FORCE IN THE X-DIRECTION
C          FY: IMAGE FORCE IN THE Y-DIRECTION
C
C.....................................................
C
      FX=0.
      FY=0.
C
C     FORCE DUE TO THE FIRST PAIR IMAGES
C
      YB=Y/H
C
C      SET THE STORAGE TO ZERO
C
```

```
      DO 767 KI=1,NTOT
      QX(KI)=0.
      QY(KI)=0.
      QXP(KI)=0.
      QYP(KI)=0.
      HQX(KI)=0.
      HQXP(KI)=0.
767   CONTINUE
C
      QX(1)=S2T*H*(1.0 - YB) + X
      QY(1)=2.0*CT2*H*(1.0 - YB)
      QXP(1)=S2T*H*(1.0 + YB) + X
      QYP(1)=2.0*CT2*H*(1.0 + YB)
C
      THE(1)=ATAN(QX(1)/QY(1))
      THEP(1)=ATAN(QXP(1)/QYP(1))
      STH1=SIN(THE(1))
      CTH1=COS(THE(1))
      STHP1=SIN(THEP(1))
      CTHP1=COS(THEP(1))
      QXQY=QX(1)*QX(1) + QY(1)*QY(1)
      QXPQYP=QXP(1)*QXP(1) + QYP(1)*QYP(1)
C
      IF(THETA.NE.0.) GO TO 75
      FX=0.
      GO TO 76
75    FX=FX + STH1/QXQY + STHP1/QXPQYP
76    FY=FY + CTH1/QXQY - CTHP1/QXPQYP
C
C     SUM UP FROM THE SECOND PAIR OF IMAGES ON
C
      DO 560 J=2,NTOT
      HQX(J-1)=1.0 - QX(J-1)*TAN(RAD)
      HQXP(J-1)=1.0 - QXP(J-1)*TAN(RAD)
      HMYPQ=HQXP(J-1) - H*YB + QYP(J-1)
      HPYPQ=HQX(J-1)  + H*YB + QY(J-1)
      QX(J)=S2T*HMYPQ + QXP(J-1)
      QY(J)=2.0*CT2*HMYPQ - QYP(J-1)
      IF(J.EQ.NTOT .AND. QY(J).LT.0.) QY(J)=-QY(J)
      QXP(J)=S2T*HPYPQ + QX(J-1)
      QYP(J)=2.0*CT2*HPYPQ - QY(J-1)
C
      THE(J)=ATAN(QX(J)/QY(J))
      THEP(J)=ATAN(QXP(J)/QYP(J))
      STHJ=SIN(THE(J))
      CTHJ=COS(THE(J))
      STHPJ=SIN(THEP(J))
      CTHPJ=COS(THEP(J))
      QXQY=QX(J)*QX(J) + QY(J)*QY(J)
      QXPQYP=QXP(J)*QXP(J) + QYP(J)*QYP(J)
      IF(THETA.EQ.0.) GO TO 78
      FX=FX + STHJ/QXQY + STHPJ/QXPQYP
78    FY=FY + CTHJ/QXQY - CTHPJ/QXPQYP
```

```
CC       K=J-1
CC       K21=K*2+1
CC       XSUM1=K21*K21+YB*YB
CC       XSUM2=(K21*K21-YB*YB)**2
CC       YSUM1=K21/XSUM2
CC       FX=FX + XSUM1/XSUM2
CC       FY=FY + YSUM1
560    CONTINUE
C
C         COMPENSATION OF THE EXTRA TERMS OF THE SUMMATION
C
       IF(THETA.NE.0. .OR. NO.LE.7) GO TO 581
CC       IF(NO.LE.7) GO TO 570
       FACTOR=2.5*NO/100.0
       IF(NO.GE.100) FACTOR=2.5
       IF(THETA.EQ.0.) GO TO 567
       FX=FX + FACTOR*(STHJ/QXQY + STHPJ/QXPQYP)
567    FY=FY + FACTOR*(CTHJ/QXQY - CTHPJ/QXPQYP)
CC       FX=FX + FACTOR*XSUM1/XSUM2
CC       FY=FY + FACTOR*YSUM1
CC       IF(THETA.EQ.0.) GO TO 580
CC570    XANGLE=0.5*SIN(RAD)/COS(RAD)**2
CC       IF(NCHAN.EQ.1) XANGLE=-XANGLE
CC       YANGLE=1.0/COS(RAD)
CC       GO TO 581
CC580    XANGLE=0.
CC       YANGLE=1.
CC581    FX=FX*Q1*XANGLE/H**2
CC       FY=FY*Q1*YB*YANGLE/H**2
C
581    FX=FX*Q1
       FY=FY*Q1
       IF(ST.EQ.0.) GO TO (5100,5200,5300,5400), INDEX
       DADT=(FX+U-A)/ST
       DBDT=(FY+V-B-G)/ST
       GO TO (510,520,530,540), INDEX
C
C.....................................................
C
C          CHECK IF THE PARTICLE HAS HIT THE WALL AND MAKE
C          ADJUSTMENTS ON THE TIME STEPS
C
C.....................................................
C
600    AY=ABS(Y)
       ADY=ABS(DY)
C
C          CHECK FOR CONVERGENT OR DIVERGENT CHANNEL
C          AND MAKE ADJUSTMENTS ON CHANNEL WIDTHS
C
       XTAN=X*TAN(RAD)
CC       IF(NCHAN.EQ.1) GO TO 608
       H=1.0-XTAN
```

```
      ADJ=.996*H
      ADJST=.998*H
      GO TO 609
608   H=1.0+XTAN
      ADJ=.996*H
      ADJST=.998*H
609   IF(AY+4.*ADY .GT. ADJ) GO TO 2500
C
C         CHECK IF THE PARTICLE HAS MOVED OUTSIDE OF THE
C         CONVERGENT CHANNEL.   STOP, IF IT IS, EVEN IF
C         IT STILL DOESN'T HIT THE CHANNEL WALL
C
      IF(NCHAN.EQ.0 .AND. X.GE.XMAX8) GO TO 2500
C
610   CONTINUE
      IF(B.EQ.0.) GO TO 615
      DBB=DB/B
      GO TO 616
615   DBB=DB
616   IN=IN+1
      IF(DX.LT. 0.0001 .AND. DBB.GT.0.09) GO TO 620
      IF(ADY.LT.0.0001) DT=DT*2.0
C
620   IF(X.LT.2. .AND. DX.GT.0.01) DT=0.01/A
      IF(ADY.GT.0.0025) DT=DT*0.002/ADY
      IF(X.LT.XMAX2 .AND. DT.GT.1.0) DT=1.0
      IF(NCHAN.EQ.0 .AND. X.GE.XMAX8) GO TO 1000
      IF(AY.LT.ADJST) GO TO 500
C      END OF THIS PARTICLE MOTION, GO ONTO NEXT WITH
C      DIFFERENT INITIAL CONDITIONS
      GO TO 1000
C
2500  IF(AY.GT.ADJST) GO TO 2600
      IF(NCHAN.EQ.0 .AND. X.GE.XMAX8) GO TO 2600
      IF(X.NE.0. .AND. XDUM.GT.X) GO TO 2600
      IF(DT.GT.0.05) DT=DT-0.01
C
      XX(200)=X
      TT(200)=T
      AYY(200)=AY
      ZZ(200)=Z
      YY(200)=YO
      GO TO 610
C
2600  L=L+1
      TT(L)=T
      XX(L)=X
      YY(L)=YO
      AYY(L)=AY
      ZZ(L)=Z
C
C         "YO" CANNOT BE EXACTLY ZERO DUE TO TRUNCATING
C         ERROR USE YO.LT.0.00001 INSTEAD OF YO.EQ.0.
```

```
C
      IF(G.EQ.0.0 .AND. YO.LT.0.00001) GO TO 938
      TOTAL=((AYY(L)-ZZ(L))*TT(200)-(AYY(200)-ZZ(200))
     **TT(L))/(ZZ(200)-ZZ(L)-AYY(200)+AYY(L))
      SL=(TOTAL-TT(200))/(TT(L)-TT(200))
      IF(G.NE.0. .AND. YO.NE.0.) XX(L)=XX(200) + SL
     **(XX(L)-XX(200))
      AYY(L)=AYY(200) + SL*(AYY(L)-AYY(200))
      ZZ(L)=ZZ(200) + SL*(ZZ(L)-ZZ(200))
C
938   PY(L)=Y
      INN(L)=IN
C
C         TO STORE THE PARTICLE INFORMATIONS --- VELOCITY,
C         ACCELERATION, FORCES AND CHANNEL WALL LOCATION
C
      WALL(L)=H
      UPAR(L)=A
      VPAR(L)=B
      ACX(L)=DADT
      ACY(L)=DBDT
      FOX(L)=FX
      FOY(L)=FY
C
C         CALCULATION OF THE PARTICLE DEPOSITION
C
C         FOR UNIFORM FLOW (COUNT ON THE WHOLE CHANNEL)
      DEPO(L)=(1.+YO)
      IF(Y.GT.0.) DEPO(L)=(1.-YO)
      IF(L.EQ.1) GO TO 610
      IF(X.GE.XMAX8) GO TO 1199
      GO TO 610
1000  CONTINUE
C
C.....................................................
C
C         PRINT OUT OF OUTPUT DATA
C
C.....................................................
C
C
1199  IF(JQ1.NE.1) GO TO 1198
      WRITE(9,50)
50    FORMAT(132('-'))
      WRITE(9,57)
      WRITE(9,49)
      WRITE(9,58)
      WRITE(9,49)
49    FORMAT('|',9X,'|',120('-'),'|')
      WRITE(9,51) DEPO(1),DEPO(2),DEPO(3),DEPO(4),DEPO(5)
     1,DEPO(6), DEPO(7),DEPO(8),DEPO(9),DEPO(10),DEPO(11)
     2,DEPO(12),DEPO(13),DEPO(14),DEPO(15)
51    FORMAT('|',9X,'|',F7.3,14F8.3,' |')
```

```
      WRITE(9,50)
1198  CONTINUE
      WRITE(9,52) Q1,XX(1),XX(2),XX(3),XX(4),XX(5),XX(6),
     1XX(7),XX(8),XX(9),XX(10),XX(11),XX(12),XX(13),XX(14)
     2,XX(15)
52    FORMAT('| ',E7.1,' | ',F6.3,14F8.3,' |')
59    WRITE(9,56)
      IF(JQ1.NE.JQTO) GO TO 55
      WRITE(9,50)
C
C      GENERATE THE PLOTFILE DATA
C      (DEPOSITION RATE VS X-DISPLACEMENT)
C
55    DO 54 KPLOT=1,15
      WRITE(10,53) XX(KPLOT),DEPO(KPLOT)
53    FORMAT(1X,2(3X,F8.4))
54    CONTINUE
56    FORMAT('|',9X,'|',120X,'|')
C57    FORMAT('|Q   ',6X,'|',120X,'|')
57    FORMAT('|',9X,'|',53X,'X-DISPLACEMENT',53X,'|')
58    FORMAT('|    Q    |',49X,'FRACTION OF DEPOSITION'
     1,49X,'|')
3000  CONTINUE
      STOP
      END
```

Table 4.1

Comparison of the Infinite Terms of Image Force (n -> ∞) and the Result from the Modified Formula; Q = 0, L = 12.5, Q = 1, St = 0

n	IMAGE FORCE PARTICLE LOCATION						
	0.1	0.3	0.5	0.7	0.8	0.9	0.95
7	0.10709	0.37768	0.91533	2.73000	6.21840	24.98369	99.99118
10	0.10716	0.37787	0.91565	2.73045	6.21892	24.98425	99.99178
20	0.10720	0.37801	0.91588	2.73078	6.21929	24.98462	99.99217
50	0.10721	0.37805	0.91594	2.73086	6.21939	24.98462	99.99217
100	0.10721	0.37805	0.91594	2.73086	6.21939	24.98462	99.99217
200	0.10721	0.37805	0.91594	2.73086	6.21939	24.98462	99.99217
7*	0.10721	0.37802	0.91590	2.73080	6.21932	24.98471	99.99228

* Modified Value

Table 5.1

Particle Trajectory along a Convergent Channel; Yo = 0.9, θ = 7.5°, L = 6.07, Q = 10, St = 10

T	ΔT	X	Y	Up	Vp	Apx	Apy	Fx	Fy	U	V	H	X/Q
0.0000	0.20E-01	0.000	0.900	1.000	0.000	0.000	0.000	3.491	25.181	1.000	-0.118	1.000	0.000
0.0200	0.43E-02	0.021	0.904	1.095	0.517	5.147	26.535	51.517	265.735	1.001	-0.119	0.997	0.002
0.0286	0.29E-02	0.030	0.910	1.164	0.763	8.787	29.326	88.014	294.080	1.004	-0.120	0.996	0.003
0.0315	0.29E-02	0.034	0.912	1.193	0.851	10.158	30.742	101.750	308.347	1.004	-0.121	0.996	0.003
0.0367	0.22E-02	0.040	0.917	1.255	1.019	12.944	33.505	129.676	336.154	1.005	-0.122	0.995	0.004
0.0389	0.22E-02	0.043	0.919	1.287	1.097	14.420	34.873	144.470	349.916	1.005	-0.122	0.994	0.004
0.0429	0.18E-02	0.048	0.924	1.354	1.246	17.957	37.863	179.907	379.962	1.006	-0.123	0.994	0.005
0.0447	0.18E-02	0.051	0.926	1.389	1.315	19.862	39.270	198.390	394.107	1.007	-0.123	0.993	0.005
0.0482	0.14E-02	0.056	0.931	1.470	1.461	24.374	42.344	244.185	424.984	1.007	-0.124	0.993	0.006
0.0496	0.14E-02	0.058	0.933	1.508	1.523	26.896	43.804	269.439	439.655	1.008	-0.125	0.992	0.006
0.0525	0.14E-02	0.062	0.937	1.594	1.652	32.306	46.432	323.627	466.068	1.008	-0.125	0.992	0.006
0.0539	0.14E-02	0.064	0.940	1.644	1.719	35.528	47.689	355.890	478.704	1.008	-0.126	0.992	0.006
0.0567	0.11E-02	0.069	0.945	1.759	1.858	43.178	49.811	432.503	500.059	1.009	-0.126	0.991	0.007
0.0578	0.11E-02	0.071	0.947	1.811	1.913	47.131	50.444	472.082	506.452	1.009	-0.127	0.991	0.007
0.0600	0.11E-02	0.075	0.951	1.926	2.025	54.902	50.757	549.904	509.697	1.010	-0.128	0.990	0.008
0.0611	0.11E-02	0.077	0.954	1.991	2.080	59.130	50.379	592.248	505.974	1.010	-0.128	0.990	0.008
0.0633	0.11E-02	0.082	0.958	2.135	2.188	67.980	48.136	680.892	483.653	1.011	-0.129	0.989	0.008
0.0644	0.11E-02	0.084	0.961	2.214	2.239	72.399	46.107	725.158	463.411	1.011	-0.129	0.989	0.008
0.0666	0.87E-03	0.089	0.966	2.387	2.332	80.473	39.943	806.065	401.867	1.012	-0.130	0.988	0.009
0.0675	0.87E-03	0.091	0.968	2.459	2.363	83.437	36.275	835.779	365.231	1.012	-0.130	0.988	0.009
0.0692	0.87E-03	0.096	0.972	2.608	2.417	87.124	28.596	872.798	288.492	1.013	-0.131	0.987	0.010
0.0701	0.87E-03	0.098	0.974	2.685	2.438	88.064	24.324	882.275	245.803	1.013	-0.131	0.987	0.010
0.0718	0.87E-03	0.103	0.978	2.838	2.470	87.903	15.403	880.818	156.624	1.014	-0.132	0.986	0.010
0.0727	0.87E-03	0.105	0.980	2.913	2.479	86.796	10.974	869.821	112.346	1.014	-0.133	0.986	0.011
0.0735	0.87E-03	0.108	0.983	2.987	2.486	85.052	6.710	852.451	69.713	1.014	-0.133	0.986	0.011

Table 5.2

Particle Trajectory along a Convergent Channel; Yo = 0.5, θ = 7.5°, L = 6.07, Q = 10, St = 10

T	ΔT	X	Y	Up	Vp	Apx	Apy	Fx	Fy	U	V	H	X/Q
0.0000	0.10E+00	0.000	0.500	1.000	0.000	0.000	0.000	0.306	0.914	1.000	-0.066	1.000	0.000
0.1255	0.51E-02	0.128	0.506	1.047	0.114	0.455	0.912	4.583	9.305	1.017	-0.069	0.983	0.013
0.1562	0.51E-02	0.160	0.510	1.061	0.142	0.497	0.915	5.014	9.360	1.021	-0.070	0.979	0.016
0.1970	0.51E-02	0.204	0.517	1.083	0.180	0.557	0.918	5.628	9.425	1.027	-0.072	0.973	0.020
0.2379	0.51E-02	0.249	0.525	1.107	0.217	0.622	0.918	6.291	9.470	1.033	-0.074	0.967	0.025
0.2736	0.51E-02	0.289	0.533	1.131	0.250	0.682	0.916	6.913	9.480	1.039	-0.076	0.962	0.029
0.3145	0.51E-02	0.336	0.544	1.160	0.287	0.756	0.908	7.671	9.441	1.046	-0.078	0.956	0.034
0.3553	0.51E-02	0.384	0.557	1.193	0.324	0.834	0.892	8.473	9.325	1.053	-0.081	0.949	0.038
0.3911	0.51E-02	0.427	0.569	1.224	0.356	0.904	0.870	9.200	9.139	1.059	-0.084	0.944	0.043
0.4268	0.51E-02	0.471	0.582	1.258	0.386	0.974	0.839	9.932	8.856	1.066	-0.087	0.938	0.047
0.4626	0.51E-02	0.517	0.596	1.294	0.415	1.043	0.796	10.647	8.460	1.072	-0.090	0.932	0.052
0.4983	0.51E-02	0.564	0.612	1.332	0.443	1.106	0.741	11.313	7.940	1.080	-0.094	0.926	0.056
0.5392	0.51E-02	0.619	0.630	1.379	0.471	1.168	0.662	11.969	7.191	1.088	-0.098	0.919	0.062
0.5790	0.41E-02	0.675	0.650	1.427	0.496	1.213	0.571	12.456	6.306	1.097	-0.103	0.911	0.067
0.6116	0.41E-02	0.722	0.666	1.467	0.513	1.234	0.489	12.700	5.511	1.105	-0.107	0.905	0.072
0.6522	0.41E-02	0.783	0.687	1.517	0.530	1.240	0.382	12.798	4.461	1.114	-0.112	0.897	0.078
0.6848	0.41E-02	0.833	0.705	1.557	0.541	1.227	0.296	12.706	3.618	1.123	-0.117	0.890	0.083
0.7174	0.41E-02	0.884	0.722	1.597	0.549	1.201	0.214	12.477	2.807	1.131	-0.122	0.884	0.088
0.7458	0.41E-02	0.930	0.738	1.630	0.554	1.169	0.147	12.179	2.146	1.139	-0.126	0.878	0.093
0.7743	0.41E-02	0.977	0.754	1.663	0.557	1.130	0.086	11.810	1.544	1.147	-0.130	0.871	0.098
0.8028	0.41E-02	1.025	0.770	1.695	0.559	1.085	0.032	11.389	1.011	1.155	-0.135	0.865	0.102
0.8354	0.41E-02	1.080	0.788	1.729	0.559	1.031	-0.021	10.870	0.488	1.165	-0.141	0.858	0.108
0.8639	0.41E-02	1.130	0.804	1.758	0.558	0.982	-0.060	10.401	0.106	1.174	-0.146	0.851	0.113
0.8923	0.41E-02	1.180	0.820	1.785	0.556	0.933	-0.092	9.933	-0.211	1.183	-0.151	0.845	0.118
0.9208	0.41E-02	1.232	0.836	1.811	0.553	0.886	-0.118	9.477	-0.468	1.193	-0.156	0.838	0.123

Table 5.3

Particle Trajectory along a Convergent Channel; Yo = 0.1, $\theta = 7.5^{\circ}$, L = 6.07, Q = 10, St = 10

T	ΔT	X	Y	Up	Vp	Apx	Apy	Fx	Fy	U	V	H	X/Q
0.0000	0.18E+00	0.000	0.100	1.000	0.000	0.000	0.000	0.225	0.106	1.000	-0.013	1.000	0.000
0.3483	0.91E-02	0.363	0.106	1.098	0.036	0.344	0.100	3.483	1.049	1.050	-0.015	0.952	0.036
0.5169	0.86E-02	0.554	0.113	1.161	0.052	0.399	0.092	4.076	0.993	1.078	-0.017	0.927	0.055
0.6762	0.81E-02	0.744	0.123	1.229	0.066	0.446	0.081	4.577	0.895	1.108	-0.020	0.902	0.074
0.8268	0.77E-02	0.934	0.134	1.299	0.077	0.480	0.066	4.962	0.761	1.139	-0.023	0.877	0.093
0.9768	0.73E-02	1.134	0.146	1.373	0.086	0.504	0.049	5.238	0.598	1.175	-0.026	0.851	0.113
1.1189	0.69E-02	1.335	0.159	1.445	0.091	0.516	0.031	5.394	0.433	1.212	-0.031	0.824	0.133
1.2935	0.65E-02	1.595	0.175	1.536	0.095	0.519	0.011	5.455	0.241	1.265	-0.037	0.790	0.159
1.4149	0.63E-02	1.785	0.186	1.599	0.095	0.514	-0.001	5.431	0.127	1.306	-0.042	0.765	0.179
1.5256	0.60E-02	1.965	0.197	1.655	0.095	0.507	-0.010	5.374	0.041	1.348	-0.047	0.741	0.197
1.6278	0.60E-02	2.137	0.207	1.706	0.093	0.499	-0.017	5.301	-0.023	1.390	-0.052	0.719	0.214
1.7360	0.60E-02	2.324	0.217	1.760	0.091	0.489	-0.023	5.211	-0.075	1.439	-0.059	0.694	0.232
1.8441	0.60E-02	2.517	0.226	1.812	0.088	0.480	-0.027	5.114	-0.113	1.494	-0.066	0.669	0.252
1.9523	0.60E-02	2.716	0.236	1.864	0.085	0.471	-0.030	5.015	-0.140	1.555	-0.075	0.642	0.272
2.0604	0.60E-02	2.921	0.245	1.914	0.082	0.463	-0.033	4.917	-0.158	1.623	-0.085	0.616	0.292
2.1685	0.60E-02	3.130	0.253	1.964	0.078	0.456	-0.034	4.822	-0.170	1.699	-0.096	0.588	0.313
2.2767	0.60E-02	3.345	0.262	2.013	0.075	0.450	-0.036	4.731	-0.177	1.784	-0.110	0.560	0.335
2.3848	0.60E-02	3.565	0.270	2.061	0.071	0.447	-0.038	4.646	-0.180	1.882	-0.126	0.531	0.357
2.4930	0.60E-02	3.791	0.277	2.109	0.066	0.445	-0.039	4.566	-0.182	1.993	-0.145	0.501	0.379
2.6011	0.60E-02	4.022	0.284	2.157	0.062	0.446	-0.041	4.493	-0.182	2.121	-0.168	0.471	0.402
2.7093	0.60E-02	4.258	0.290	2.206	0.057	0.449	-0.044	4.425	-0.182	2.271	-0.197	0.439	0.426
2.8174	0.60E-02	4.499	0.296	2.255	0.053	0.456	-0.047	4.364	-0.181	2.447	-0.233	0.408	0.450
2.9256	0.60E-02	4.745	0.302	2.305	0.047	0.466	-0.051	4.310	-0.180	2.658	-0.281	0.375	0.475
3.0337	0.60E-02	4.997	0.306	2.356	0.042	0.482	-0.056	4.261	-0.178	2.915	-0.343	0.342	0.500
3.1298	0.60E-02	5.226	0.310	2.403	0.036	0.502	-0.063	4.224	-0.177	3.196	-0.417	0.312	0.523

Table 5.4

Image Charge Distribution at various Particle Vertical Positions

(a) θ = 7.5° (Total No. of Image Pairs = 12)

Y	X-Force	Y-Force	Resultant
0.1000	0.22512	0.10617	0.24890
0.2000	0.23182	0.22544	0.32336
0.3000	0.24460	0.37535	0.44802
0.4000	0.26682	0.58528	0.64323
0.5000	0.30581	0.91380	0.96361
0.6000	0.37949	1.49872	1.54602
0.7000	0.54035	2.74006	2.79283
0.8000	1.00135	6.25642	6.33604
0.8200	1.19605	7.73783	7.82972
0.8400	1.46826	9.80777	9.91706
0.8600	1.86530	12.82568	12.96061
0.8800	2.47702	17.47389	17.64857
0.9000	3.49149	25.18127	25.42218
0.9200	5.35895	39.36771	39.73077
0.9300	6.94689	51.43002	51.89708
0.9400	9.39345	70.01424	70.64154
0.9500	13.45095	100.83475	101.72792
0.9600	20.92026	157.57170	158.95439
0.9700	37.05769	280.14575	282.58594
0.9800	83.16460	630.36353	635.82568
0.9900	332.13770	2521.52490	2543.30542
0.9950	1328.05762	10086.26170	10173.31640
0.9990	33198.09770	252163.62500	254339.56200

Table 5.4 (cont.)

(b) θ = 5° (Total No. of Image Pairs = 18)

Y	X-Force	Y-Force	Resultant
0.1000	0.16597	0.10659	0.19725
0.2000	0.17044	0.22624	0.28325
0.3000	0.17896	0.37638	0.41676
0.4000	0.19375	0.58627	0.61745
0.5000	0.21966	0.91419	0.94021
0.6000	0.26854	1.49732	1.52121
0.7000	0.37511	2.73379	2.75941
0.8000	0.68022	6.23446	6.27146
0.8200	0.80904	7.70903	7.75137
0.8400	0.98913	9.76933	9.81927
0.8600	1.25175	12.77308	12.83426
0.8800	1.65637	17.39928	17.47794
0.9000	2.32737	25.07016	25.17795
0.9200	3.56251	39.18915	39.35074
0.9300	4.61276	51.19411	51.40149
0.9400	6.23088	69.68987	69.96782
0.9500	8.91443	100.36340	100.75851
0.9600	13.85455	156.82991	157.44066
0.9700	24.52728	278.81934	279.89600
0.9800	55.02124	627.36719	629.77515
0.9900	219.68710	2509.51050	2519.10791
0.9950	878.35718	10038.16020	10076.51560
0.9990	21956.32420	250961.31200	251919.93700

Table 5.4 (cont.)

(c) θ = 2.5° (Total No. of Image Pairs = 36)

Y	X-Force	Y-Force	Resultant
0.1000	0.09734	0.10699	0.14465
0.2000	0.09958	0.22701	0.24789
0.3000	0.10384	0.37744	0.39146
0.4000	0.11123	0.58745	0.59789
0.5000	0.12417	0.91518	0.92357
0.6000	0.14855	1.49739	1.50474
0.7000	0.20165	2.73111	2.73854
0.8000	0.35356	6.22260	6.23264
0.8200	0.41768	7.69313	7.70446
0.8400	0.50731	9.74770	9.76089
0.8600	0.63803	12.74306	12.75902
0.8800	0.83939	17.35599	17.37627
0.9000	1.17328	25.00516	25.03267
0.9200	1.78793	39.08395	39.12483
0.9300	2.31057	51.05475	51.10701
0.9400	3.11580	69.49780	69.56758
0.9500	4.45119	100.08385	100.18277
0.9600	6.90953	156.38919	156.54175
0.9700	12.22063	278.02637	278.29468
0.9800	27.39459	625.57910	626.17871
0.9900	109.33597	2502.34863	2504.73584
0.9950	437.09937	10009.45310	10018.99220
0.9990	10925.92970	250244.50000	250482.87500

Table 5.5

Particle Deposition along a Convergent Channel for various Charge Parameter Q; $\theta = 7.5^{\circ}$, L = 6.07, St = 100

Q	X-DISPLACEMENT FRACTION OF DEPOSITION													
	0.020	0.060	0.100	0.140	0.200	0.300	0.400	0.500	0.600	0.700	0.800	0.900	0.950	0.990	0.999
100	0.012	0.055	0.110	0.177	0.296	0.538	0.836	1.211	1.688	2.347	3.345	4.967	6.077	-----	-----
10	0.027	0.136	0.286	0.469	0.771	1.351	2.021	2.764	3.584	4.488	5.471	6.091	-----	-----	-----
1	0.070	0.322	0.600	0.898	1.340	2.110	2.904	3.714	4.822	5.405	6.425	-----	-----	-----	-----
0.1	0.125	0.432	0.730	1.038	1.500	2.310	3.103	3.920	4.735	5.394	6.231	-----	-----	-----	-----
0.01	0.135	0.442	0.750	1.058	1.520	2.310	3.113	3.909	4.652	5.547	6.229	-----	-----	-----	-----
0	0.145	0.452	0.750	1.058	1.520	2.310	3.113	3.909	4.652	5.547	6.229	-----	-----	-----	-----

Table 5.6

Particle Deposition along a Convergent Channel for various Charge Parameter Q; $\theta = 7.5^{\circ}$, L = 6.07, St = 10

Q	X-DISPLACEMENT FRACTION OF DEPOSITION													
	0.020	0.060	0.100	0.140	0.200	0.300	0.400	0.500	0.600	0.700	0.800	0.900	0.950	0.990	0.999
100	0.006	0.024	0.050	0.079	0.129	0.230	0.359	0.520	0.735	1.044	1.561	2.762	4.309	6.081	-----
10	0.012	0.055	0.111	0.178	0.296	0.542	0.849	1.239	1.740	2.448	3.522	5.240	6.122	-----	-----
1	0.027	0.136	0.287	0.469	0.781	1.411	2.151	3.011	4.096	5.076	6.081	-----	-----	-----	-----
0.1	0.070	0.322	0.610	0.928	1.420	2.302	3.241	4.213	5.157	6.048	6.104	-----	-----	-----	-----
0.01	0.125	0.432	0.760	1.088	1.600	2.504	3.452	4.412	5.335	6.091	-----	-----	-----	-----	-----
0	0.145	0.452	0.780	1.108	1.630	2.535	3.473	4.435	5.359	6.092	-----	-----	-----	-----	-----

Table 5.7

Particle Deposition along a Convergent Channel for various Charge Parameter Q; $\theta = 7.5^{o}$, L = 6.07, St = 1

Q	X-DISPLACEMENT													
	FRACTION OF DEPOSITION													
	0.020	0.060	0.100	0.140	0.200	0.300	0.400	0.500	0.600	0.700	0.800	0.900	0.950	0.990	0.999
100	0.004	0.015	0.030	0.045	0.070	0.125	0.195	0.289	0.419	0.609	0.936	1.720	2.943	6.077	-----
10	0.006	0.025	0.051	0.079	0.129	0.232	0.364	0.537	0.769	1.111	1.706	3.226	5.335	6.298	-----
1	0.011	0.055	0.111	0.182	0.310	0.591	0.989	1.579	2.622	3.753	5.507	6.109	-----	-----	-----
0.1	0.029	0.143	0.310	0.531	1.029	2.478	4.353	5.611	6.181	-----	-----	-----	-----	-----	-----
0.01	0.074	0.368	0.830	1.640	3.114	5.023	5.982	6.120	-----	-----	-----	-----	-----	-----	-----
0	0.151	0.577	1.210	2.103	3.623	5.182	6.091	-----	-----	-----	-----	-----	-----	-----	-----

Table 5.8

Particle Deposition along a Convergent Channel for various Charge Parameter Q; $\theta = 7.5^{o}$, L = 6.07, St = 0.1

Q	X-DISPLACEMENT													
	FRACTION OF DEPOSITION													
	0.020	0.060	0.100	0.140	0.200	0.300	0.400	0.500	0.600	0.700	0.800	0.900	0.950	0.990	0.999
100	0.003	0.013	0.023	0.033	0.052	0.090	0.143	0.215	0.318	0.473	0.741	1.384	2.454	6.190	-----
10	0.004	0.016	0.029	0.045	0.071	0.130	0.206	0.311	0.457	0.682	1.084	2.405	5.957	6.207	-----
1	0.006	0.026	0.051	0.083	0.141	0.277	0.491	0.899	2.172	4.231	5.782	6.130	-----	-----	-----
0.1	0.011	0.058	0.128	0.236	0.622	3.892	5.731	6.198	-----	-----	-----	-----	-----	-----	-----
0.01	0.028	0.204	2.953	5.156	6.098	-----	-----	-----	-----	-----	-----	-----	-----	-----	-----
0	2.433	6.078	-----	-----	-----	-----	-----	-----	-----	-----	-----	-----	-----	-----	-----

Table 5.9

Particle Deposition along a Conversent Channel for various Charge Parameter Q; $\theta = 7.5^{\circ}$, L = 6.07, St = 0.01

Q	X-DISPLACEMENT													
	FRACTION OF DEPOSITION													
	0.020	0.060	0.100	0.140	0.200	0.300	0.400	0.500	0.600	0.700	0.800	0.900	0.950	0.990	0.999
100	0.003	0.012	0.020	0.030	0.046	0.080	0.127	0.192	0.287	0.432	0.680	1.284	2.660	6.102	-----
10	0.003	0.013	0.022	0.033	0.054	0.097	0.159	0.249	0.379	0.595	1.062	3.591	5.570	6.202	-----
1	0.004	0.017	0.032	0.051	0.089	0.195	0.407	1.078	2.485	4.208	5.677	6.120	-----	-----	-----
0.1	0.007	0.029	0.071	0.147	0.789	4.024	5.784	6.119	-----	-----	-----	-----	-----	-----	-----
0.01	0.013	0.143	3.792	5.752	6.120	-----	-----	-----	-----	-----	-----	-----	-----	-----	-----
0	-----	-----	-----	-----	-----	-----	-----	-----	-----	-----	-----	-----	-----	-----	-----

Table 5.10

Particle Deposition along a Conversent Channel for various Charge Parameter Q; $\theta = 7.5^{\circ}$, L = 6.07, St = 0

Q	X-DISPLACEMENT													
	FRACTION OF DEPOSITION													
	0.020	0.060	0.100	0.140	0.200	0.300	0.400	0.500	0.600	0.700	0.800	0.900	0.950	0.990	0.999
100	0.003	0.021	0.043	0.065	0.102	0.178	0.265	0.384	0.547	0.759	1.174	2.786	4.646	6.147	-----
10	0.004	0.021	0.043	0.066	0.107	0.189	0.290	0.434	0.637	0.969	1.841	3.774	5.492	6.201	-----
1	0.006	0.023	0.047	0.079	0.138	0.304	0.598	1.184	2.513	4.194	5.679	6.131	-----	-----	-----
0.1	0.008	0.031	0.089	0.208	0.836	3.998	5.785	6.128	-----	-----	-----	-----	-----	-----	-----
0.01	0.009	0.190	3.775	5.735	6.130	-----	-----	-----	-----	-----	-----	-----	-----	-----	-----
0	-----	-----	-----	-----	-----	-----	-----	-----	-----	-----	-----	-----	-----	-----	-----

Table 5.11

Particle Deposition along a Convergent Channel for various Charge Parameter Q; $\theta = 5^{\circ}$, L = 9.14, St = 100

Q	X-DISPLACEMENT													
	FRACTION OF DEPOSITION													
	0.020	0.060	0.100	0.140	0.200	0.300	0.400	0.500	0.600	0.700	0.800	0.900	0.950	0.990	0.999
100	0.011	0.054	0.112	0.178	0.301	0.555	0.880	1.280	1.815	2.589	3.864	6.319	8.446	9.177	-----
10	0.029	0.151	0.315	0.529	0.891	1.631	2.506	3.543	4.748	6.132	7.702	9.149	-----	-----	-----
1	0.084	0.412	0.800	1.228	1.890	3.064	4.280	5.519	6.818	8.156	9.201	-----	-----	-----	-----
0.1	0.175	0.632	1.090	1.548	2.362	3.496	4.716	6.010	7.175	8.518	9.205	-----	-----	-----	-----
0.01	0.215	0.672	1.130	1.598	2.380	3.548	4.770	6.073	7.248	8.604	9.207	-----	-----	-----	-----
0	0.215	0.672	1.140	1.630	2.430	3.584	4.817	6.134	7.319	8.606	9.210	-----	-----	-----	-----

Table 5.12

Particle Deposition along a Convergent Channel for various Charge Parameter Q; $\theta = 5^{\circ}$, L = 9.14, St = 10

Q	X-DISPLACEMENT													
	FRACTION OF DEPOSITION													
	0.020	0.060	0.100	0.140	0.200	0.300	0.400	0.500	0.600	0.700	0.800	0.900	0.950	0.990	0.999
100	0.005	0.021	0.047	0.075	0.121	0.220	0.342	0.497	0.702	0.997	1.497	2.747	4.753	9.156	-----
10	0.011	0.054	0.112	0.179	0.305	0.560	0.888	1.306	1.874	2.708	4.138	6.813	8.924	9.248	-----
1	0.029	0.151	0.318	0.529	0.911	1.718	2.728	3.960	5.404	7.418	9.086	9.615	-----	-----	-----
0.1	0.084	0.412	0.830	1.288	2.060	3.459	4.941	6.396	7.764	9.032	9.301	-----	-----	-----	-----
0.01	0.175	0.642	1.140	1.658	2.462	3.923	5.397	6.801	8.060	9.072	9.305	-----	-----	-----	-----
0	0.215	0.692	1.200	1.752	2.573	4.026	5.496	6.917	8.193	9.099	9.330	-----	-----	-----	-----

Table 5.13

Particle Deposition along a Convergent Channel for various Charge Parameter Q; $\theta = 5^{o}$, L = 9.14, St = 1

Q	X-DISPLACEMENT													
	FRACTION OF DEPOSITION													
	0.020	0.060	0.100	0.140	0.200	0.300	0.400	0.500	0.600	0.700	0.800	0.900	0.950	0.990	0.999
100	0.003	0.013	0.024	0.037	0.062	0.109	0.171	0.252	0.364	0.530	0.809	1.482	2.626	7.808	9.242
10	0.005	0.023	0.046	0.074	0.121	0.222	0.349	0.514	0.736	1.062	1.643	3.261	6.092	10.135	-----
1	0.011	0.054	0.113	0.184	0.317	0.612	1.035	1.687	2.915	5.408	7.994	9.278	-----	-----	-----
0.1	0.028	0.150	0.348	0.611	1.239	3.852	7.034	8.794	9.240	-----	-----	-----	-----	-----	-----
0.01	0.085	0.488	1.270	2.968	6.126	8.607	9.261	-----	-----	-----	-----	-----	-----	-----	-----
0	0.241	1.057	2.917	5.424	7.589	9.308	9.182	-----	-----	-----	-----	-----	-----	-----	-----

Table 5.14

Particle Deposition along a Convergent Channel for various Charge Parameter Q; $\theta = 5^{o}$, L = 9.14, St = 0.1

Q	X-DISPLACEMENT													
	FRACTION OF DEPOSITION													
	0.020	0.060	0.100	0.140	0.200	0.300	0.400	0.500	0.600	0.700	0.800	0.900	0.950	0.990	0.999
100	0.003	0.010	0.017	0.026	0.040	0.071	0.115	0.174	0.258	0.382	0.601	1.115	1.966	7.817	9.614
10	0.003	0.013	0.025	0.038	0.062	0.112	0.180	0.273	0.403	0.598	0.944	1.962	6.369	9.442	-----
1	0.005	0.023	0.047	0.076	0.133	0.266	0.474	0.865	2.621	5.671	8.234	9.304	-----	-----	-----
0.1	0.012	0.056	0.128	0.239	0.644	5.704	8.428	9.252	-----	-----	-----	-----	-----	-----	-----
0.01	0.029	0.227	4.949	8.046	9.259	-----	-----	-----	-----	-----	-----	-----	-----	-----	-----
0	6.498	9.157	-----	-----	-----	-----	-----	-----	-----	-----	-----	-----	-----	-----	-----

Table 5.15

Particle Deposition along a Convergent Channel for various Charge Parameter Q; $\theta = 5^{\circ}$, L = 9.14, St = 0.01

Q	X-DISPLACEMENT FRACTION OF DEPOSITION													
	0.020	0.060	0.100	0.140	0.200	0.300	0.400	0.500	0.600	0.700	0.800	0.900	0.950	0.990	0.999
100	0.002	0.008	0.015	0.021	0.034	0.060	0.097	0.150	0.224	0.338	0.534	0.984	1.777	9.170	-----
10	0.002	0.010	0.017	0.027	0.042	0.079	0.130	0.206	0.315	0.491	0.841	3.649	6.813	9.192	-----
1	0.003	0.013	0.027	0.043	0.077	0.175	0.374	1.160	3.123	5.674	8.106	9.205	-----	-----	-----
0.1	0.005	0.027	0.067	0.144	1.027	5.861	8.540	9.260	-----	-----	-----	-----	-----	-----	-----
0.01	0.012	0.138	5.729	8.649	9.258	-----	-----	-----	-----	-----	-----	-----	-----	-----	-----
0	-----	-----	-----	-----	-----	-----	-----	-----	-----	-----	-----	-----	-----	-----	-----

Table 5.16

Particle Deposition along a Convergent Channel for various Charge Parameter Q; $\theta = 5^{\circ}$, L = 9.14, St = 0

Q	X-DISPLACEMENT FRACTION OF DEPOSITION													
	0.020	0.060	0.100	0.140	0.200	0.300	0.400	0.500	0.600	0.700	0.800	0.900	0.950	0.990	0.999
100	0.002	0.014	0.032	0.051	0.083	0.150	0.231	0.342	0.482	0.690	1.035	2.311	4.968	9.153	-----
10	0.003	0.015	0.033	0.053	0.088	0.161	0.267	0.402	0.611	0.903	1.555	4.136	6.680	9.282	-----
1	0.003	0.017	0.037	0.067	0.132	0.308	0.613	1.340	3.166	5.660	8.115	9.304	-----	-----	-----
0.1	0.004	0.027	0.088	0.212	1.108	5.827	8.536	9.240	-----	-----	-----	-----	-----	-----	-----
0.01	0.008	0.218	5.638	8.578	9.263	-----	-----	-----	-----	-----	-----	-----	-----	-----	-----
0	-----	-----	-----	-----	-----	-----	-----	-----	-----	-----	-----	-----	-----	-----	-----

Table 5.17

Particle Deposition along a Convergent Channel for various Charge Parameter Q; $\theta = 2.5^{\circ}$, L = 18.3, St = 100

Q	X-DISPLACEMENT FRACTION OF DEPOSITION													
	0.020	0.060	0.100	0.140	0.200	0.300	0.400	0.500	0.600	0.700	0.800	0.900	0.950	0.990	0.999
100	0.011	0.053	0.109	0.179	0.308	0.572	0.911	1.342	1.933	2.816	4.427	8.447	13.273	18.329	-----
10	0.028	0.159	0.348	0.599	1.051	2.021	3.296	4.914	6.990	9.643	13.056	17.428	18.330	-----	-----
1	0.099	0.552	1.190	1.928	3.143	5.409	7.814	10.361	12.986	16.829	18.516	-----	-----	-----	-----
0.1	0.285	1.152	2.110	3.059	4.451	6.818	9.216	11.640	14.165	16.916	18.696	-----	-----	-----	-----
0.01	0.405	1.332	2.450	3.389	4.776	7.200	9.841	12.185	14.581	17.061	18.907	-----	-----	-----	-----
0	0.425	1.352	2.460	3.487	4.963	7.278	9.939	12.306	14.728	17.234	19.096	-----	-----	-----	-----

Table 5.18

Particle Deposition along a Convergent Channel for various Charge Parameter Q; $\theta = 2.5^{\circ}$, L = 18.3, St = 10

Q	X-DISPLACEMENT FRACTION OF DEPOSITION													
	0.020	0.060	0.100	0.140	0.200	0.300	0.400	0.500	0.600	0.700	0.800	0.900	0.950	0.990	0.999
100	0.004	0.018	0.042	0.068	0.113	0.206	0.322	0.465	0.652	0.917	1.360	2.498	4.684	15.038	18.450
10	0.011	0.053	0.110	0.179	0.309	0.575	0.923	1.374	1.995	2.970	4.857	9.672	15.013	18.520	-----
1	0.028	0.159	0.350	0.599	1.081	2.173	3.685	5.821	8.722	12.847	17.113	19.432	-----	-----	-----
0.1	0.099	0.572	1.250	2.078	3.585	6.897	10.434	13.772	16.591	18.676	-----	-----	-----	-----	-----
0.01	0.295	1.212	2.300	3.480	5.416	9.035	12.547	15.508	17.880	18.679	-----	-----	-----	-----	-----
0	0.435	1.432	2.551	3.819	5.815	9.444	12.954	15.926	18.215	18.942	-----	-----	-----	-----	-----

Table 5.19

Particle Deposition along a Convergent Channel for various Charge Parameter Q; $\theta = 2.5^{\circ}$, L = 18.3, St = 1

Q	X-DISPLACEMENT													
	FRACTION OF DEPOSITION													
	0.020	0.060	0.100	0.140	0.200	0.300	0.400	0.500	0.600	0.700	0.800	0.900	0.950	0.990	0.999
100	0.004	0.010	0.019	0.029	0.049	0.089	0.141	0.208	0.295	0.423	0.633	1.122	1.929	8.316	18.330
10	0.004	0.020	0.041	0.067	0.113	0.207	0.327	0.480	0.684	0.982	1.506	3.040	7.345	19.195	-----
1	0.010	0.053	0.112	0.184	0.322	0.629	1.085	1.842	3.661	9.832	15.805	19.000	-----	-----	-----
0.1	0.030	0.163	0.380	0.710	1.608	9.276	15.561	18.509	-----	-----	-----	-----	-----	-----	-----
0.01	0.103	0.717	3.300	10.918	16.288	18.537	-----	-----	-----	-----	-----	-----	-----	-----	-----
0	0.541	6.860	13.826	17.012	18.517	-----	-----	-----	-----	-----	-----	-----	-----	-----	-----

Table 5.20

Particle Deposition along a Convergent Channel for various Charge Parameter Q; $\theta = 2.5^{\circ}$, L = 18.3, St = 0.1

Q	X-DISPLACEMENT													
	FRACTION OF DEPOSITION													
	0.020	0.060	0.100	0.140	0.200	0.300	0.400	0.500	0.600	0.700	0.800	0.900	0.950	0.990	0.999
100	0.002	0.006	0.011	0.017	0.028	0.051	0.081	0.123	0.182	0.271	0.418	0.753	1.263	5.670	18.772
10	0.002	0.010	0.019	0.031	0.050	0.093	0.151	0.227	0.334	0.492	0.761	1.465	6.575	18.456	-----
1	0.004	0.021	0.042	0.071	0.125	0.250	0.455	0.836	3.970	10.019	15.477	18.990	-----	-----	-----
0.1	0.010	0.055	0.128	0.241	0.728	11.399	16.823	18.523	-----	-----	-----	-----	-----	-----	-----
0.01	0.030	0.253	10.920	16.772	18.535	-----	-----	-----	-----	-----	-----	-----	-----	-----	-----
0	-----	-----	-----	-----	-----	-----	-----	-----	-----	-----	-----	-----	-----	-----	-----

Table 5.21

Particle Deposition along a Convergent Channel for various Charge Parameter Q; $\theta = 2.5^{\circ}$, L = 18.3, St = 0.01

Q	X-DISPLACEMENT													
	FRACTION OF DEPOSITION													
	0.020	0.060	0.100	0.140	0.200	0.300	0.400	0.500	0.600	0.700	0.800	0.900	0.950	0.990	0.999
100	0.001	0.005	0.008	0.013	0.021	0.038	0.063	0.097	0.146	0.222	0.349	0.623	1.015	12.597	18.410
10	0.001	0.006	0.012	0.018	0.029	0.056	0.096	0.152	0.238	0.370	0.612	2.185	8.410	18.546	-----
1	0.003	0.011	0.020	0.035	0.065	0.153	0.335	1.382	4.838	9.770	14.960	18.575	-----	-----	-----
0.1	0.004	0.024	0.061	0.135	1.844	11.365	16.870	18.508	-----	-----	-----	-----	-----	-----	-----
0.01	0.011	0.145	11.516	17.293	18.539	-----	-----	-----	-----	-----	-----	-----	-----	-----	-----
0	-----	-----	-----	-----	-----	-----	-----	-----	-----	-----	-----	-----	-----	-----	-----

Table 5.22

Particle Deposition along a Convergent Channel for various Charge Parameter Q; $\theta = 2.5^{\circ}$, L = 18.3, St = 0

Q	X-DISPLACEMENT													
	FRACTION OF DEPOSITION													
	0.020	0.060	0.100	0.140	0.200	0.300	0.400	0.500	0.600	0.700	0.800	0.900	0.950	0.990	0.999
100	0.006	0.007	0.019	0.031	0.052	0.102	0.173	0.263	0.394	0.567	0.848	1.546	5.476	12.295	18.330
10	0.006	0.011	0.020	0.032	0.058	0.125	0.223	0.365	0.552	0.861	1.463	4.672	8.460	18.157	18.654
1	0.006	0.011	0.024	0.049	0.115	0.307	0.697	1.784	4.911	9.729	15.034	18.602	-----	-----	-----
0.1	0.006	0.021	0.080	0.243	2.046	11.276	16.828	18.513	-----	-----	-----	-----	-----	-----	-----
0.01	0.007	0.344	11.317	17.170	18.547	-----	-----	-----	-----	-----	-----	-----	-----	-----	-----
0	-----	-----	-----	-----	-----	-----	-----	-----	-----	-----	-----	-----	-----	-----	-----

Table 5.23

Particle Deposition along a Parallel Plate Channel for various Charge Parameter Q; $\theta = 0^{o}$, L = 12.5, St = 0

Q	X-DISPLACEMENT FRACTION OF DEPOSITION														
	0.020	0.060	0.100	0.140	0.200	0.300	0.400	0.500	0.600	0.700	0.800	0.900	0.950	0.990	0.999
100	0.000	0.000	0.000	0.000	0.000	0.000	0.001	0.002	0.003	0.005	0.009	0.015	0.022	0.037	0.059
10	0.000	0.000	0.000	0.000	0.001	0.004	0.009	0.017	0.031	0.053	0.087	0.150	0.215	0.368	0.590
1	0.000	0.000	0.001	0.004	0.011	0.036	0.087	0.174	0.312	0.525	0.867	1.499	2.151	3.682	5.877
0.1	0.000	0.003	0.013	0.037	0.107	0.363	0.872	1.739	3.116	5.250	8.664	14.988	-----	-----	-----
0.01	0.001	0.029	0.134	0.367	1.070	3.632	8.715	17.393	-----	-----	-----	-----	-----	-----	-----
0	-----	-----	-----	-----	-----	-----	-----	-----	-----	-----	-----	-----	-----	-----	-----

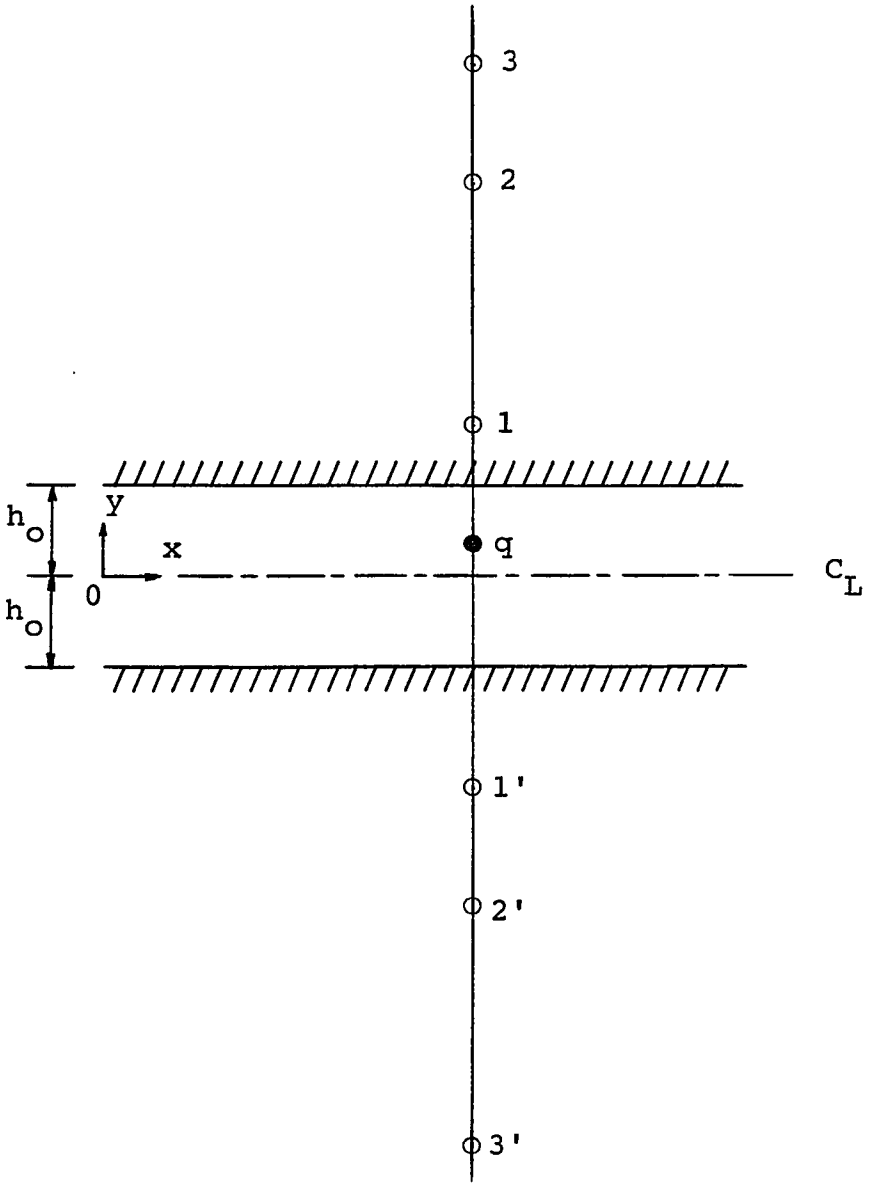

Figure 3.1 Coordinate System in a Parallel Plate Channel with Charged Particle and Image Pairs

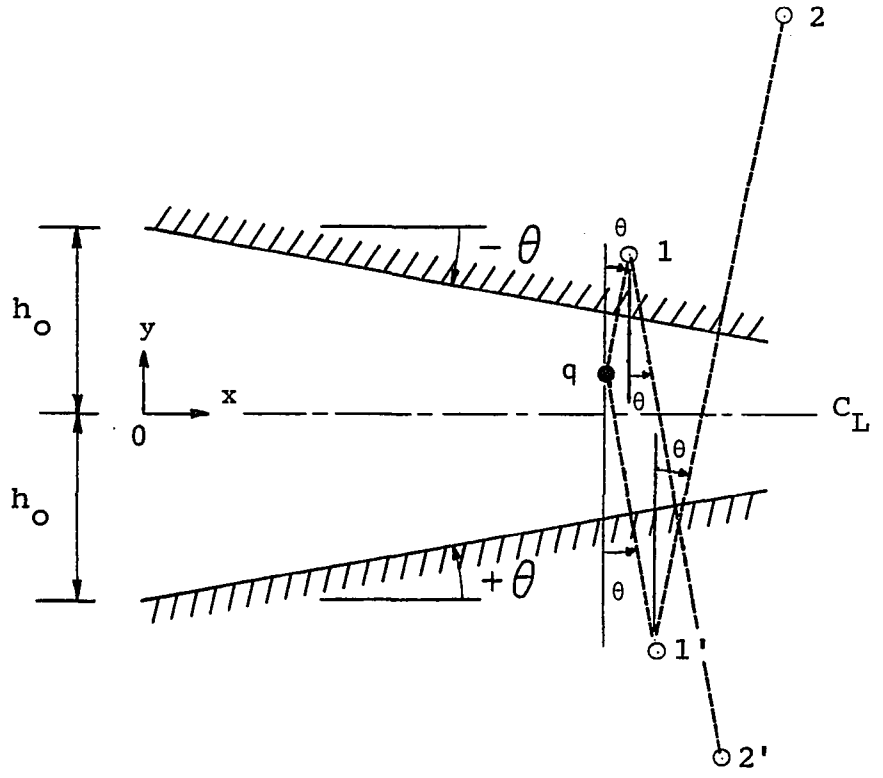

Figure 3.2 Coordinate System in a Convergent Channel with Charged Particle and Image Pairs

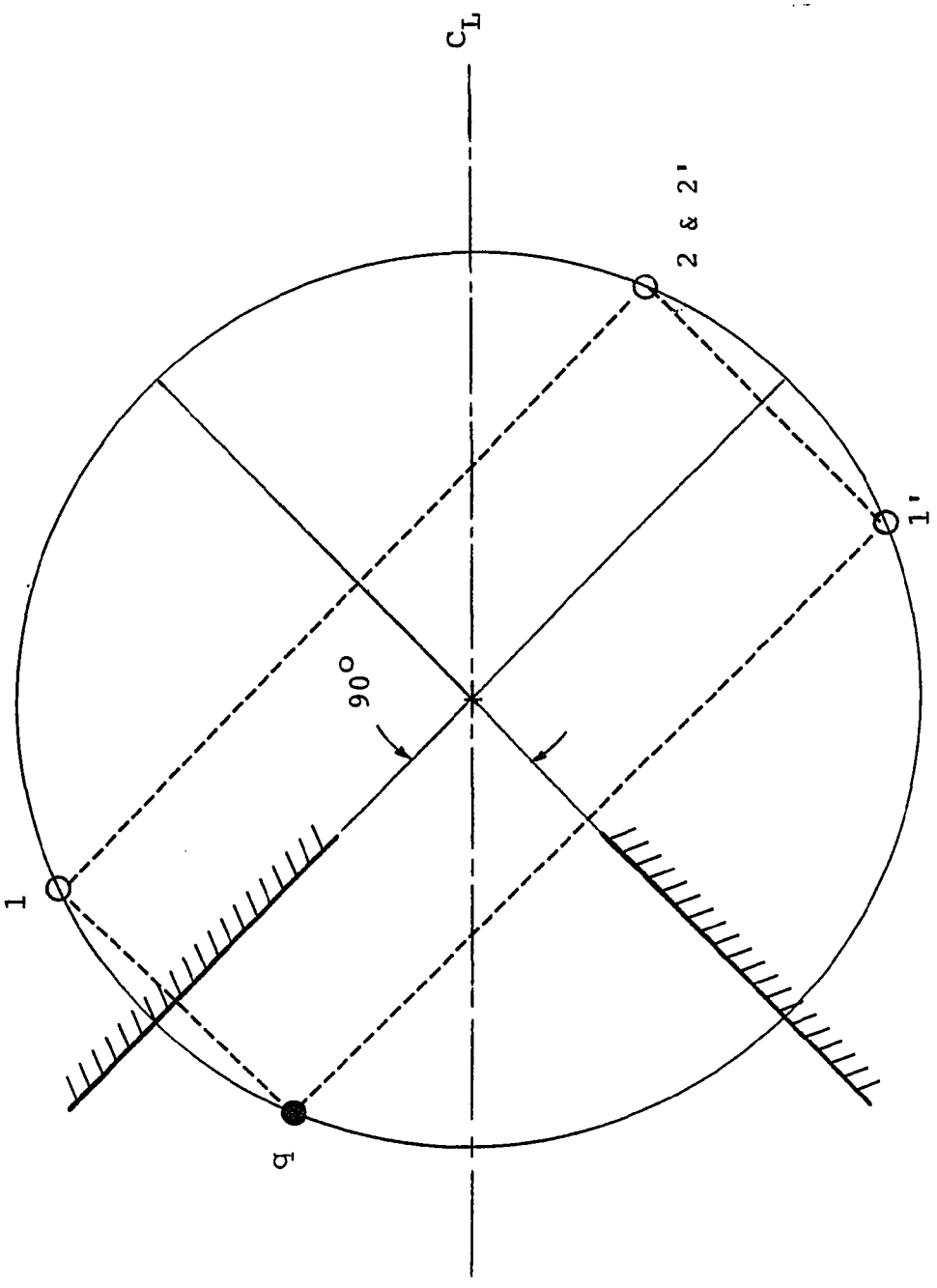

Figure 3.3 Distribution of Image Pairs on Image Circle of a Convergent Channel of 90 Degrees

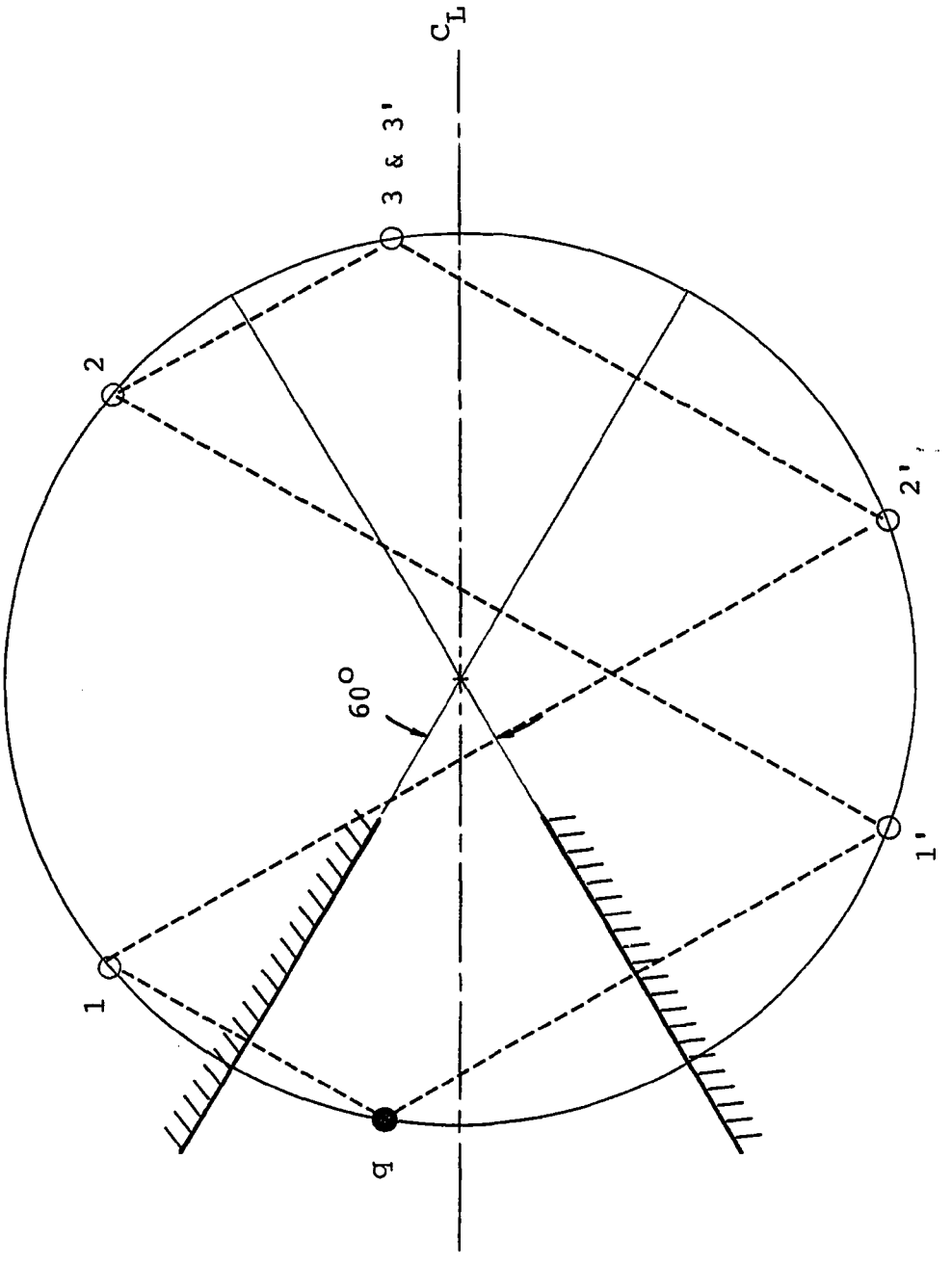

Figure 3.4 Distribution of Image Pairs on Image Circle of a Convergent Channel of 60 Degrees

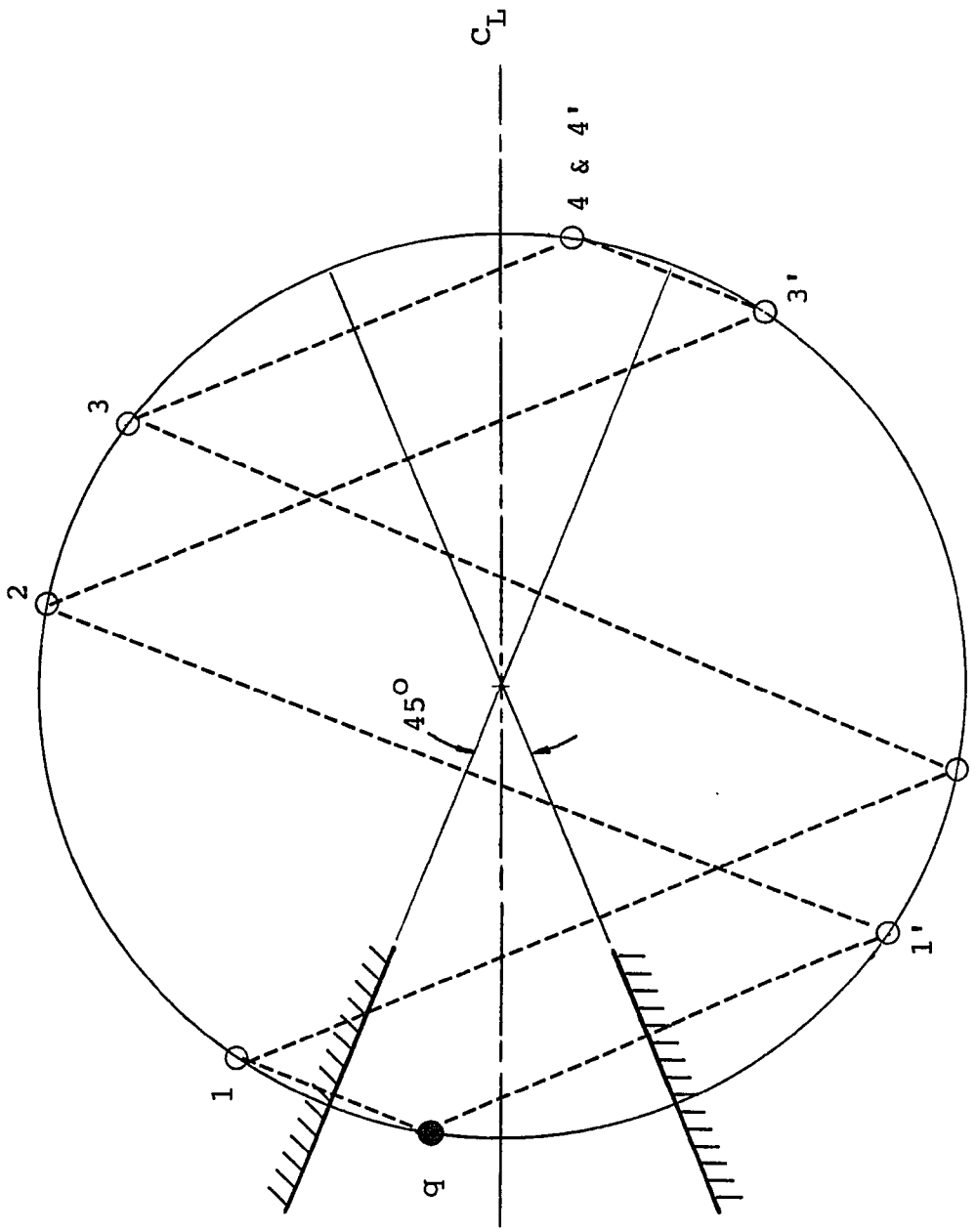

Figure 3.5 Distribution of Image Pairs on Image Circle of a Convergent Channel of 45 Degrees

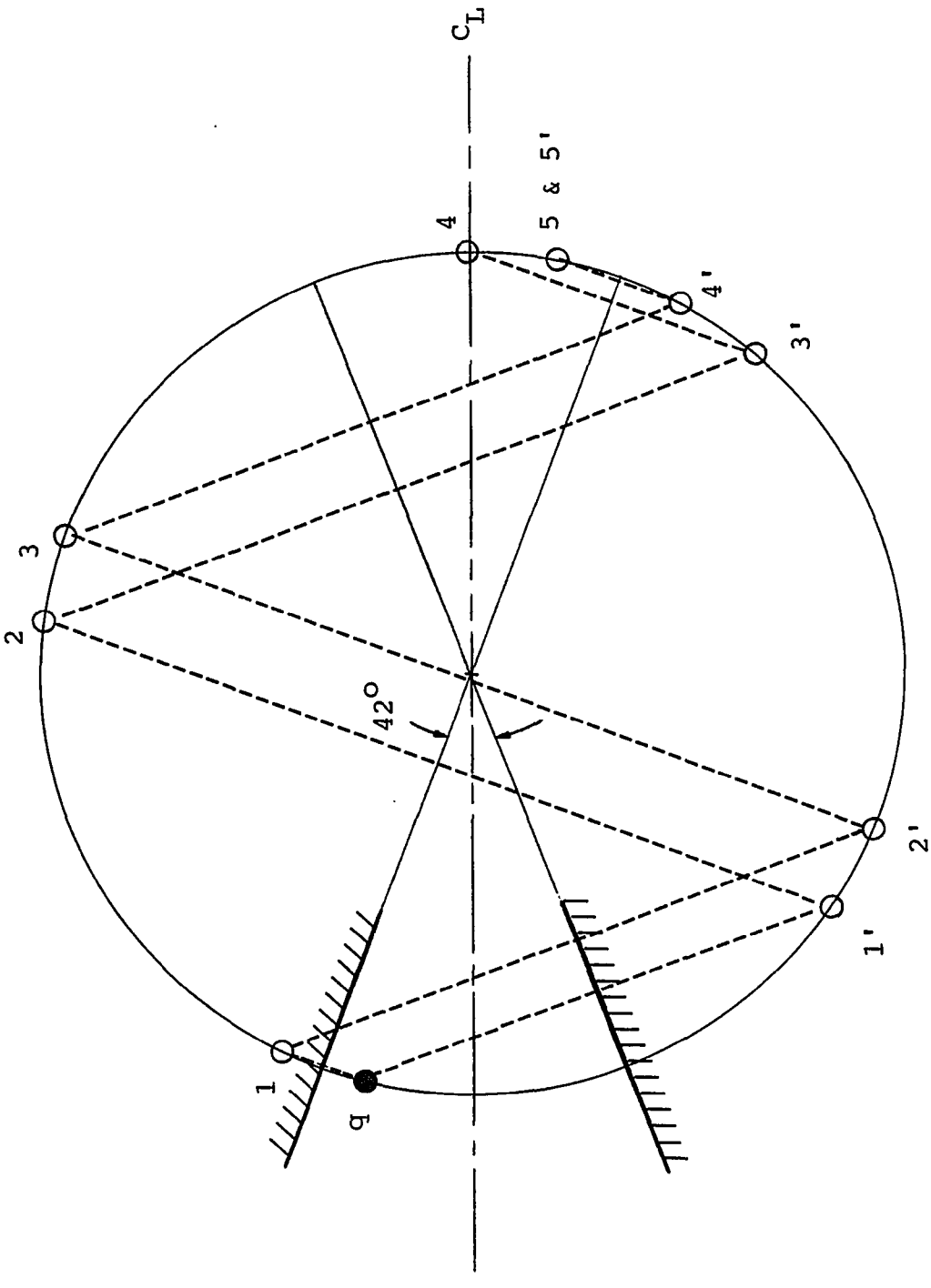

Figure 3.6 Distribution of Image Pairs on Image Circle of a Convergent Channel of 42 Degrees

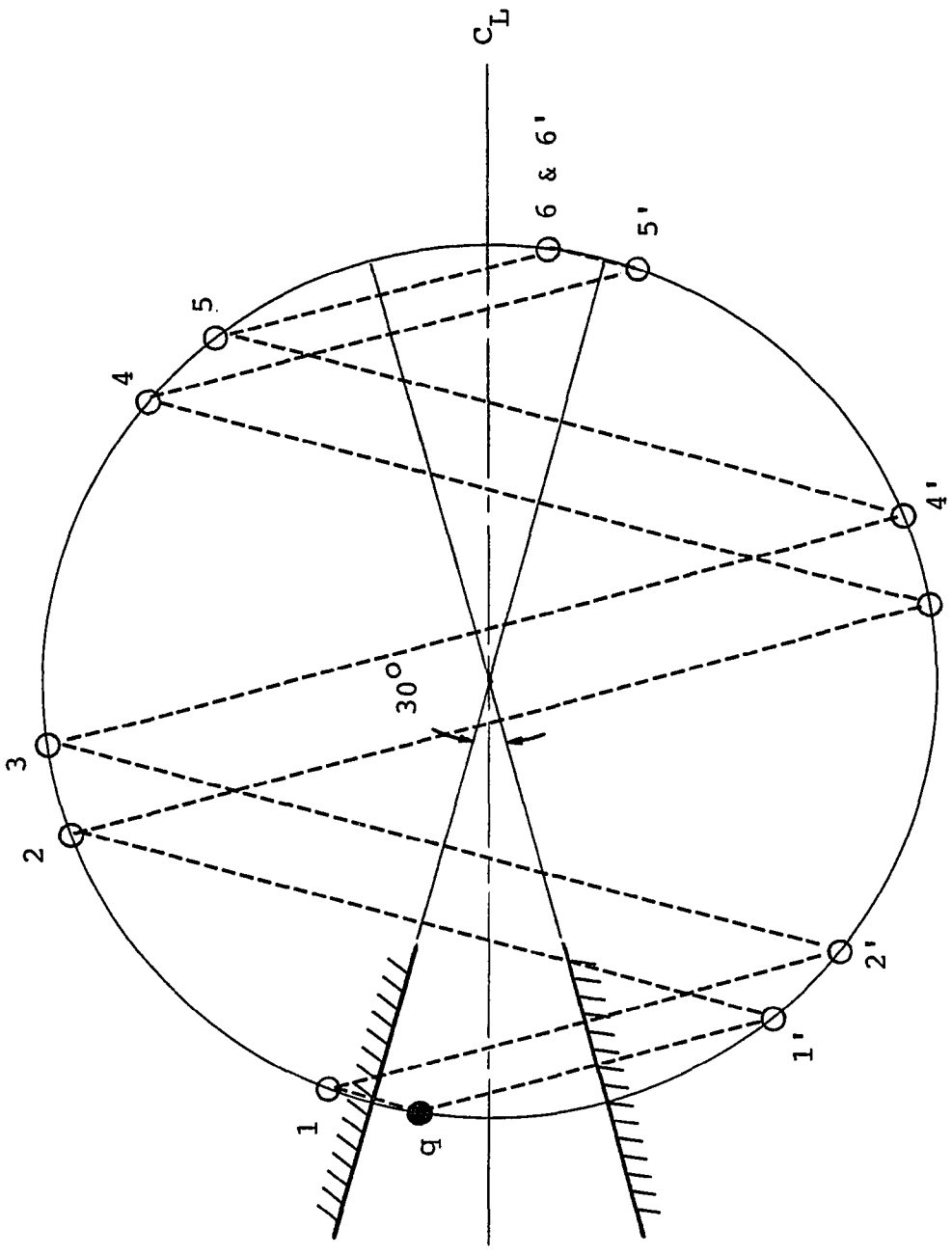

Figure 3.7 Distribution of Image Pairs on Image Circle of a Convergent Channel of 30 Degrees

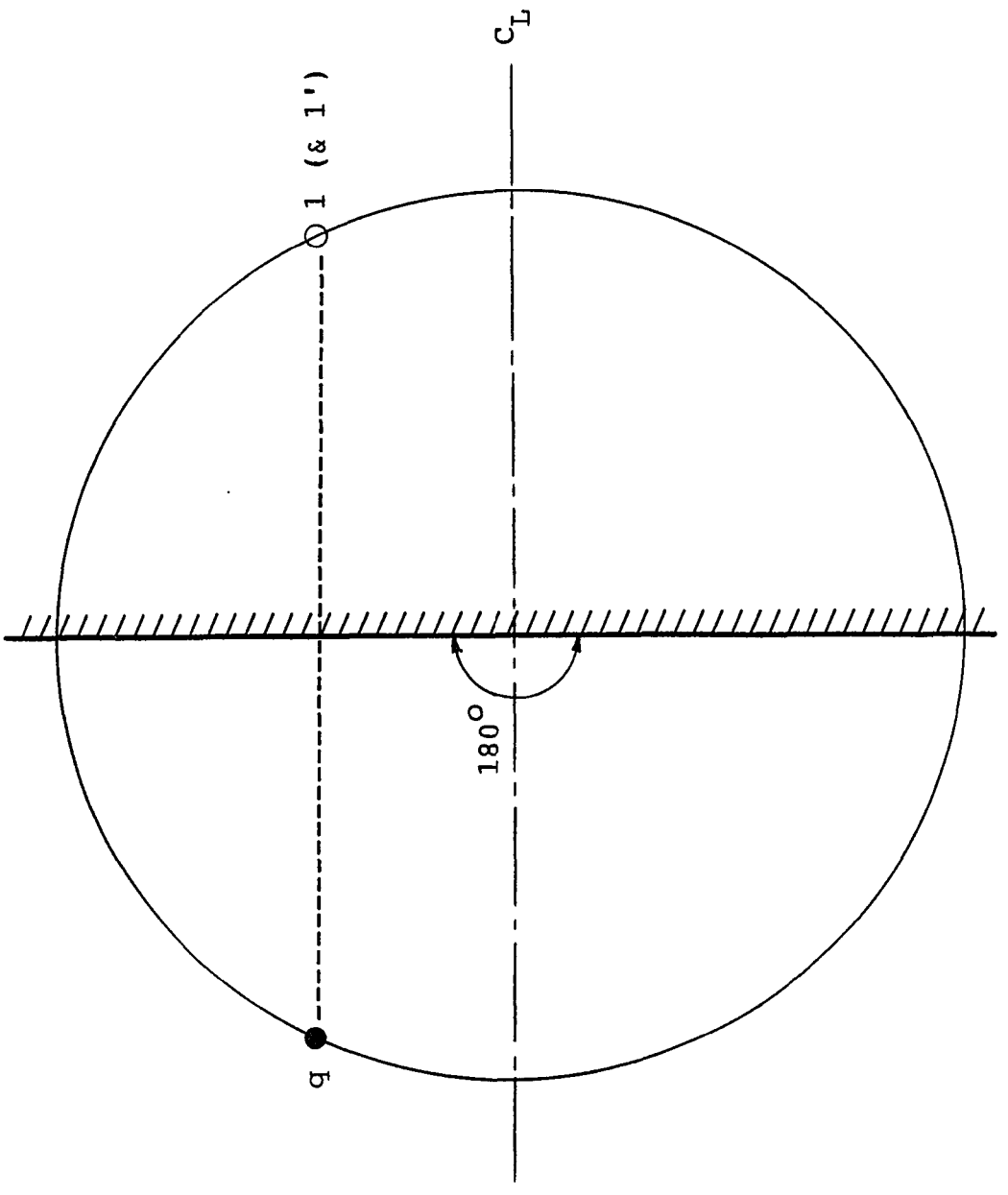

Figure 3.8 Limiting Case of a Convergent Channel of 180 Degrees

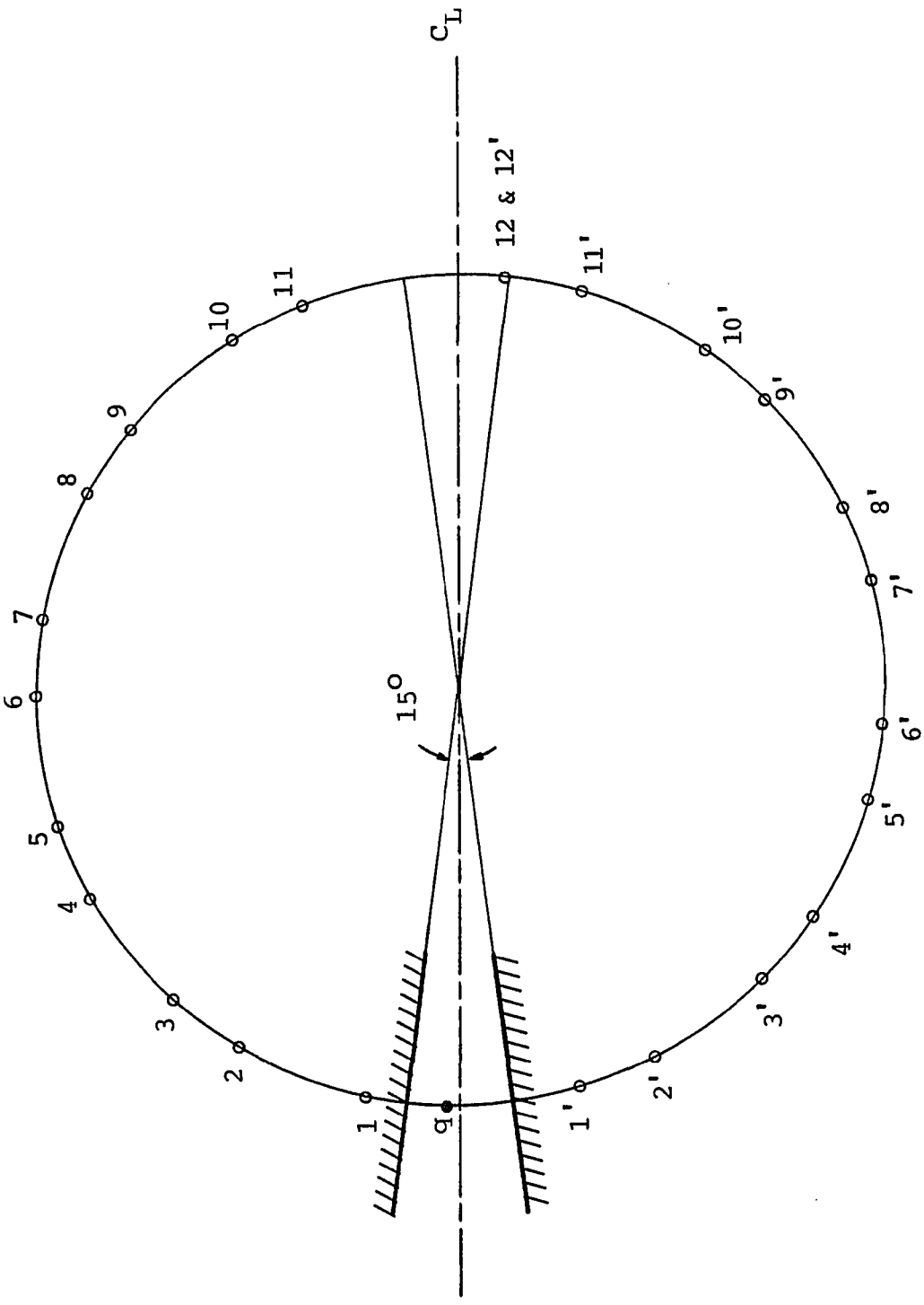

Figure 3.9 Distribution of Image Pairs on Image Circle of a Convergent Channel of 15 Degrees

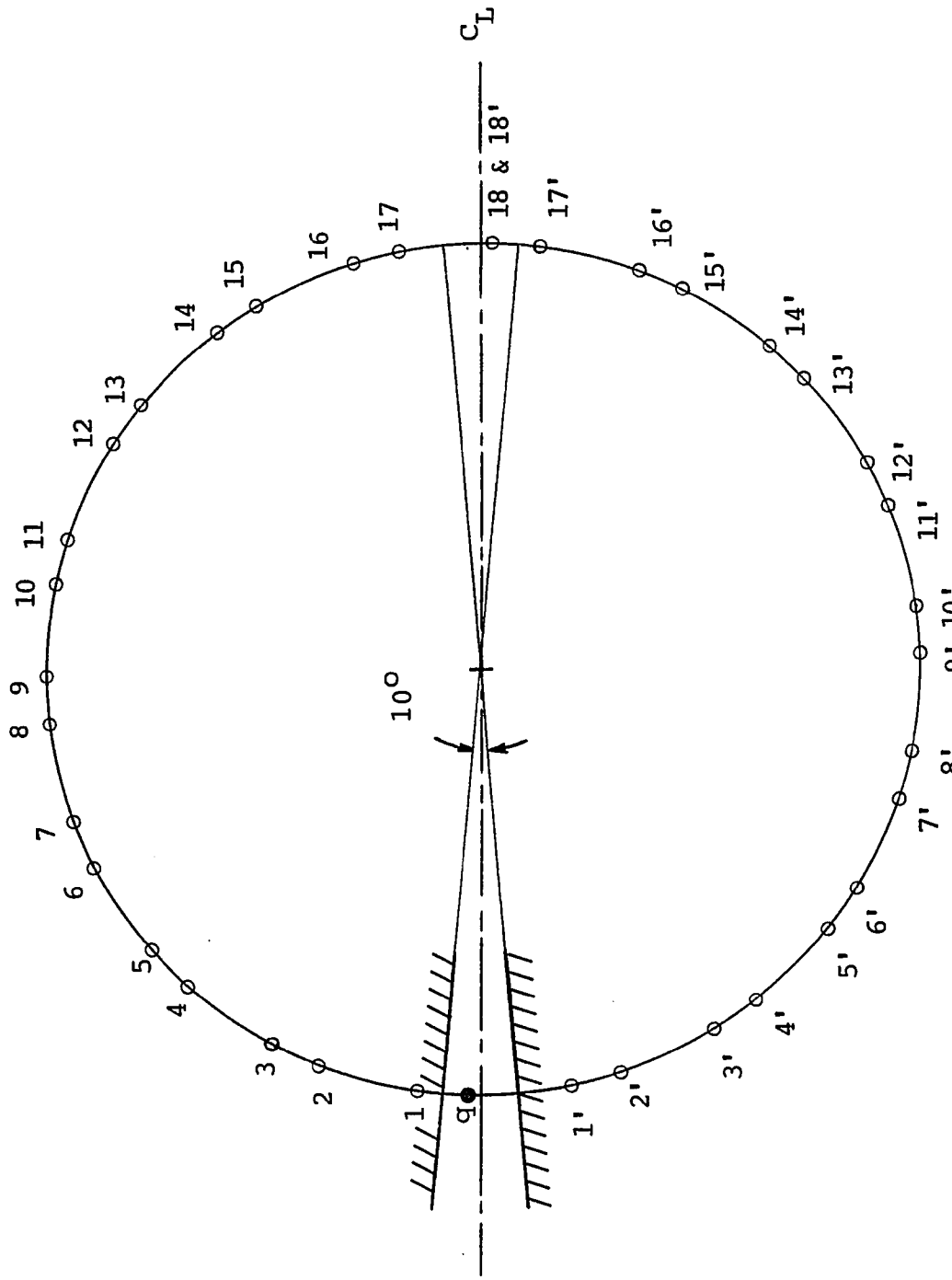

Figure 3.10 Distribution of Image Pairs on Image Circle of a Convergent Channel of 10 Degrees

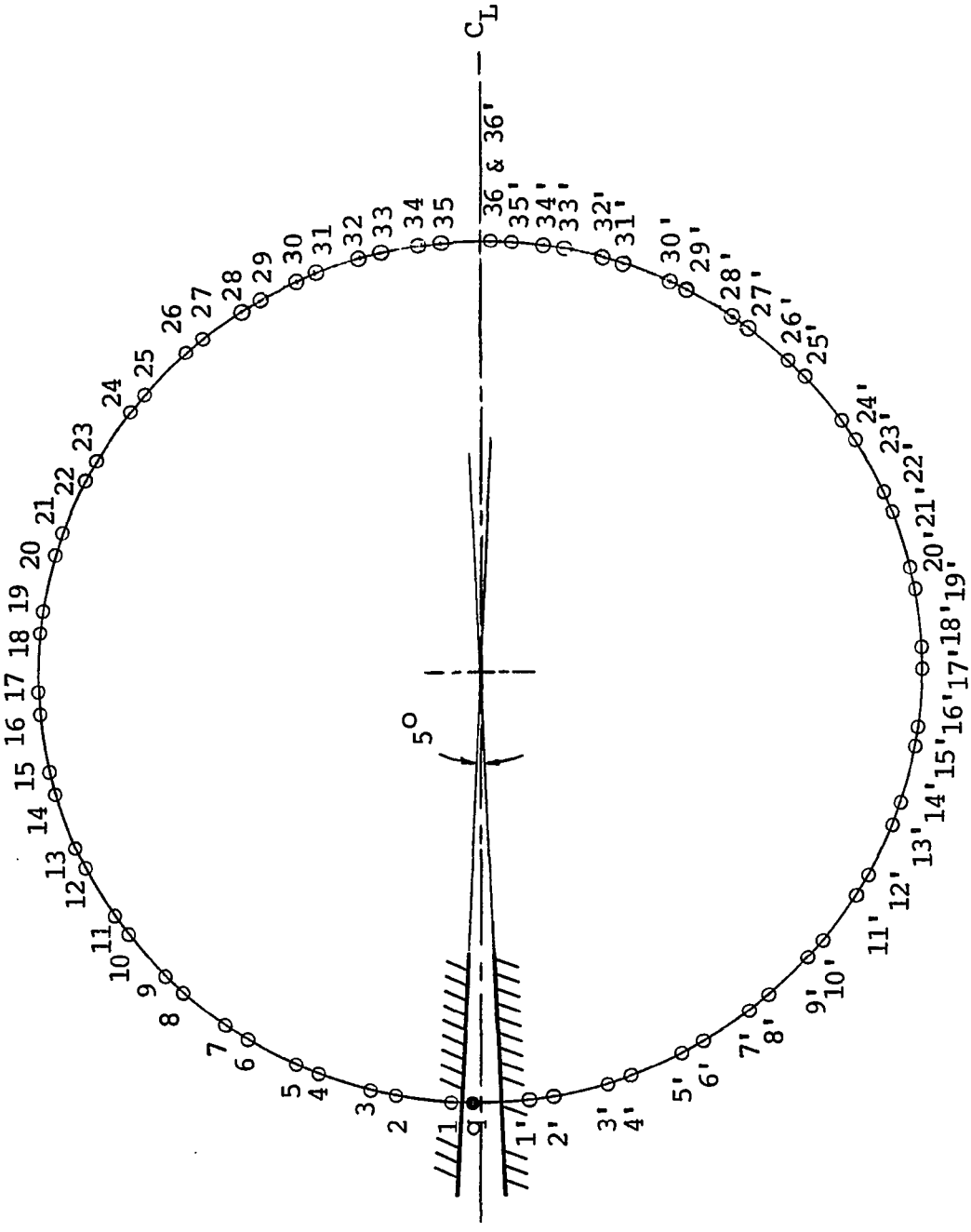

Figure 3.11 Distribution of Image Pairs on Image Circle of a Convergent Channel of 5 Degrees

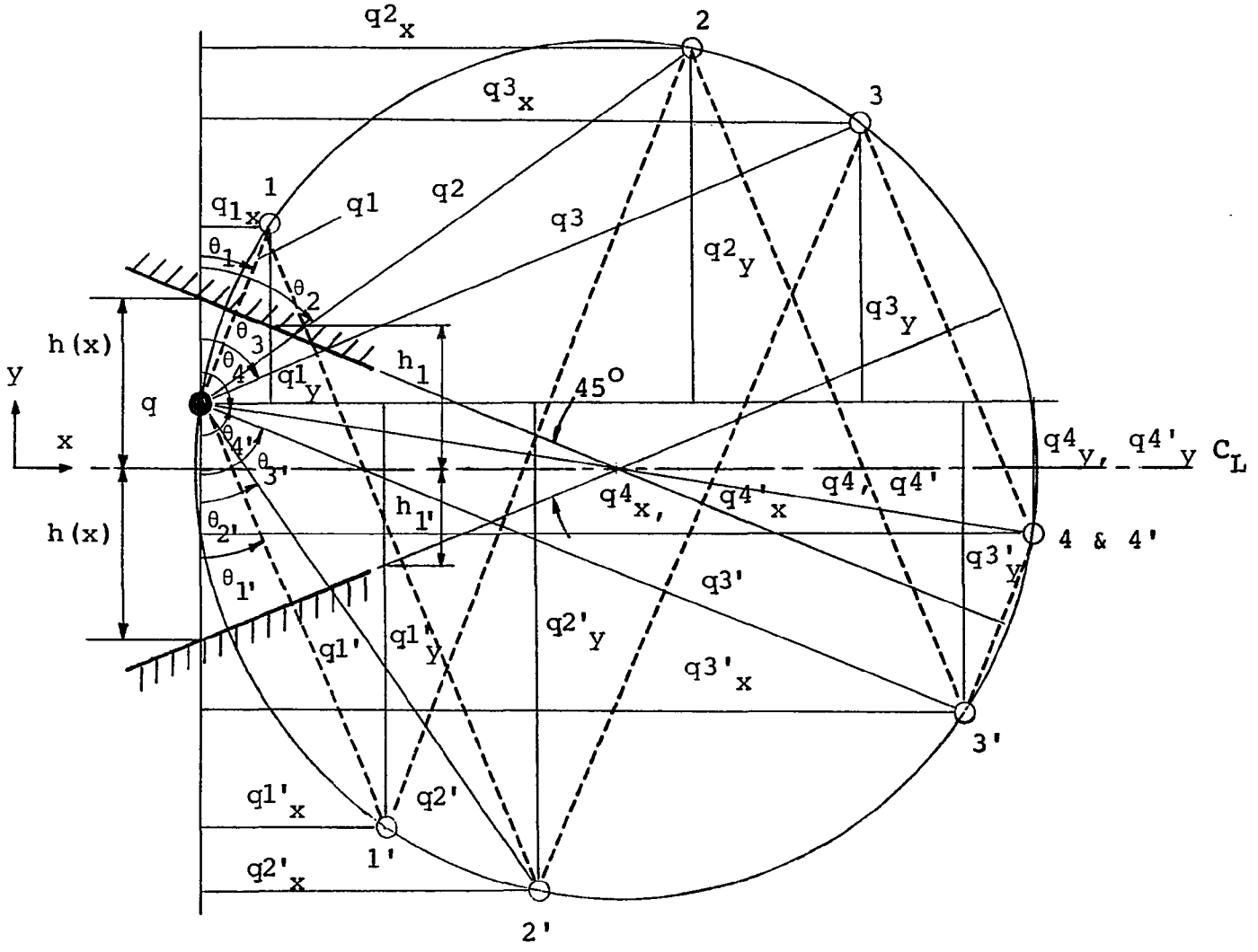

Figure 3.12 Scheme of Image Pairs on Image Circle of a Convergnet Channel of 45 Degrees

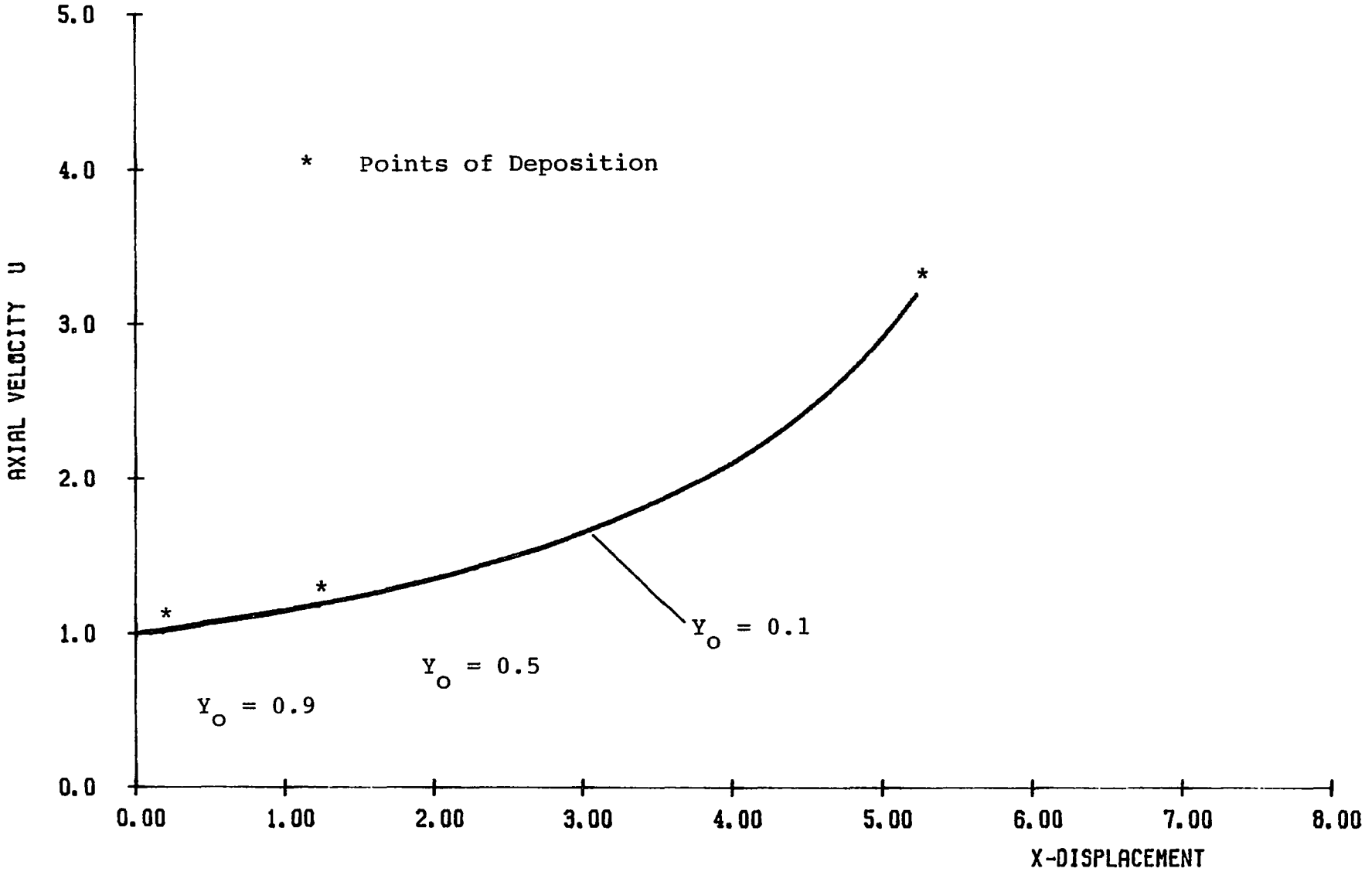

Fig. 5.1 Axial Velocity of Fluid along a Convergent Channel; $\theta = 7.5°$, L = 6.07, Q = 10, St = 10

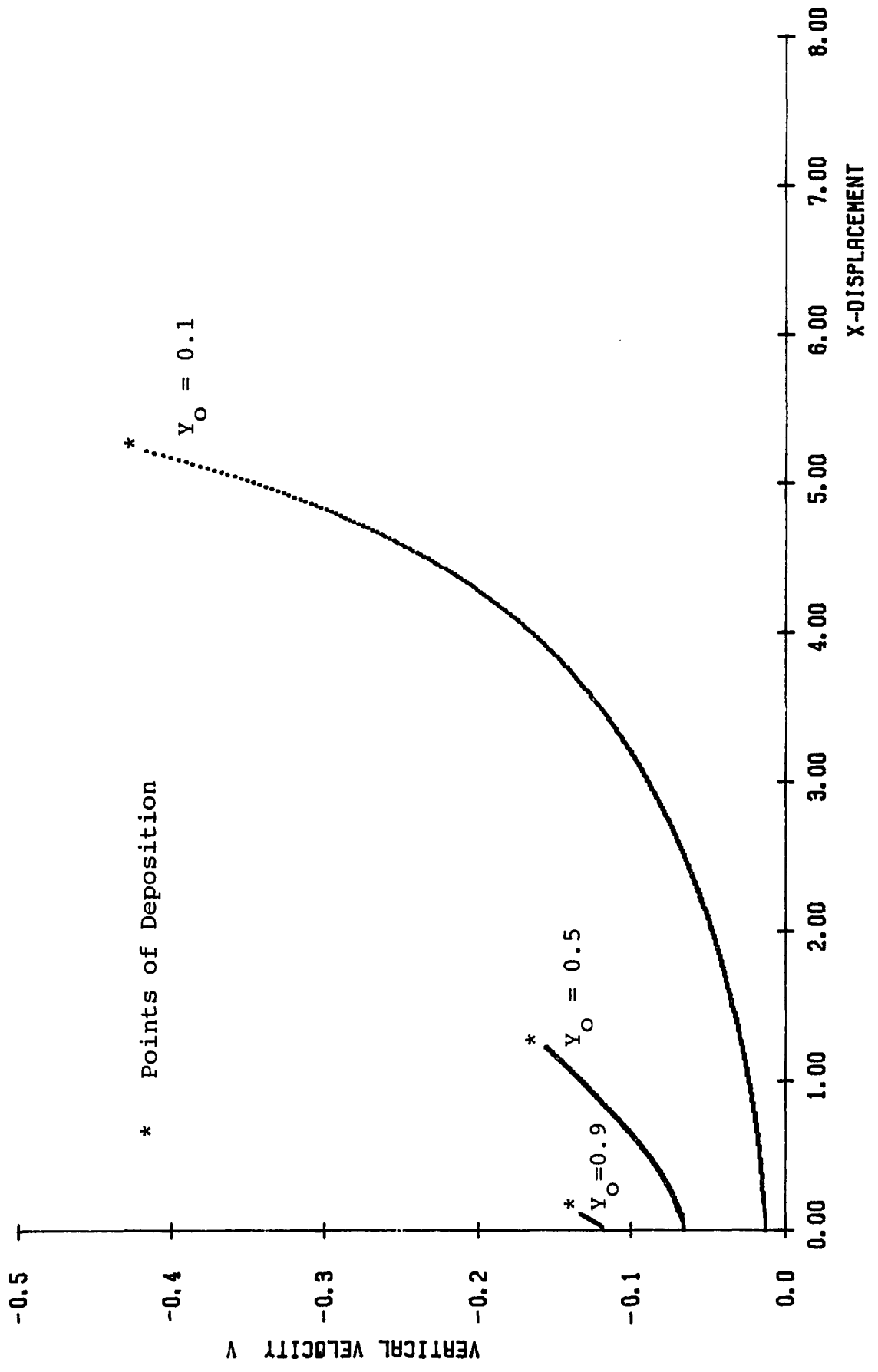

Fig. 5.2 Vertical Velocity of Fluid along a Convergent Channel; $\theta = 7.5^\circ$, L = 6.07, Q = 10, St = 10

140

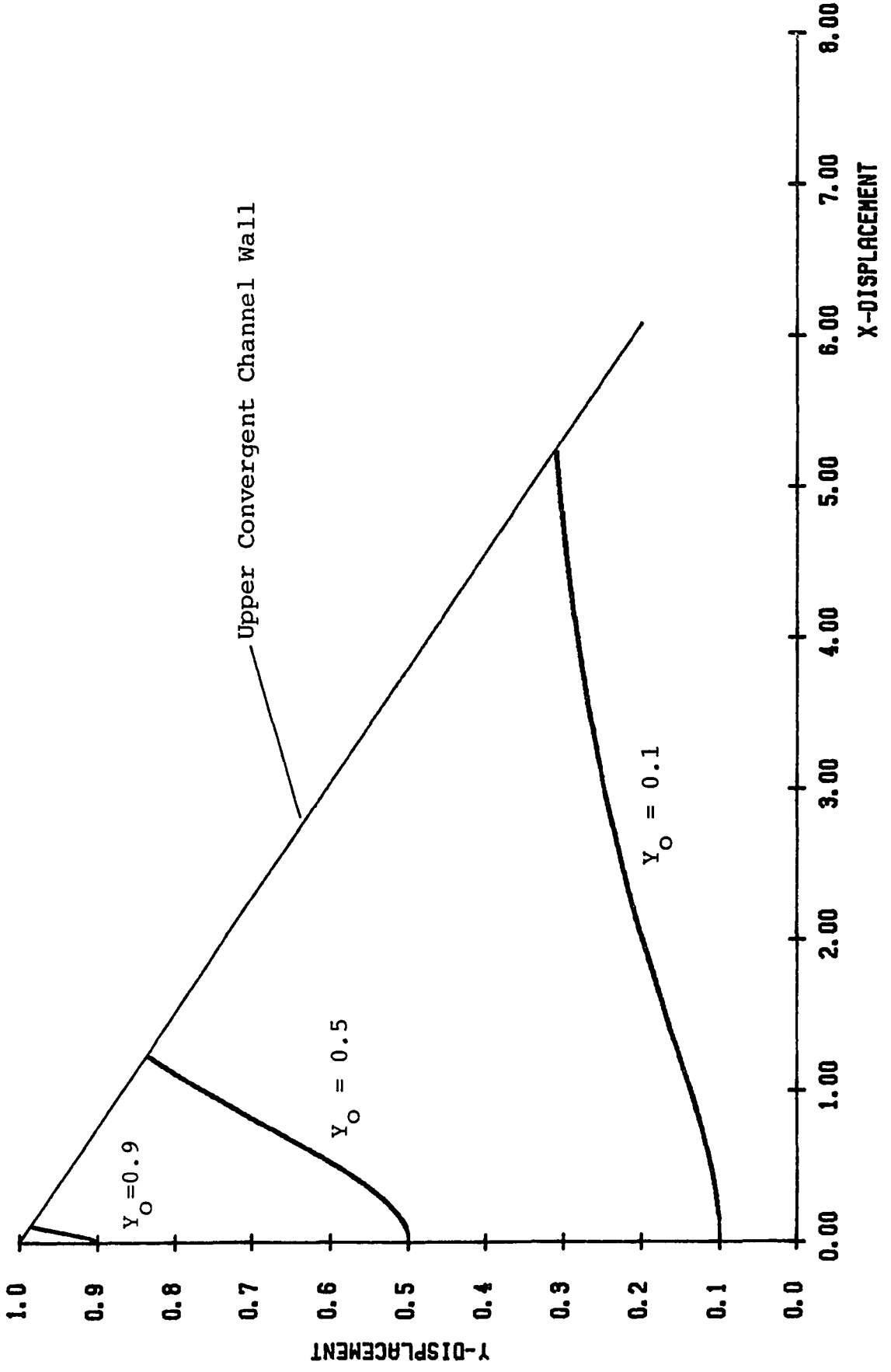

Fig. 5.3 Particle Trajectory along a Convergent Channel; $\theta = 7.5°$, L = 6.07, Q = 10, St = 10

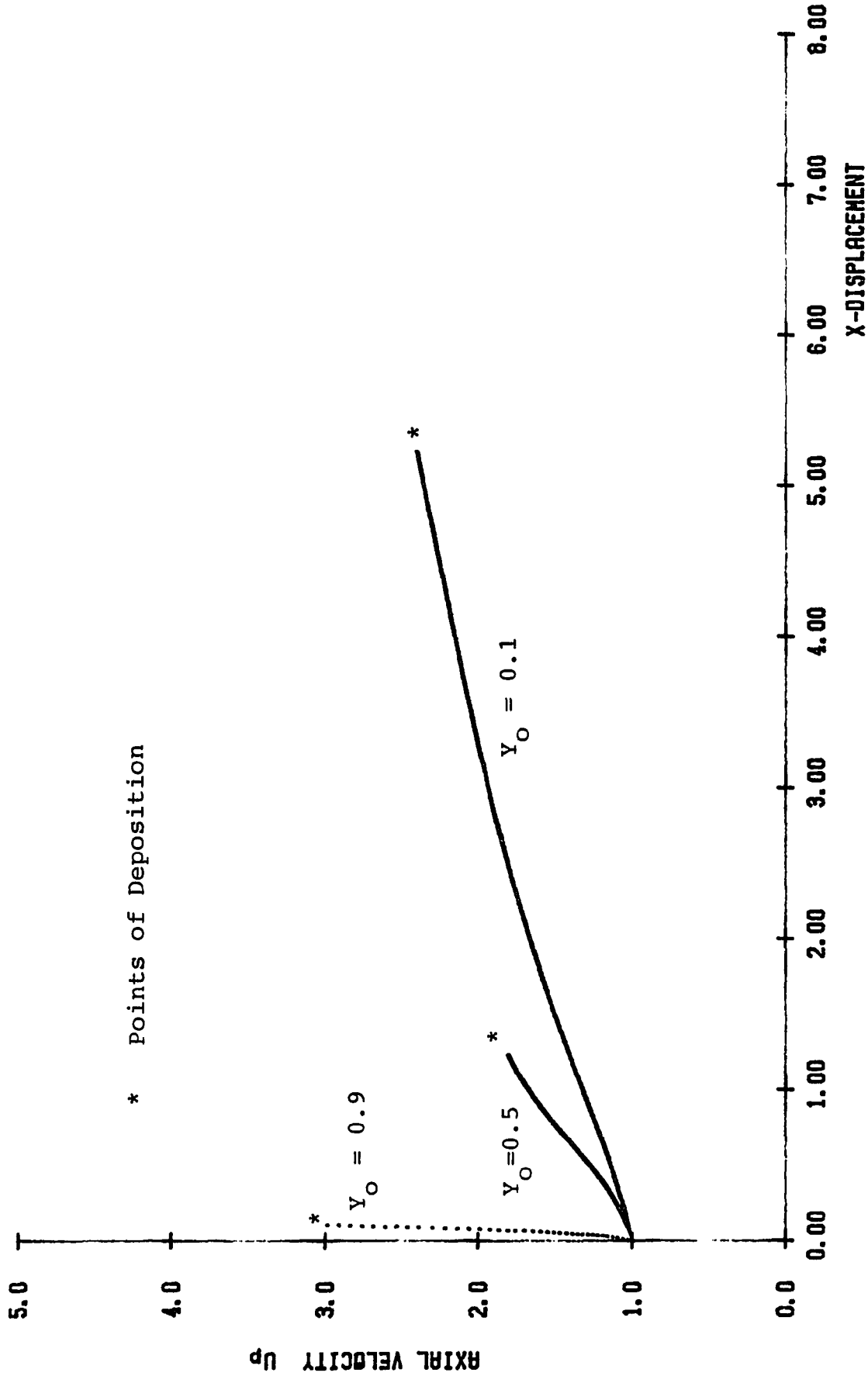

Fig. 5.4 Particle Axial Velocity along a Convergent Channel; $\theta = 7.5^\circ$, L = 6.07, Q = 10, St = 10

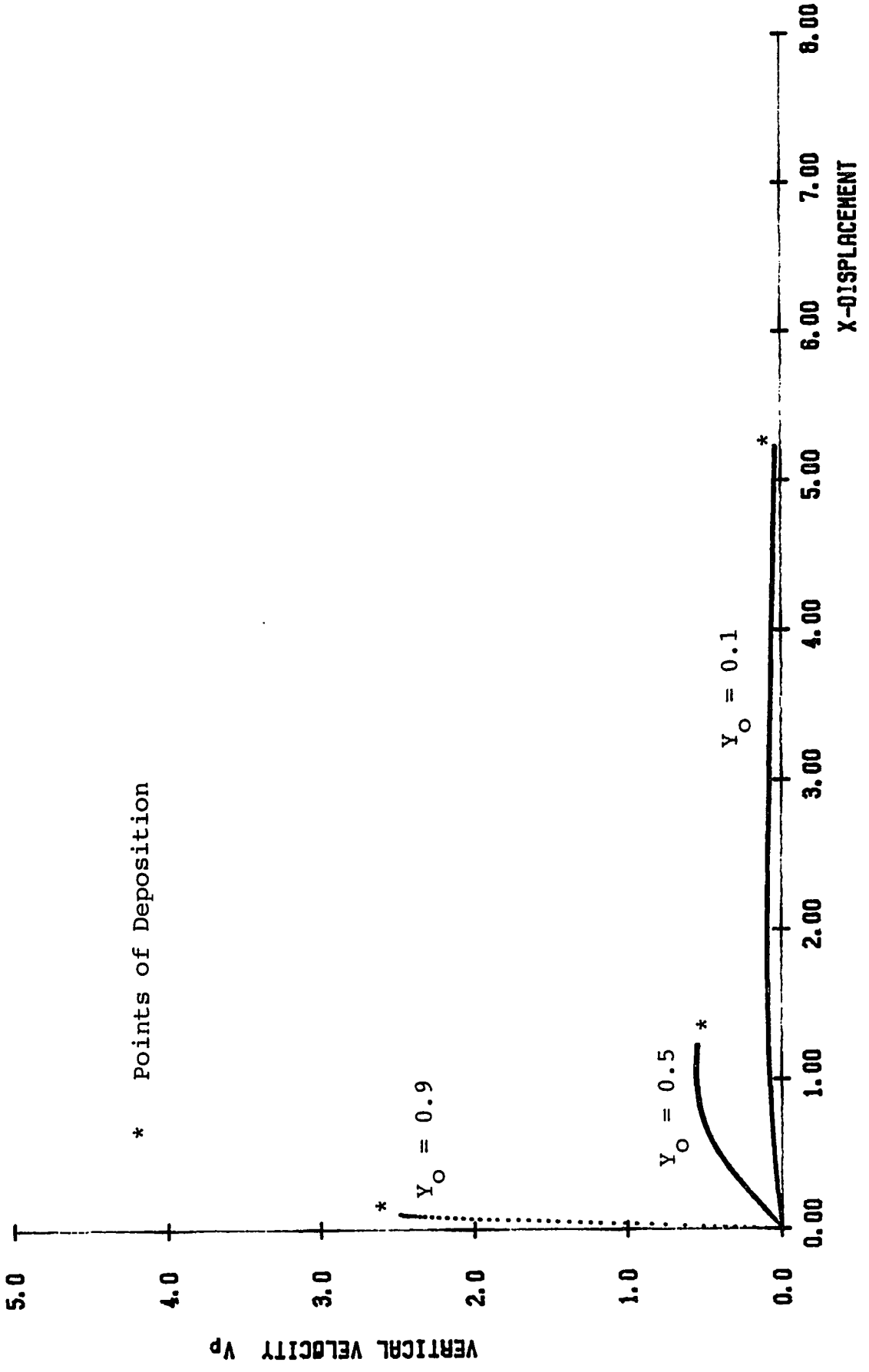

Fig. 5.5 Particle Vertical Velocity along a Convergent Channel: $\theta = 7.5°$, L = 6.07, Q = 10, St = 10

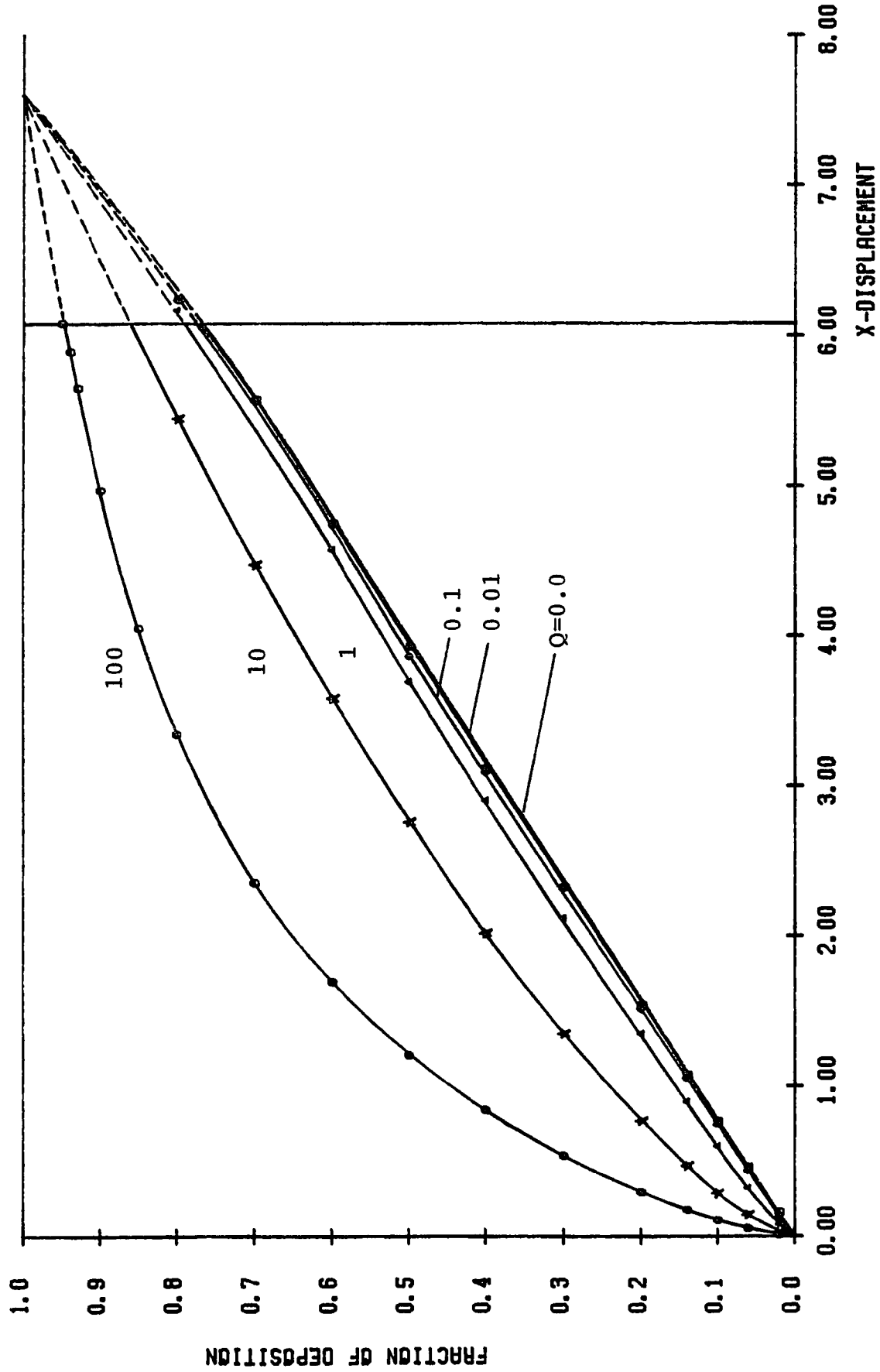

Fig. 5.6 Effect of Charge Parameter Q on Deposition for Uniform Flow in a Convergent Channel; $\theta = 7.5$, $L = 6.07$, $St = 100$

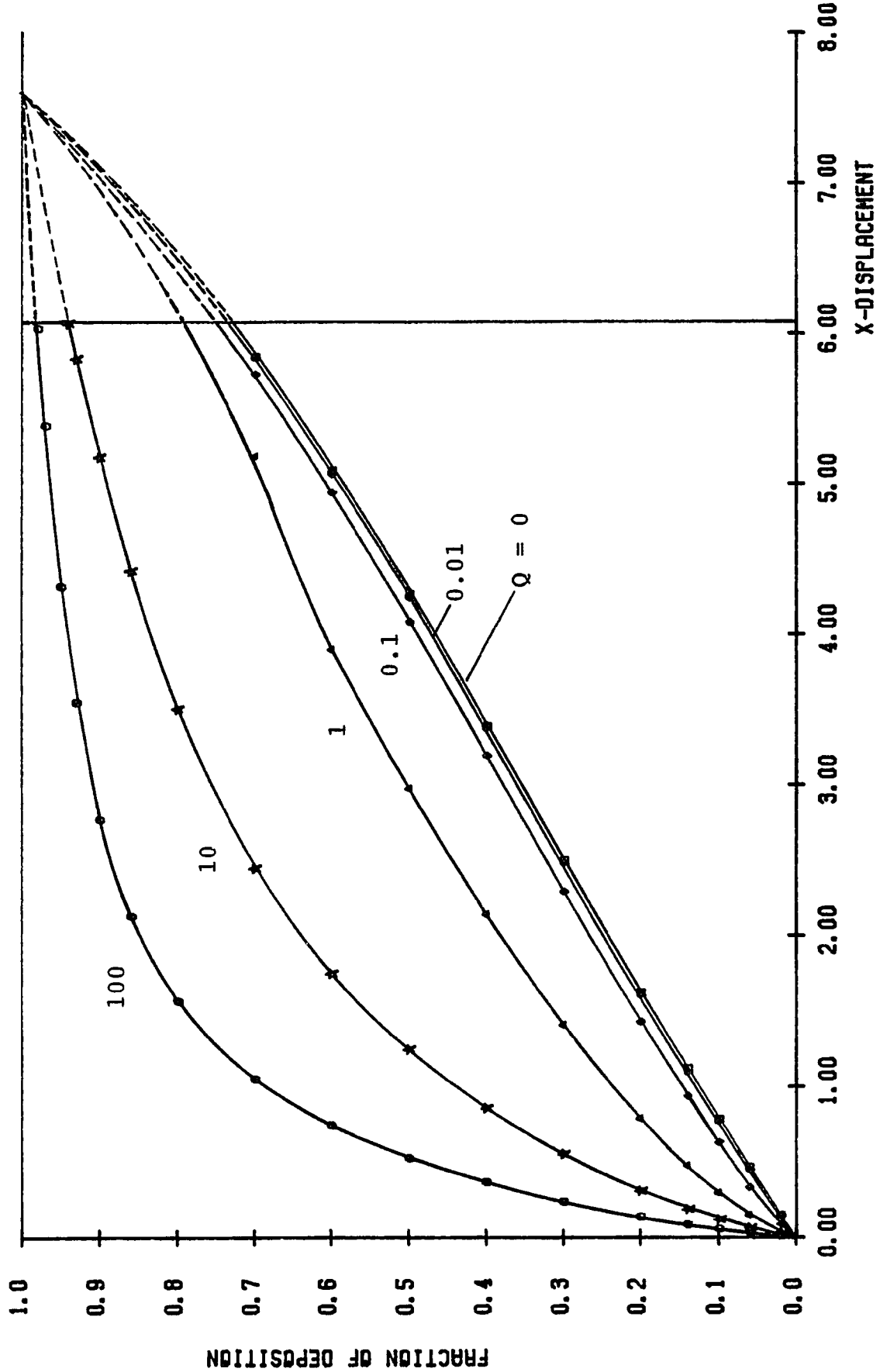

Fig. 5.7 Effect of Charge Parameter Q on Deposition for Uniform Flow in a Convergent Channel; $\theta = 7.5°$, $L = 6.07$, $St = 10$

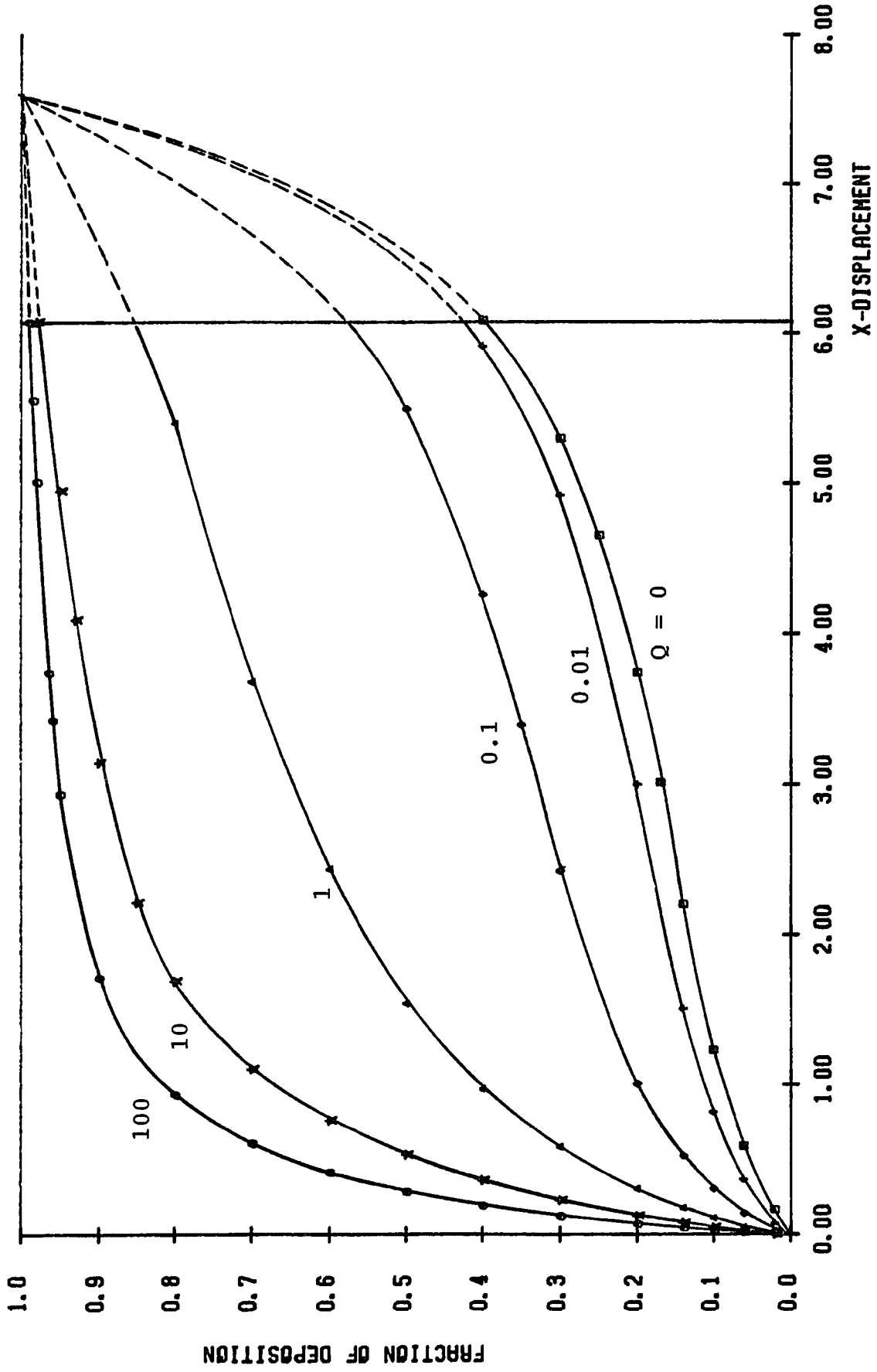

Fig. 5.8 Effect of Charge Parameter Q on Deposition for Uniform Flow in a Convergent Channel; $\theta = 7.5°$, $L = 6.07$, $St = 1$

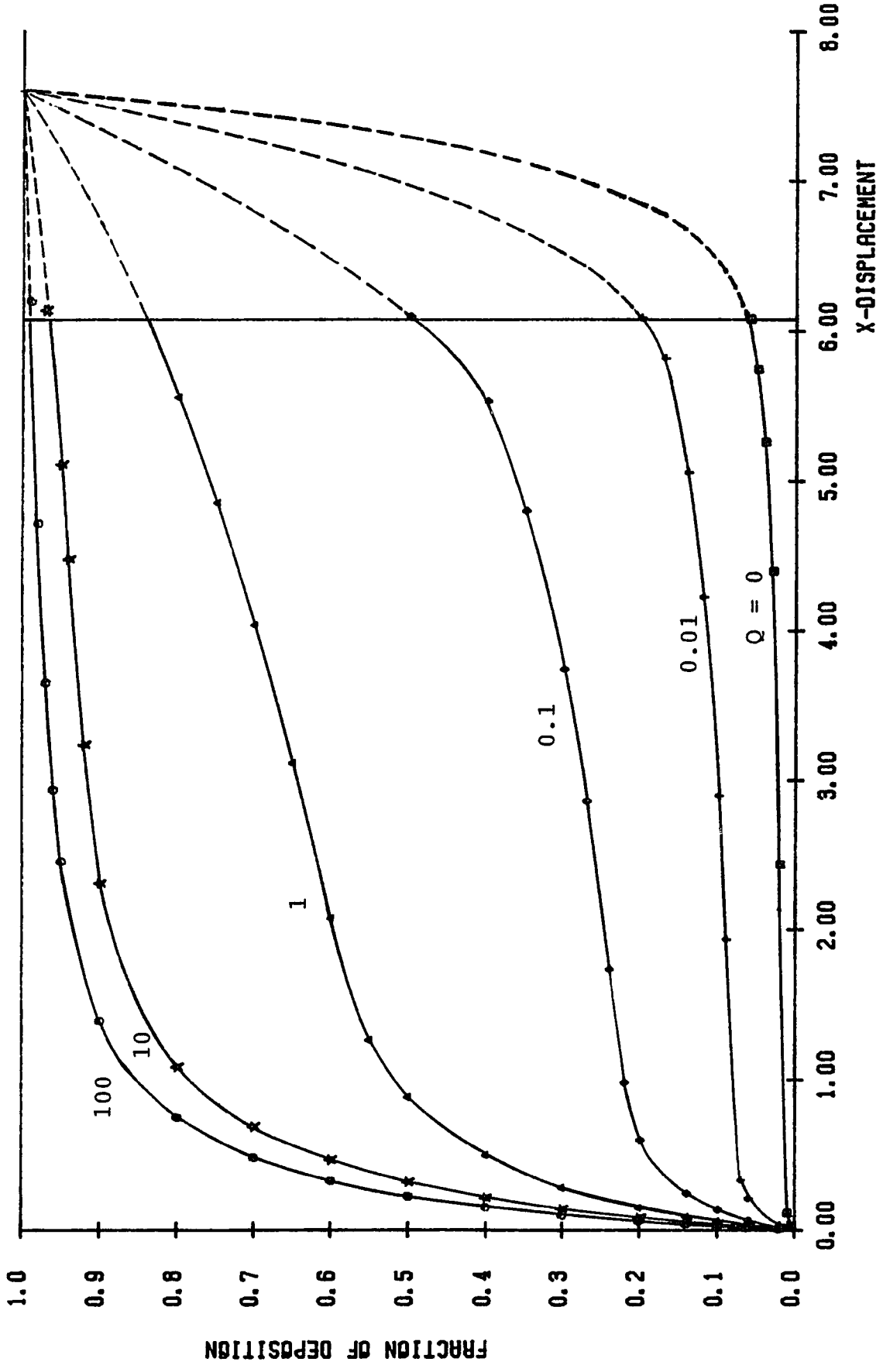

Fig. 5.9 Effect of Charge Parameter Q on Deposition for Uniform Flow in a Convergent Channel; $\theta = 7.5°$, $L = 6.07$, $St = 0.1$

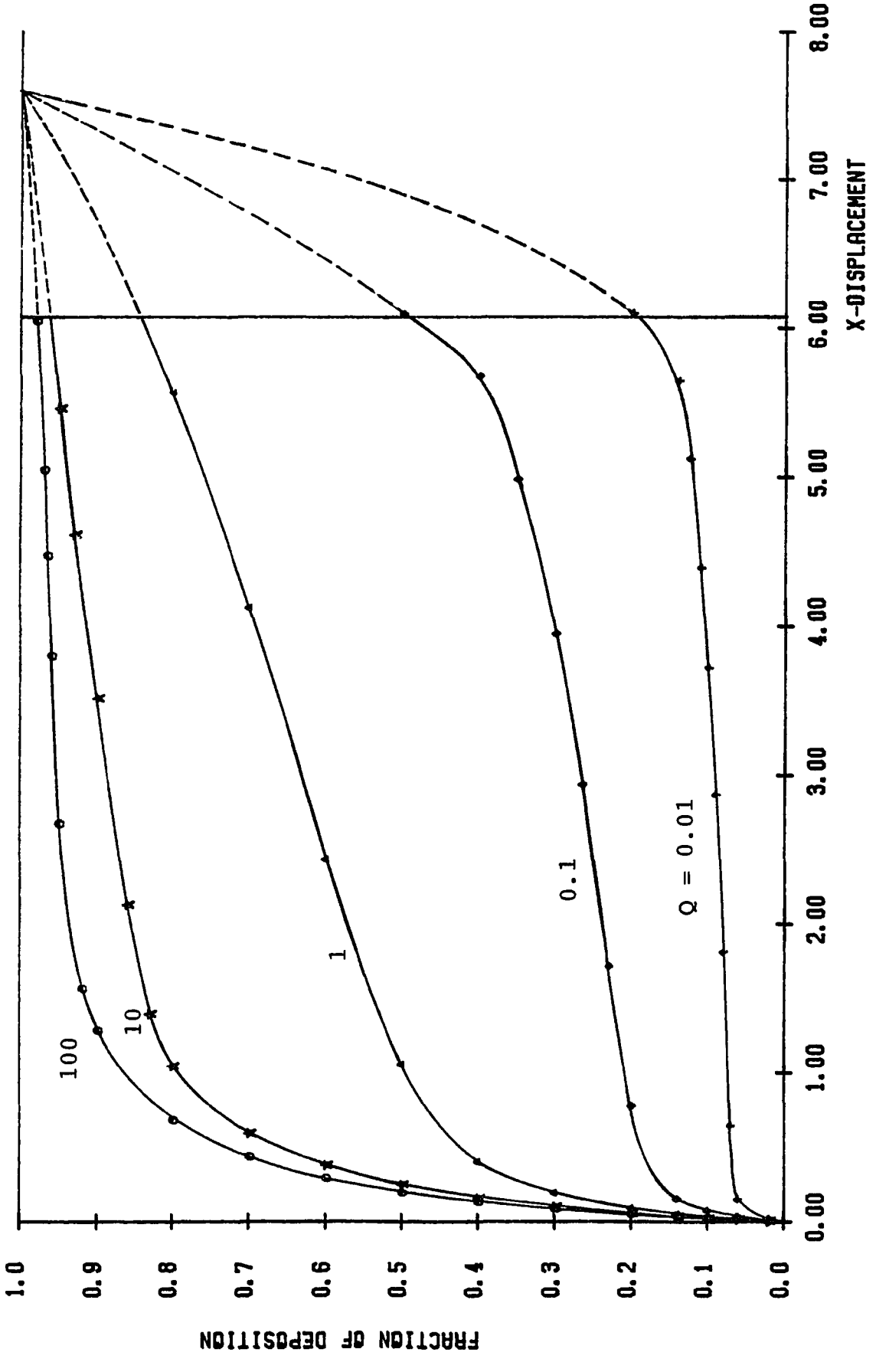

Fig. 5.10 Effect of Charge Parameter Q on Deposition for Uniform Flow in a Convergent Channel; $\theta = 7.5°$, $L = 6.07$, $St = 0.01$

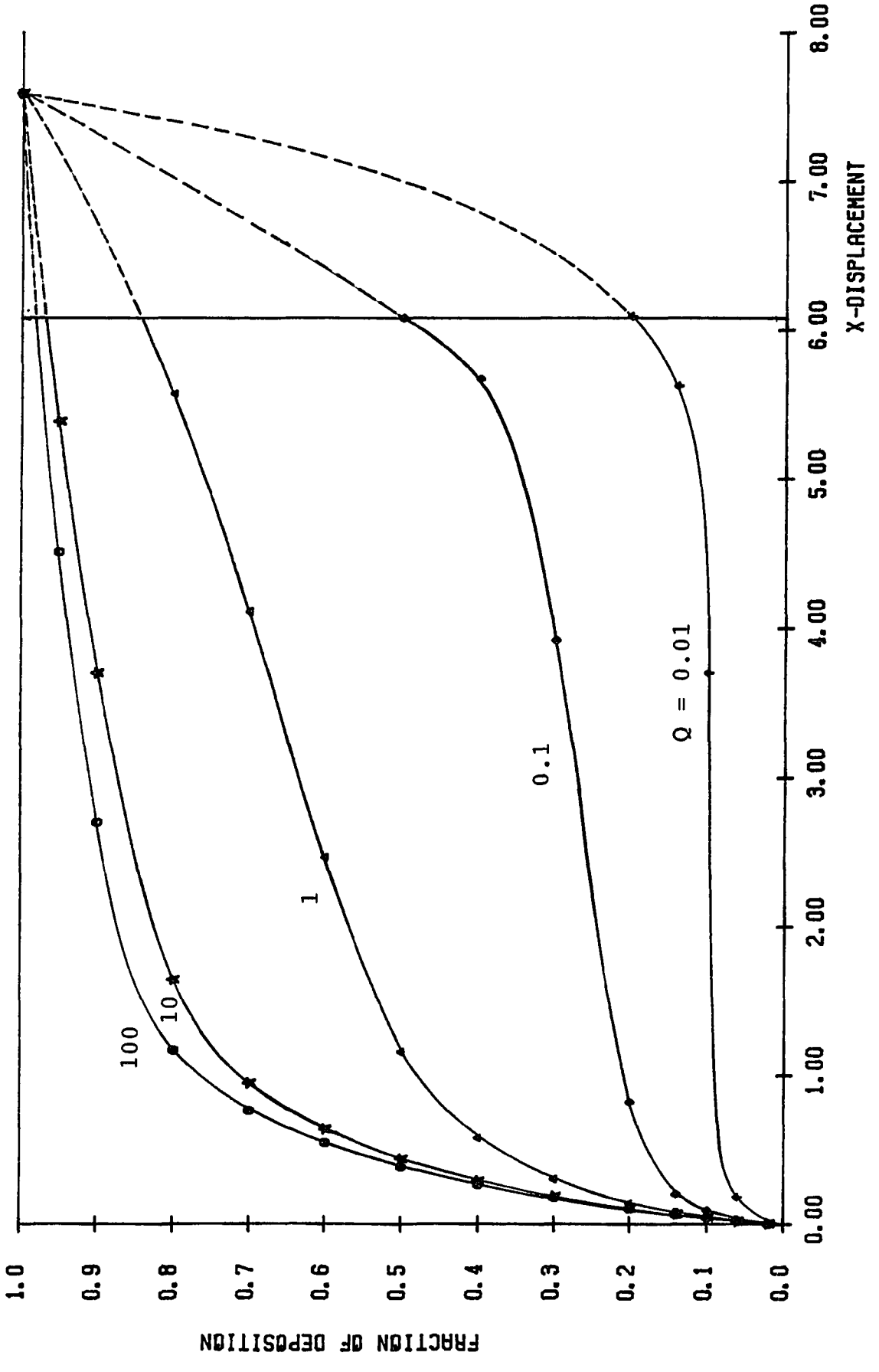

Fig. 5.11 Effect of Charge Parameter Q on Deposition for Uniform Flow in a Convergent Channel; $\theta = 7.5°$, $L = 6.07$, $St = 0$

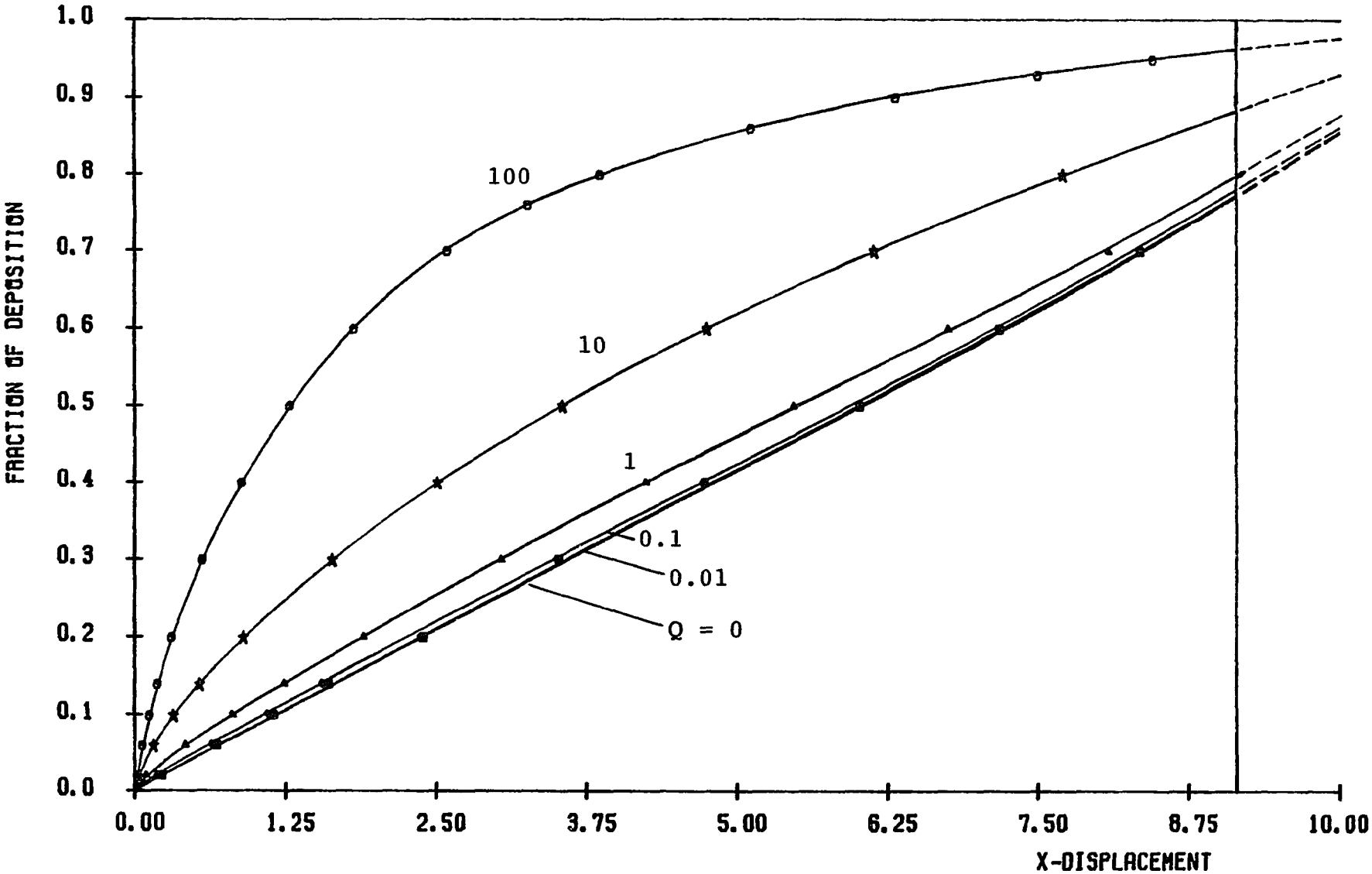

Fig. 5.12 Effect of Charge Parameter Q on Deposition for Uniform Flow in a Convergent Channel; $\theta = 5°$, $L = 9.14$, $St = 100$

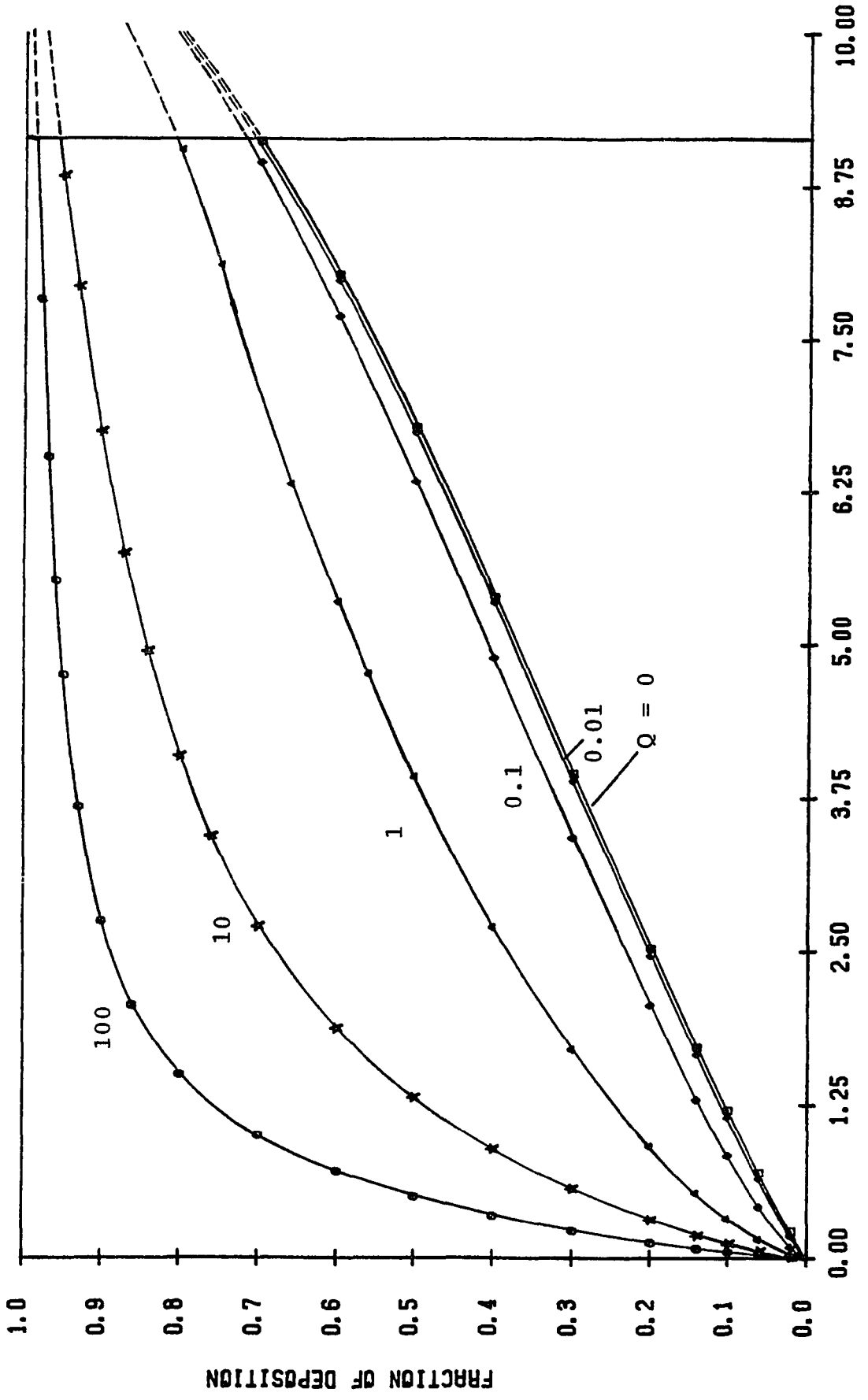

Fig. 5.13 Effect of Charge Parameter Q on Deposition for Uniform Flow in a Convergent Channel; $\theta = 5°$, $L = 9.14$, $St = 10$

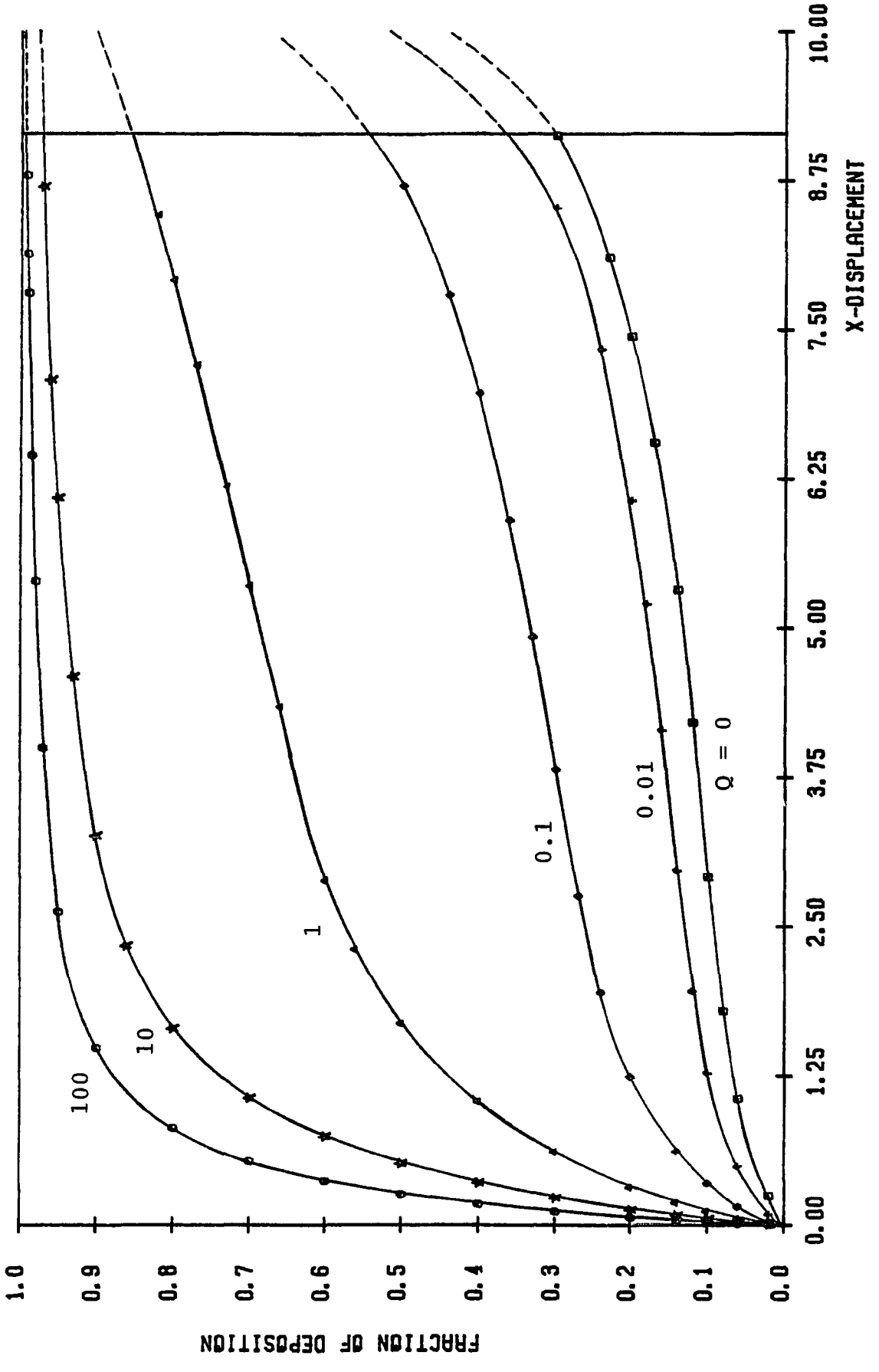

Fig. 5.14 Effect of Charge Parameter Q on Deposition for Uniform Flow in a Convergent Channel; $\theta = 5°$, $L = 9.14$, $St = 1$

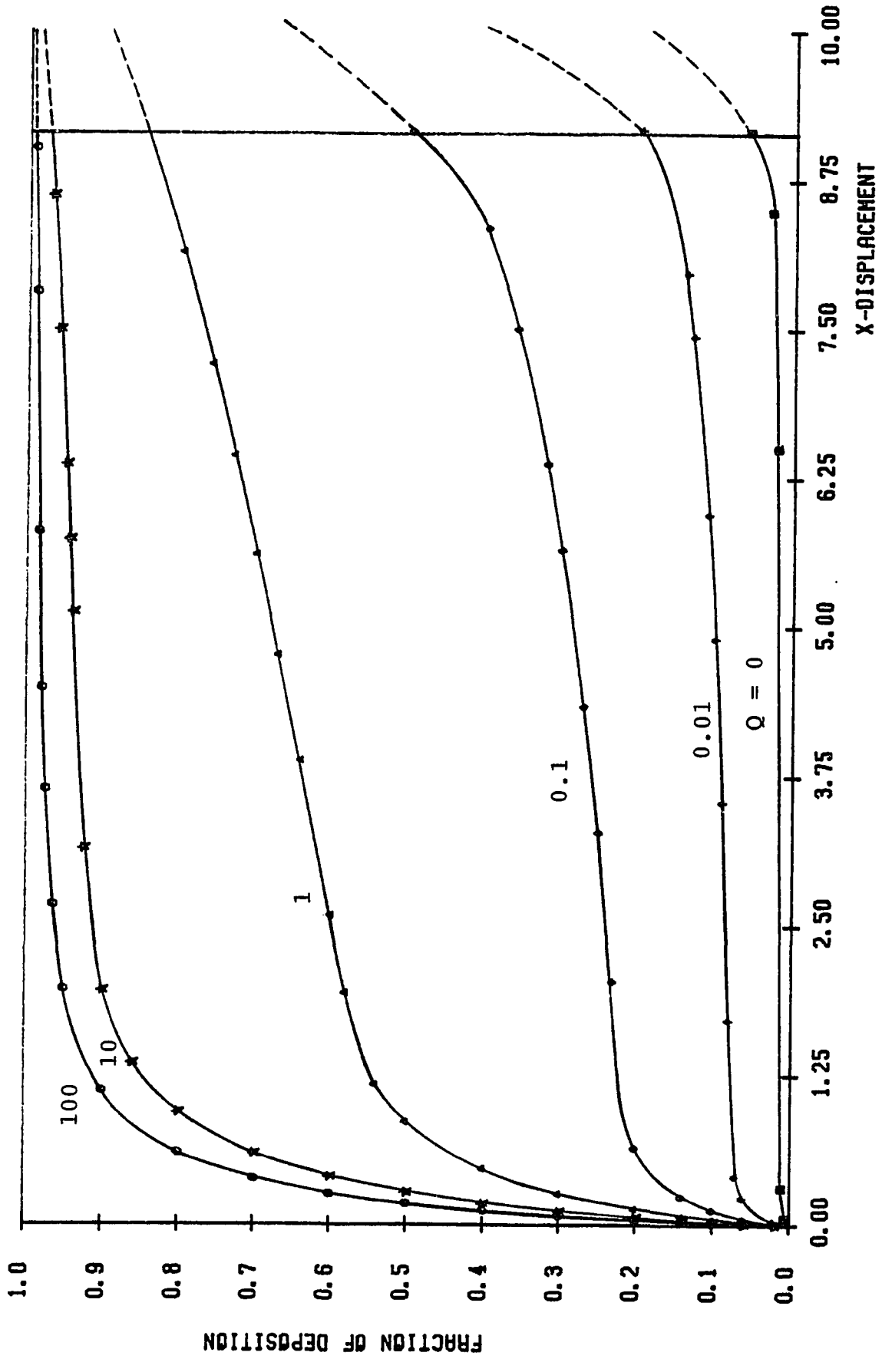

Fig. 5.15 Effect of Charge Parameter Q on Deposition for Uniform Flow in a Convergent Channel; $\theta = 5^{\circ}$, $L = 9.14$, $St = 0.1$

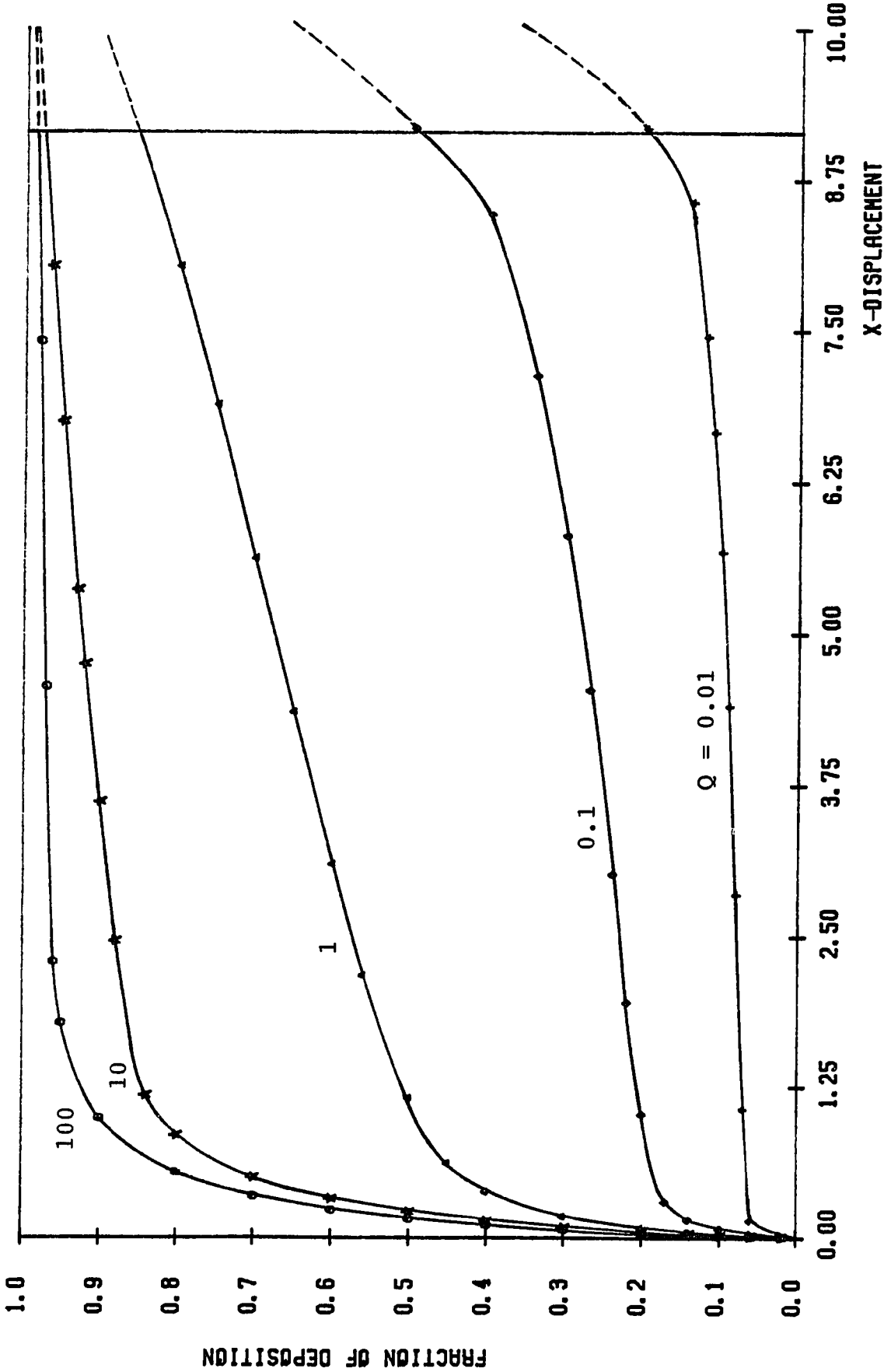

Fig. 5.16 Effect of Charge Parameter Q on Deposition for Uniform Flow in a Convergent Channel; $\theta = 5^{\circ}$, $L = 9.14$, $St = 0.01$

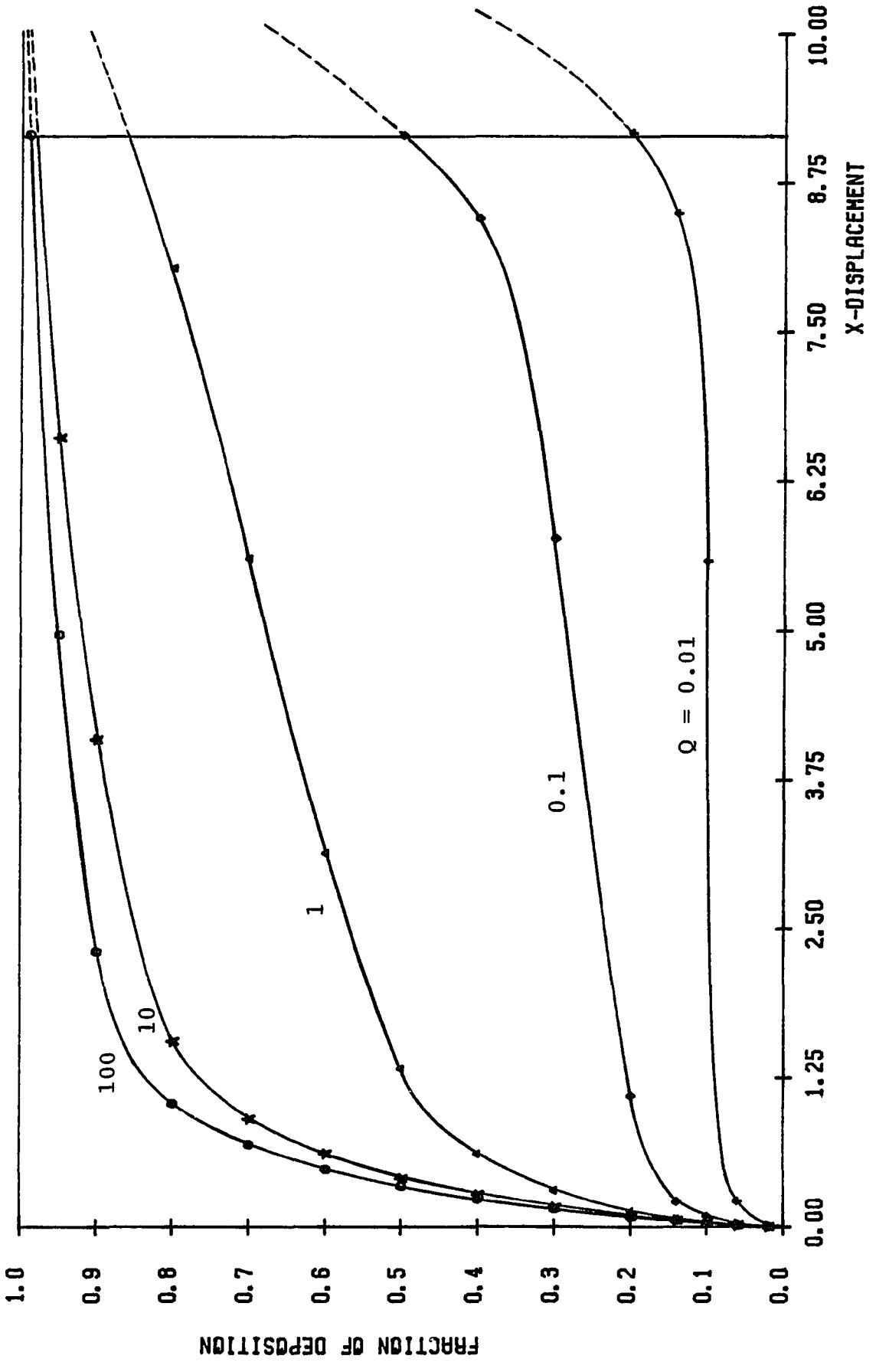

Fig. 5.17 Effect of Charge Parameter Q on Deposition for Uniform Flow in a Convergent Channel; $\theta = 5^{\circ}$, $L = 9.14$, $St = 0$

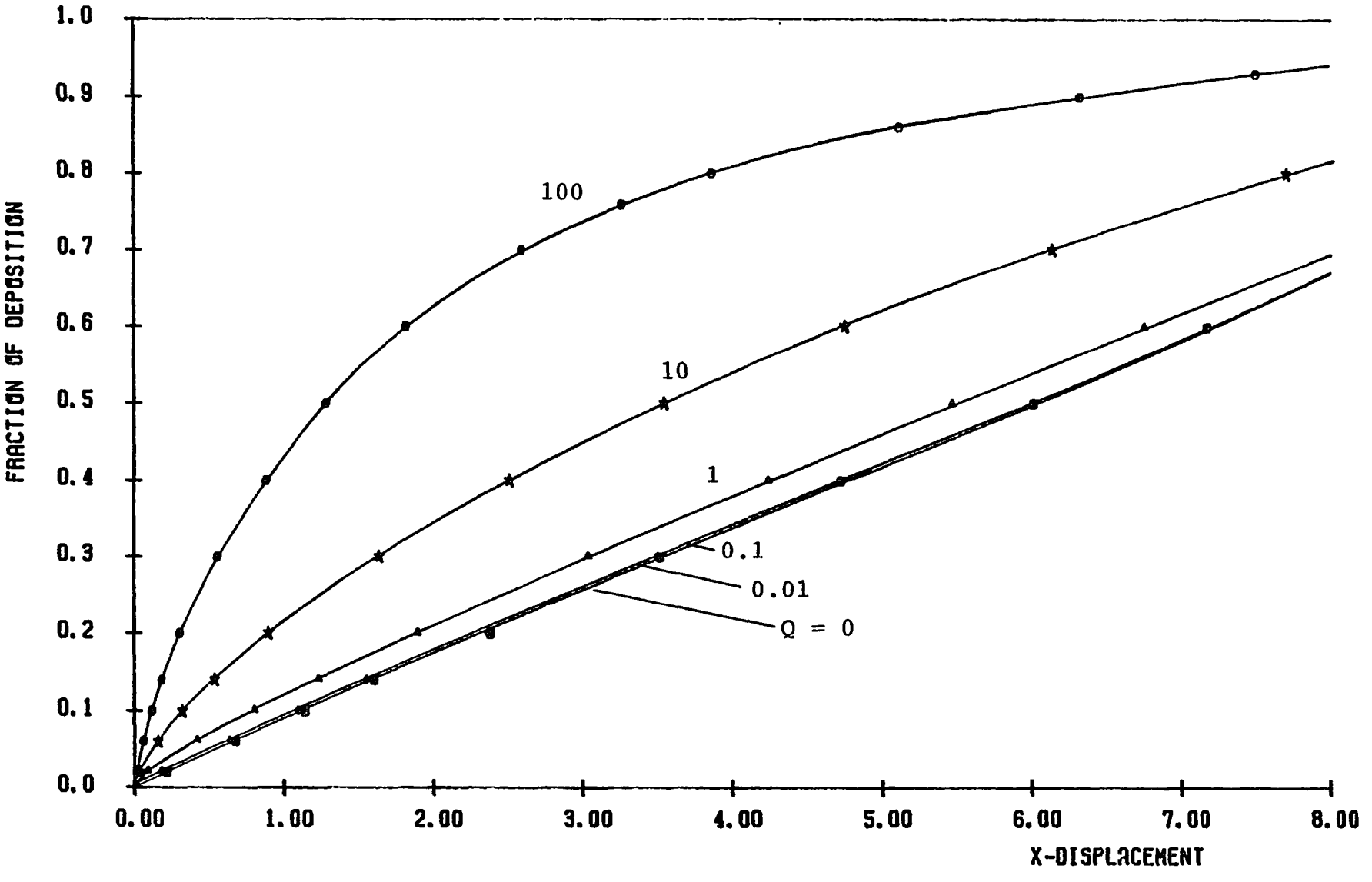

Fig. 5.18 Effect of Charge Parameter Q on Deposition for Uniform Flow in a Convergent Channel; $\theta = 5°$, $L = 9.14$, $St = 100$

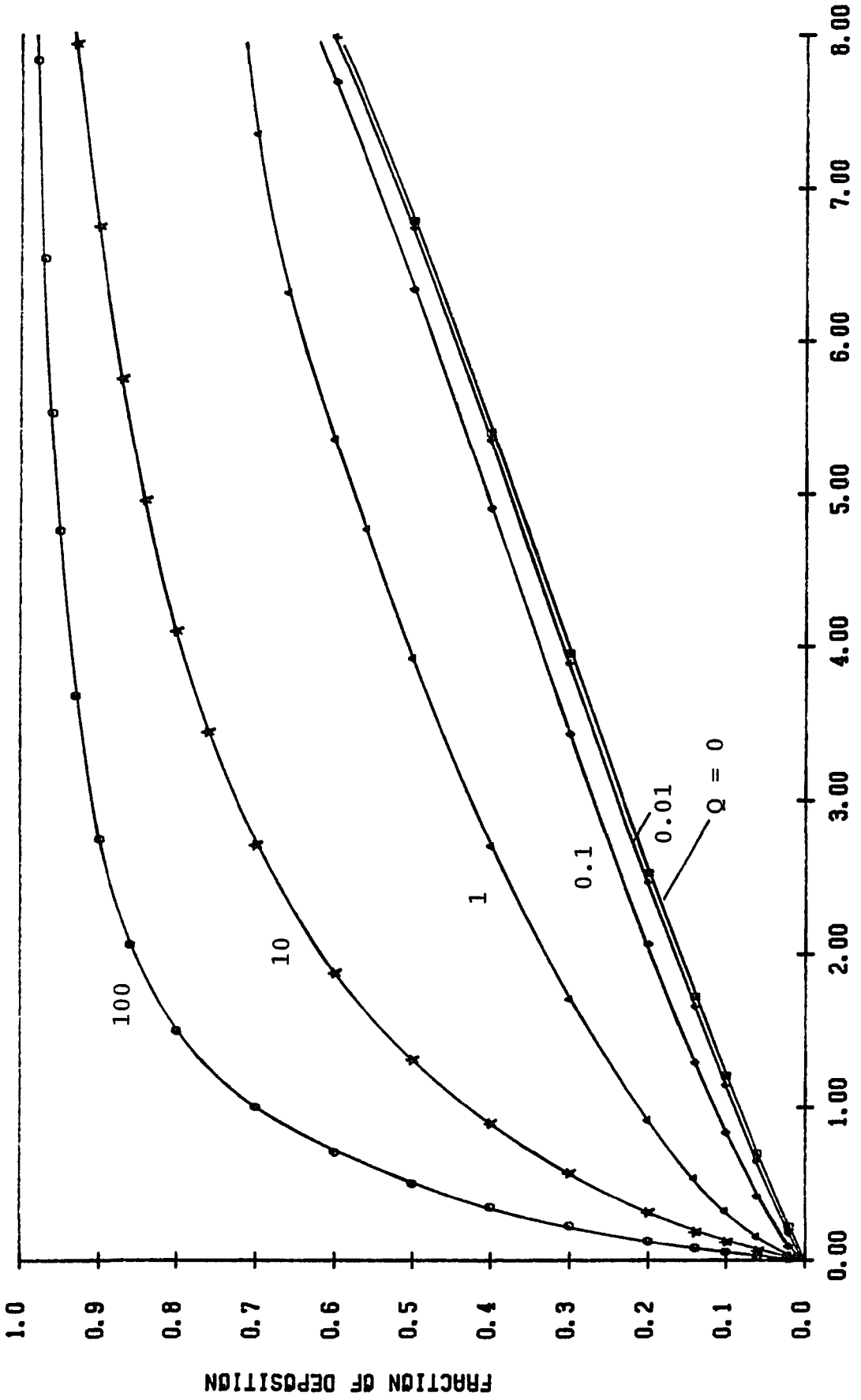

Fig. 5.19 Effect of Charge Parameter Q on Deposition for Uniform Flow in a Convergent Channel; $\theta = 5^{\circ}$, $L = 9.14$, $St = 10$

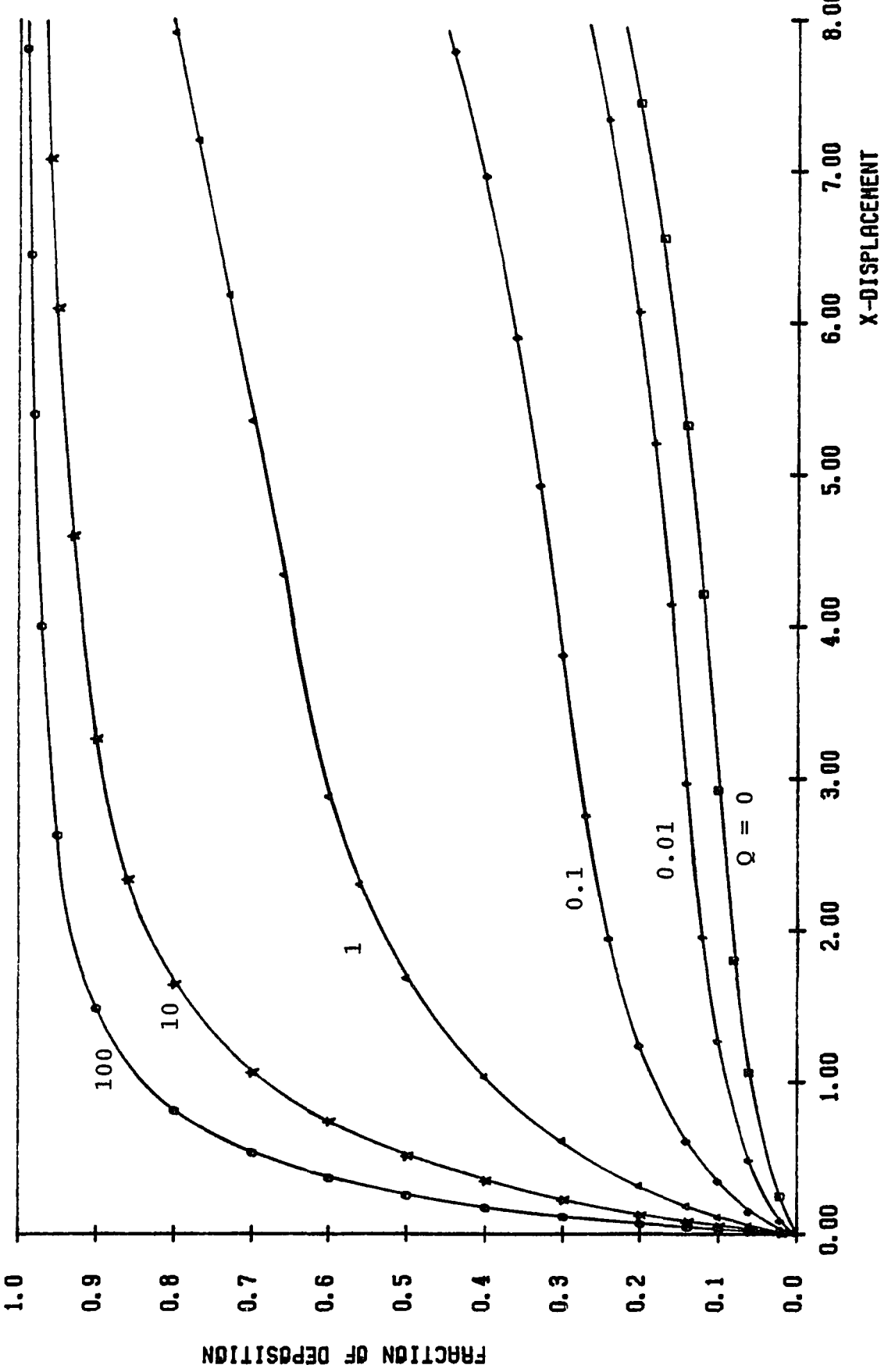

Fig. 5.20 Effect of Charge Parameter Q on Deposition for Uniform Flow in a Convergent Channel; $\theta = 5°$, $L = 9.14$, $St = 1$

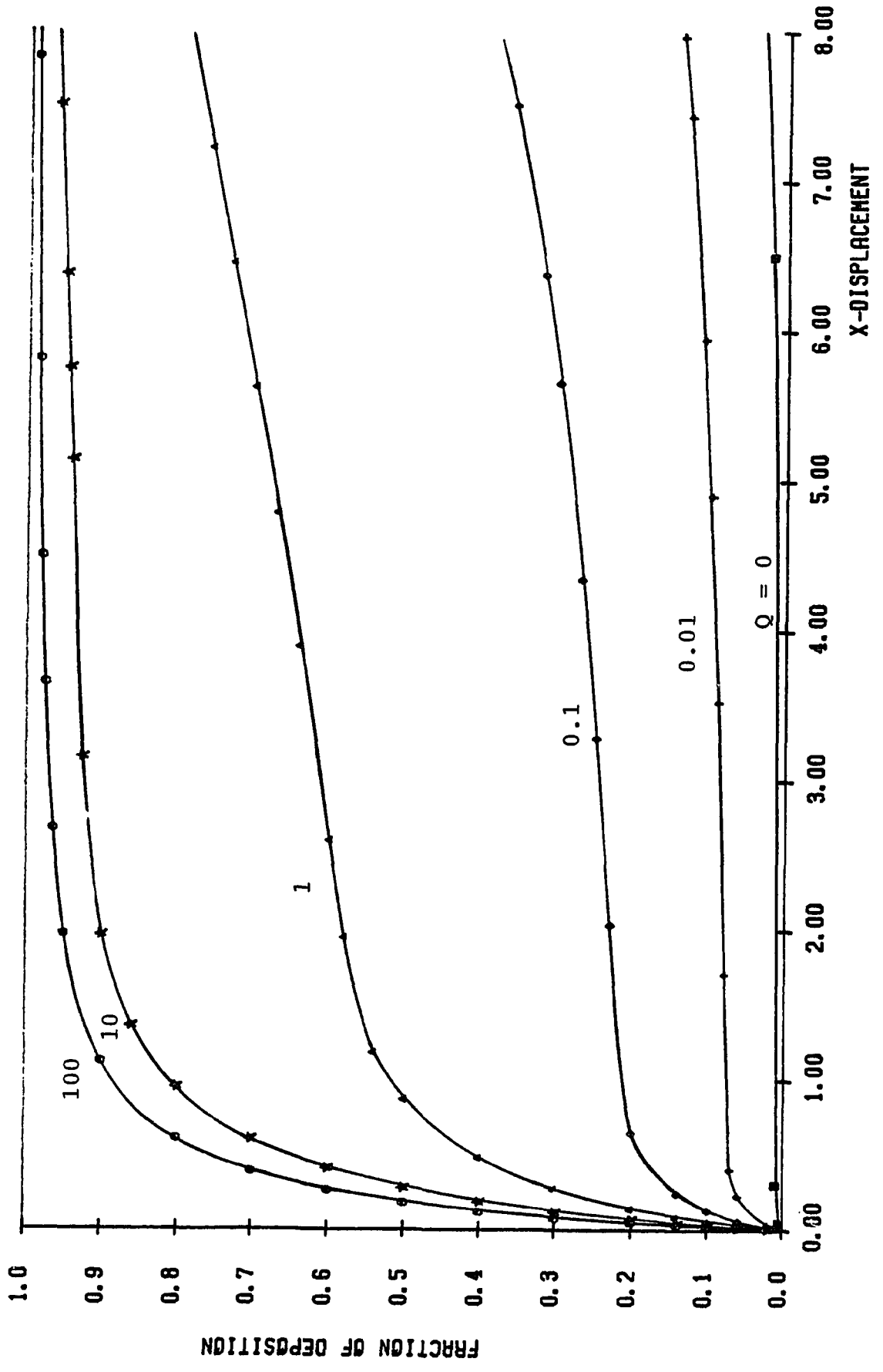

Fig. 5.21 Effect of Charge Parameter Q on Deposition for Uniform Flow in a Convergent Channel; $\theta = 5^{\circ}$, $L = 9.14$, $St = 0.1$

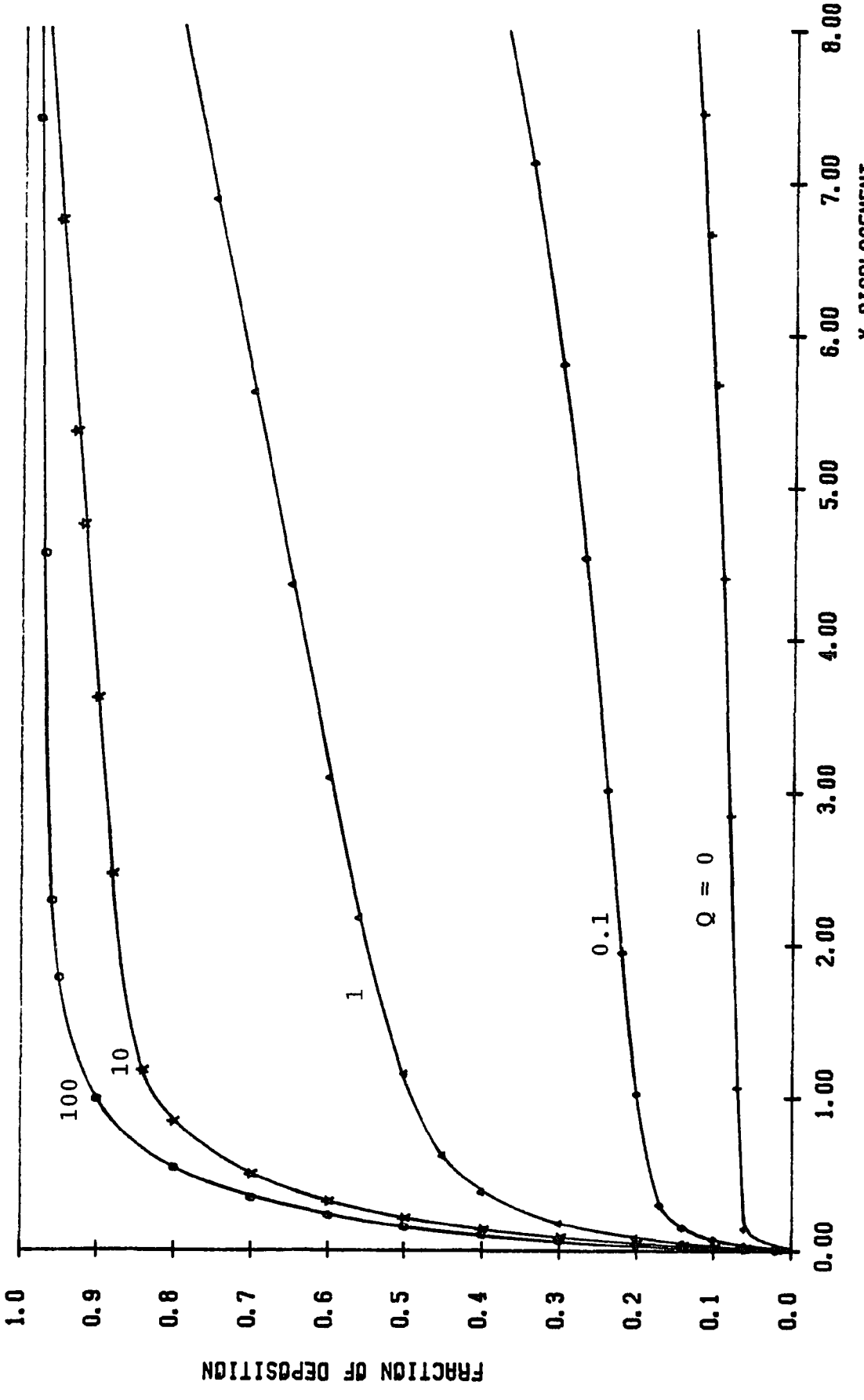

Fig. 5.22 Effect of Charge Parameter Q on Deposition for Uniform Flow in a Convergent Channel; $\theta = 5^{\circ}$, $L = 9.14$, $St = 0.01$

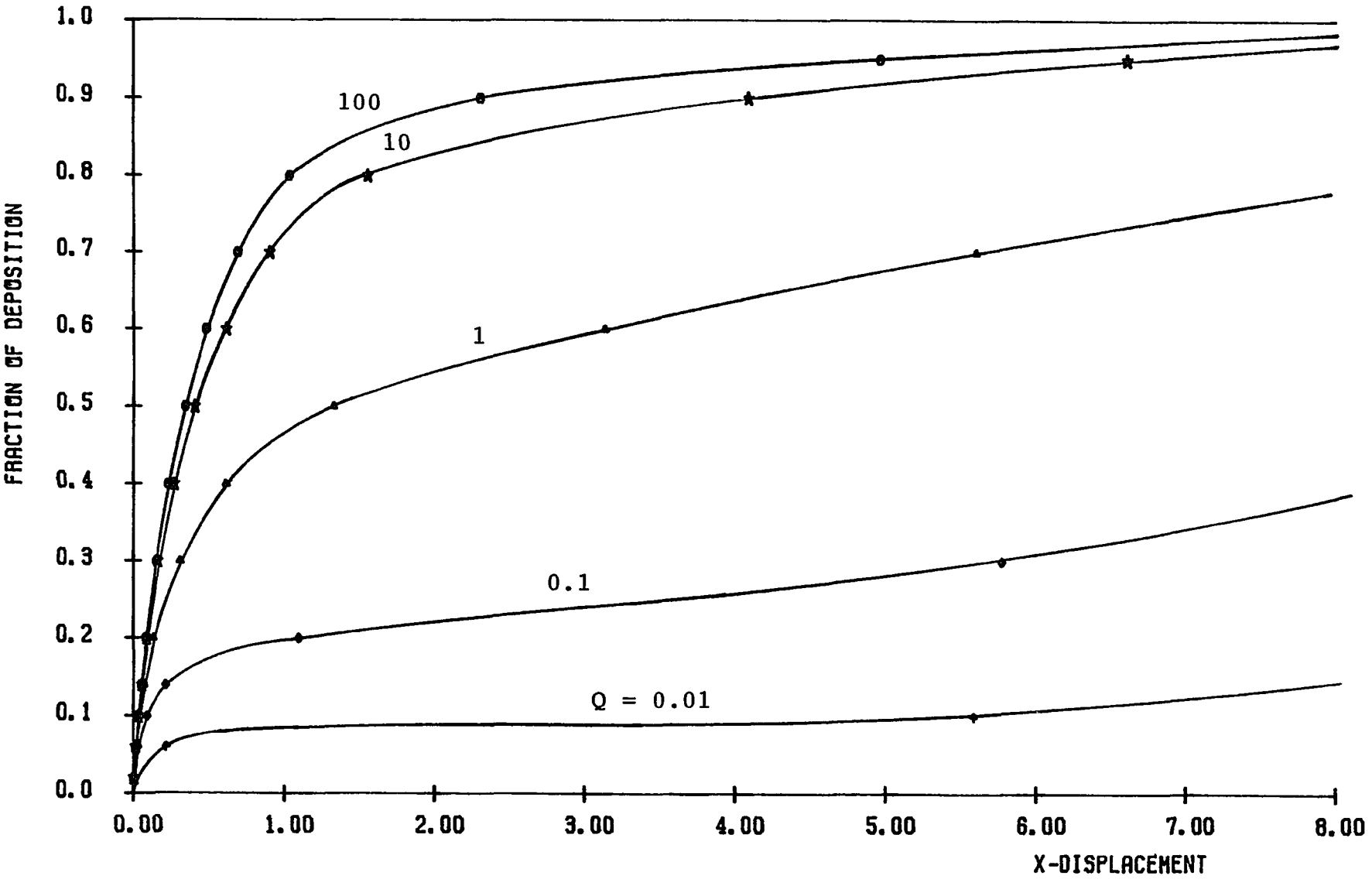

Fig. 5.23 Effect of Charge Parameter Q on Deposition for Uniform Flow in a Convergent Channel; $\theta = 5^\circ$, $L = 9.14$, $St = 0$

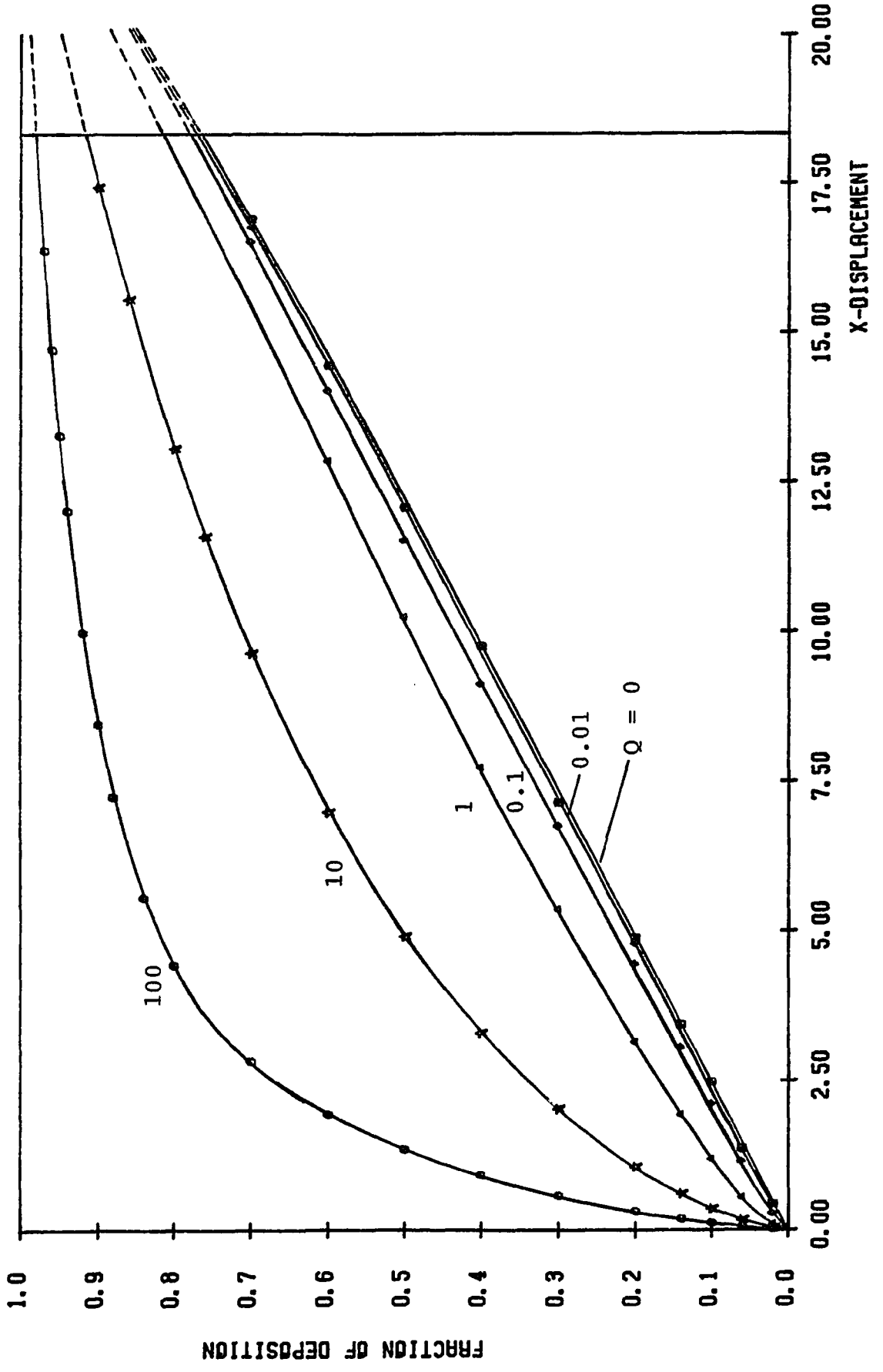

Fig. 5.24 Effect of Charge Parameter Q on Deposition for Uniform Flow in a Convergent Channel; $\theta = 2.5^{\circ}$, L = 18.3, St = 100

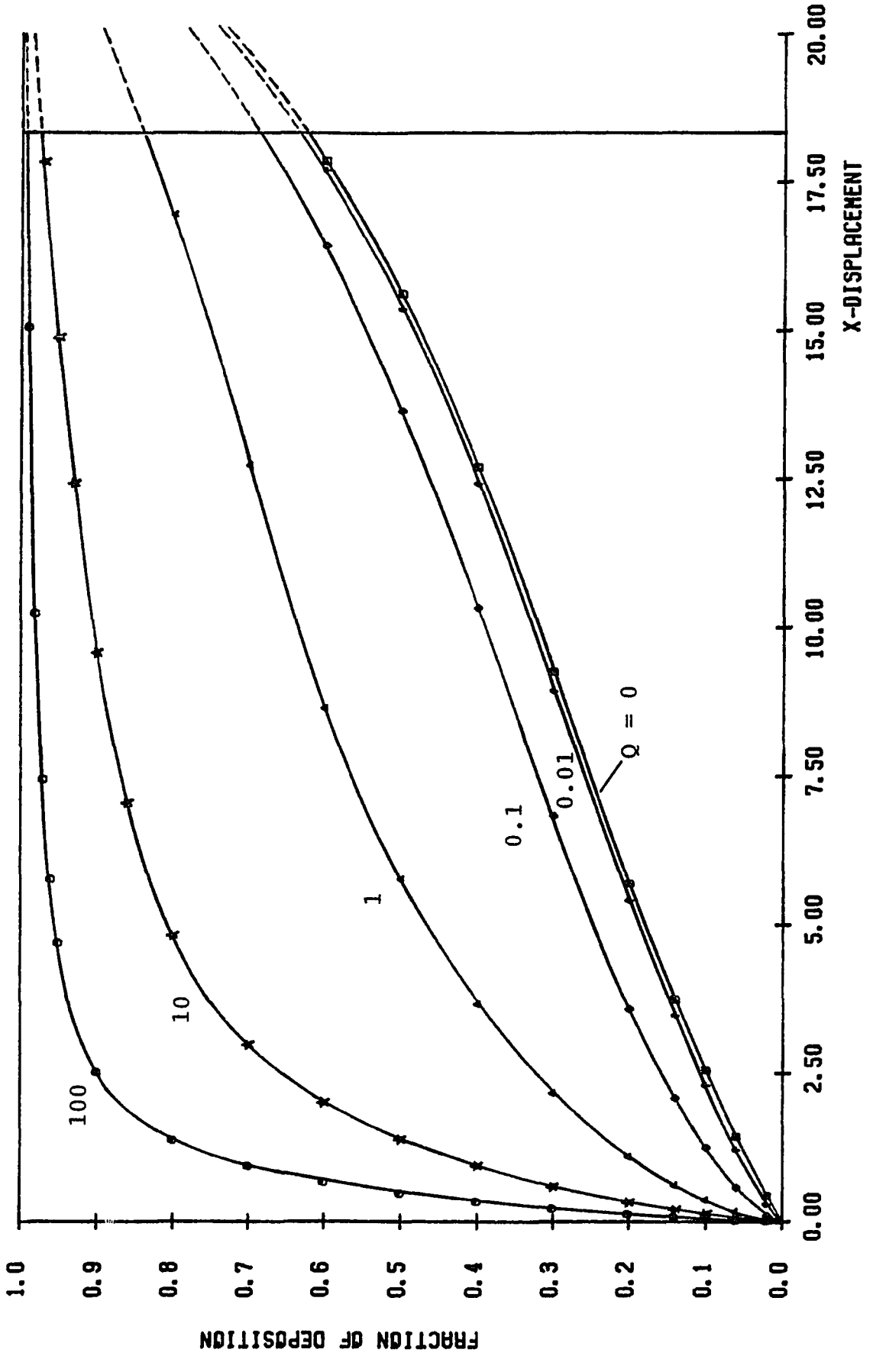

Fig. 5.25 Effect of Charge Parameter Q on Deposition for Uniform Flow in a Convergent Channel; $\theta = 2.5^{\circ}$, $L = 18.3$, $St = 10$

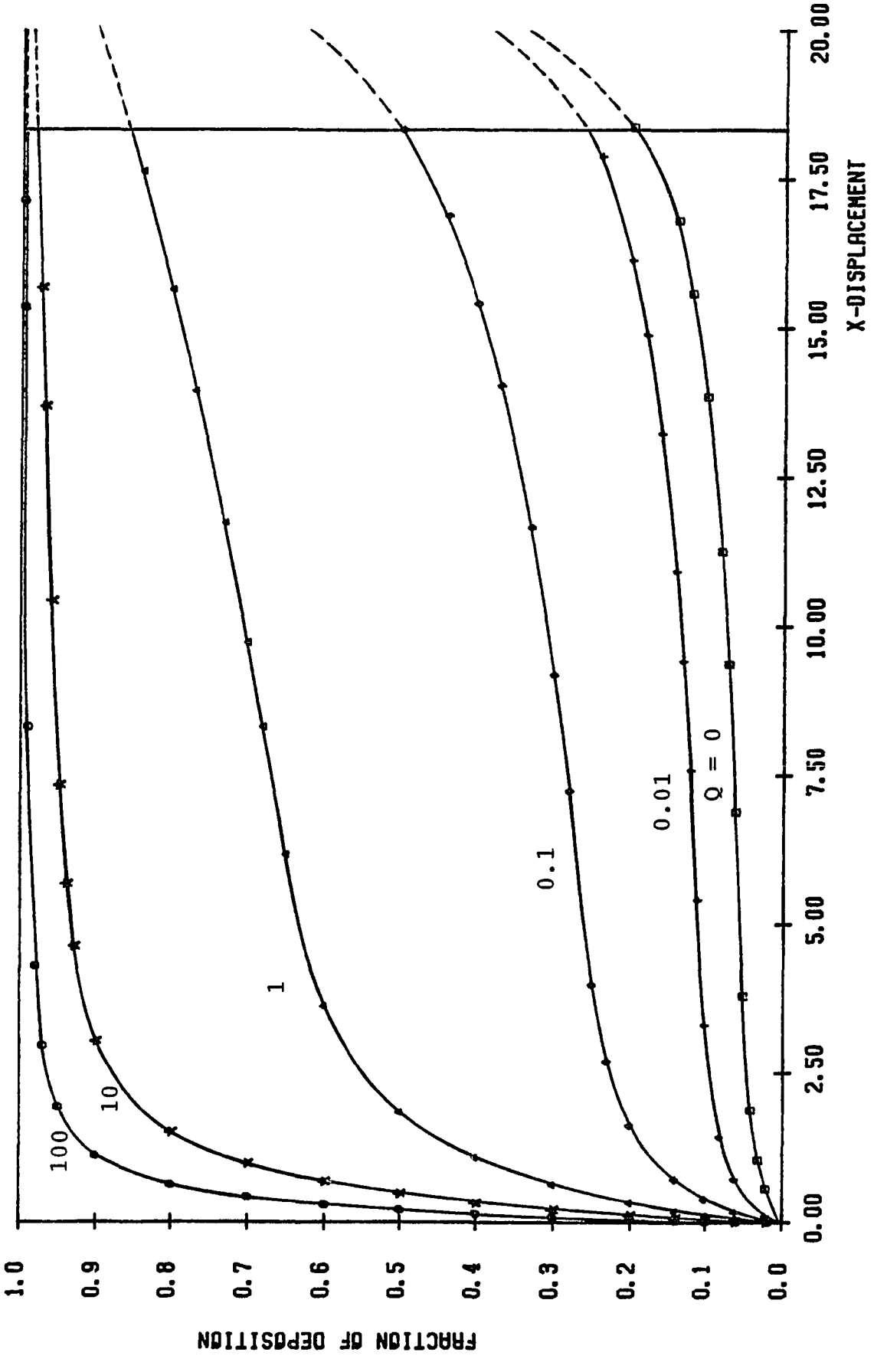

Fig. 5.26 Effect of Charge Parameter Q on Deposition for Uniform Flow in a Convergent Channel; $\theta = 2.5^{\circ}$, $L = 18.3$, $St = 1$

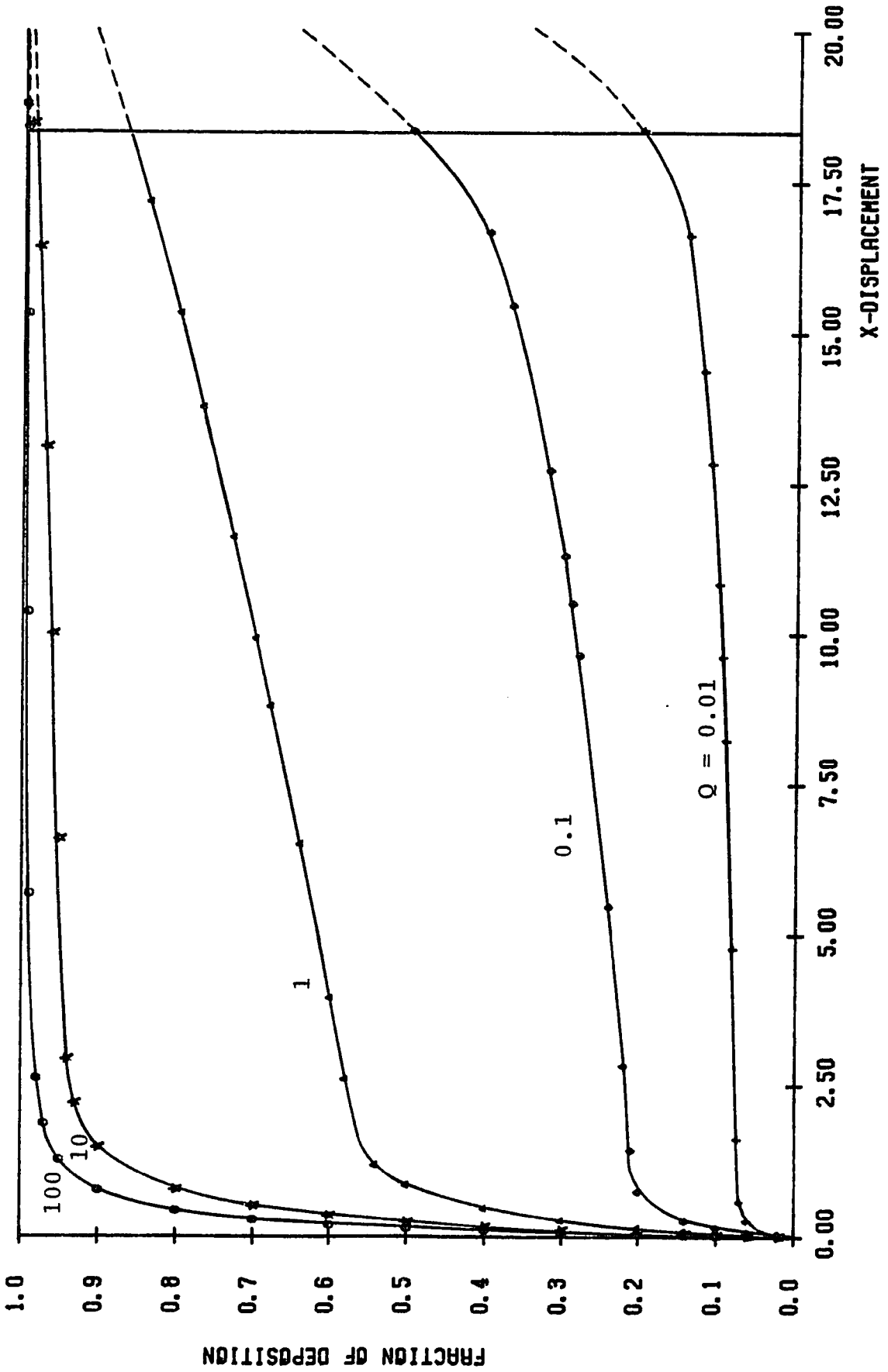

Fig. 5.27 Effect of Charge Parameter Q on Deposition for Uniform Flow in a Convergent Channel; $\theta = 2.5^{\circ}$, L = 18.3, St = 0.1

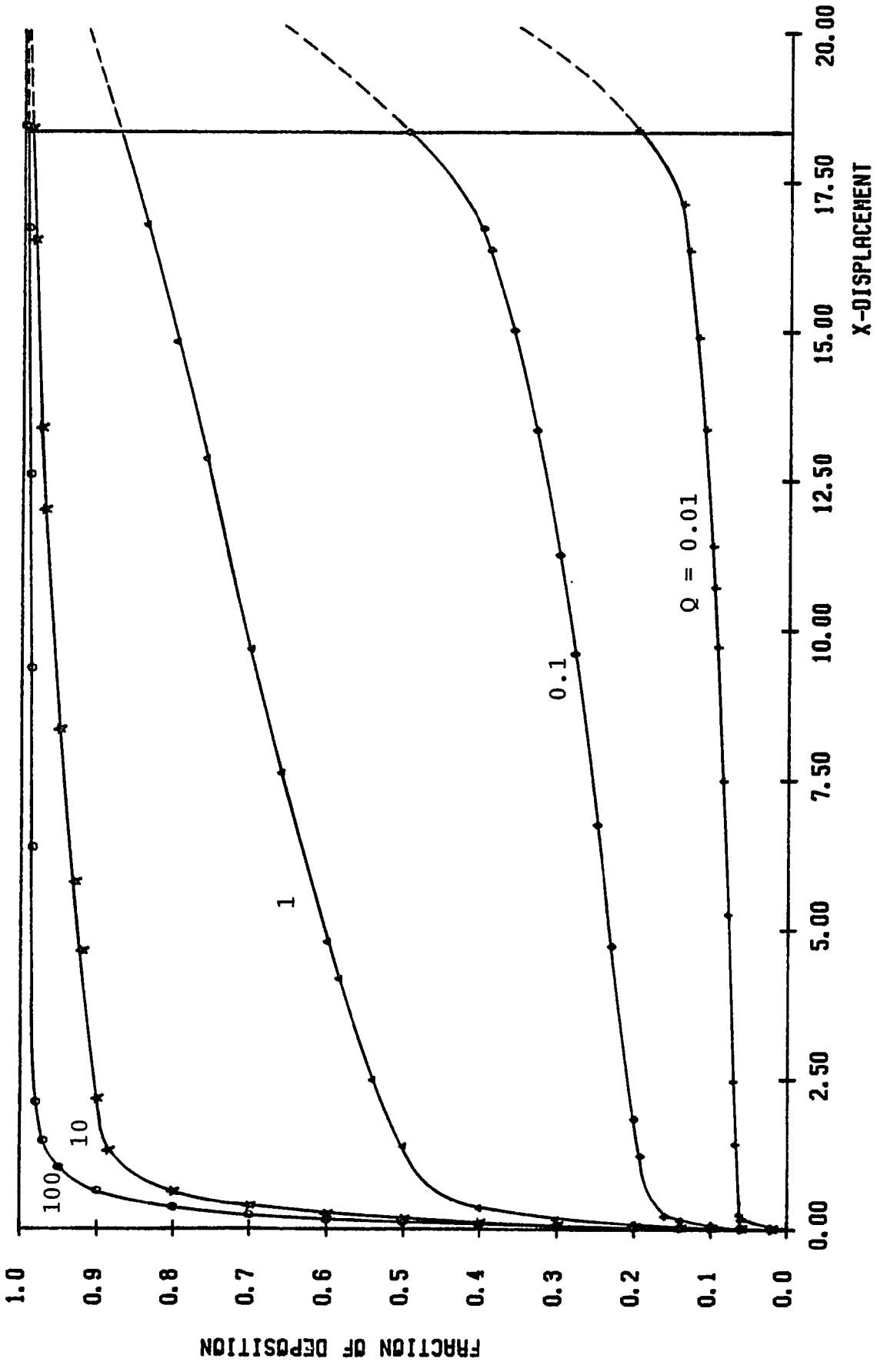

Fig. 5.28 Effect of Charge Parameter Q on Deposition for Uniform Flow in a Convergent Channel; $\theta = 2.5^{\circ}$, $L = 18.3$, $St = 0.01$

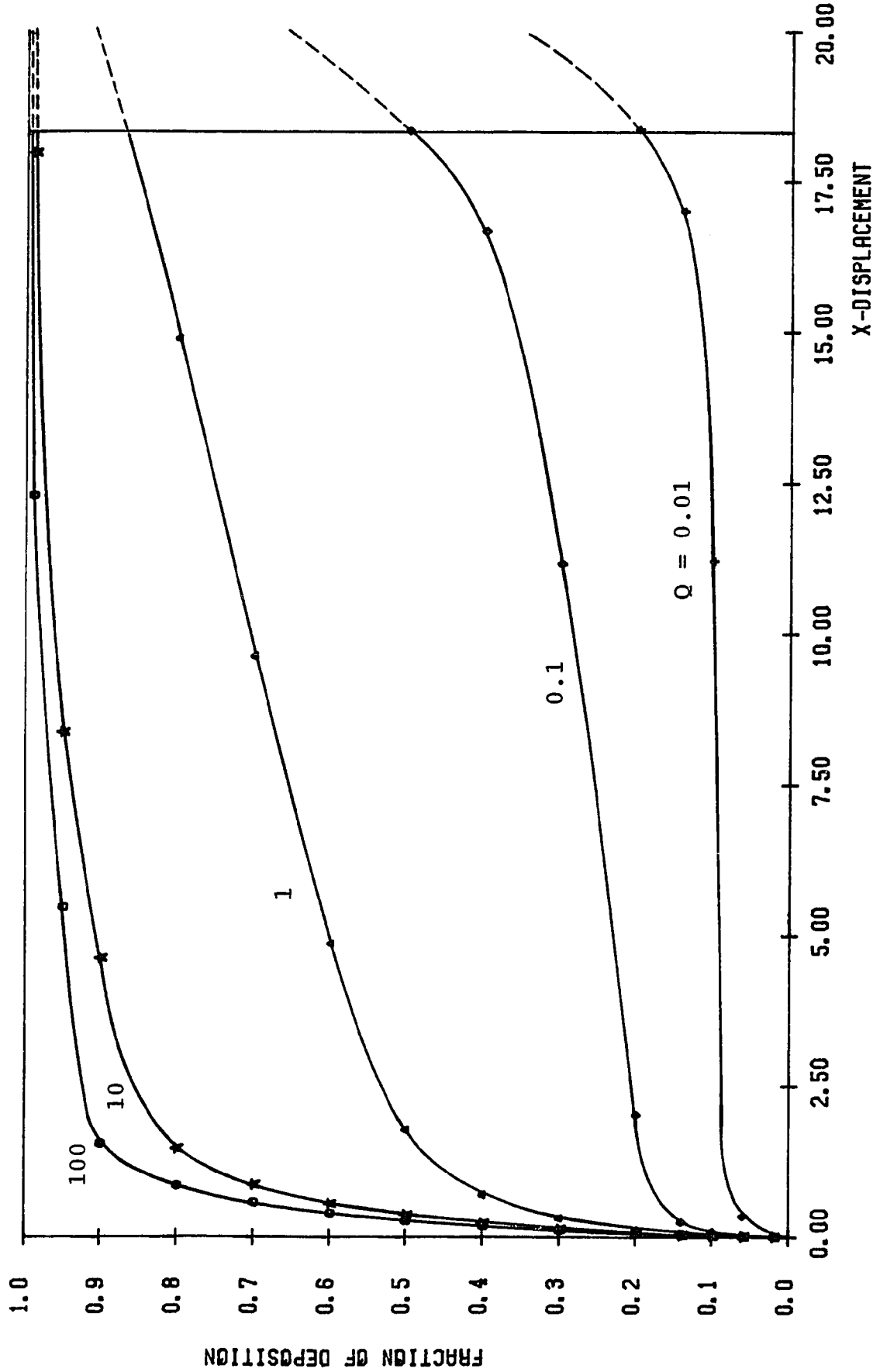

Fig. 5.29 Effect of Charge Parameter Q on Deposition for Uniform Flow in a Convergent Channel; $\theta = 2.5°$, $L = 18.3$, $St = 0$

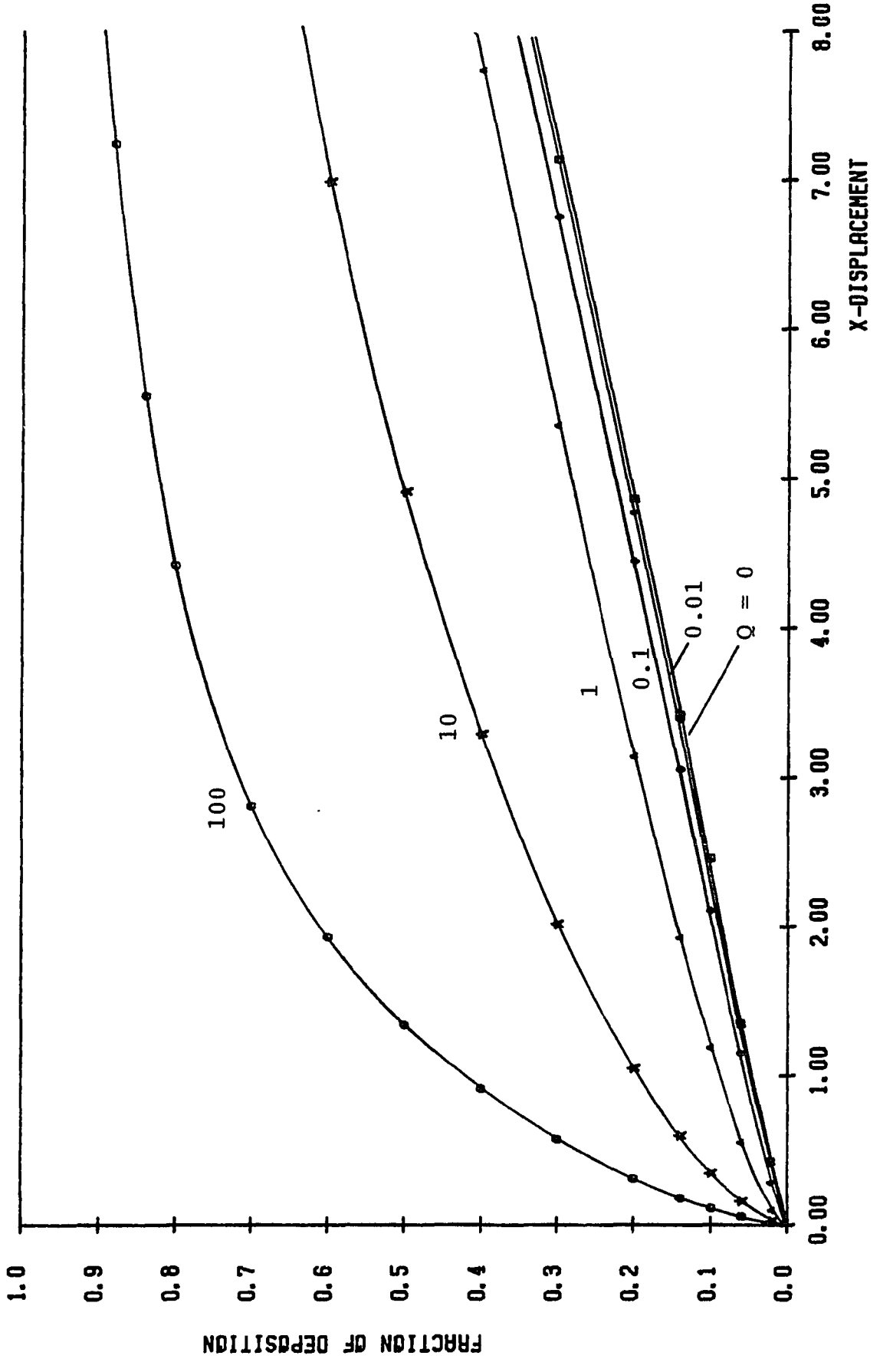

Fig. 5.30 Effect of Charge Parameter Q on Deposition for Uniform Flow in a Convergent Channel; $\theta = 2.5^{\circ}$, L = 18.3, St = 100

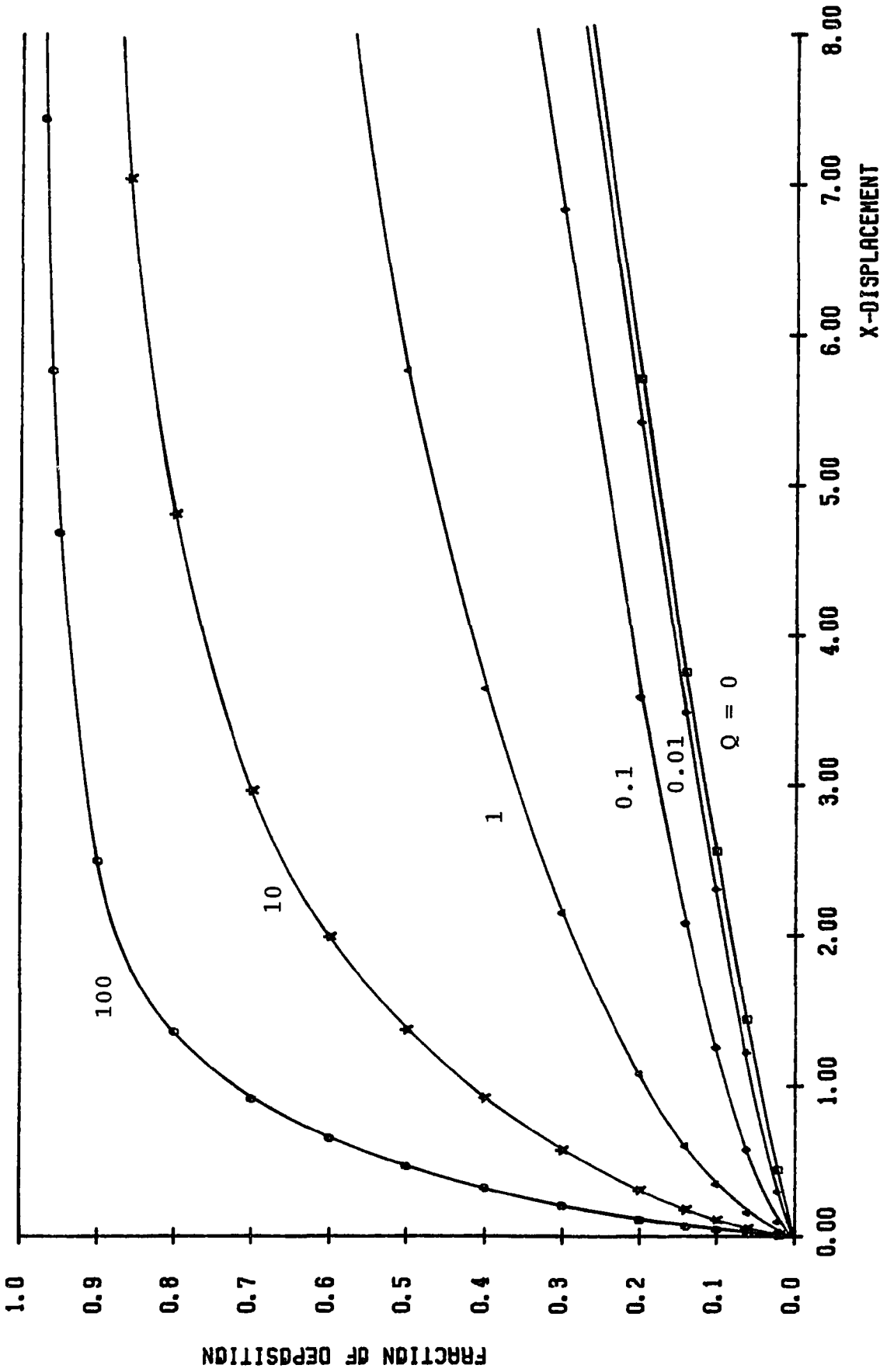

Fig. 5.31 Effect of Charge Parameter Q on Deposition for Uniform Flow in a Convergent Channel; $\theta = 2.5^{\circ}$, L = 18.3, St = 10

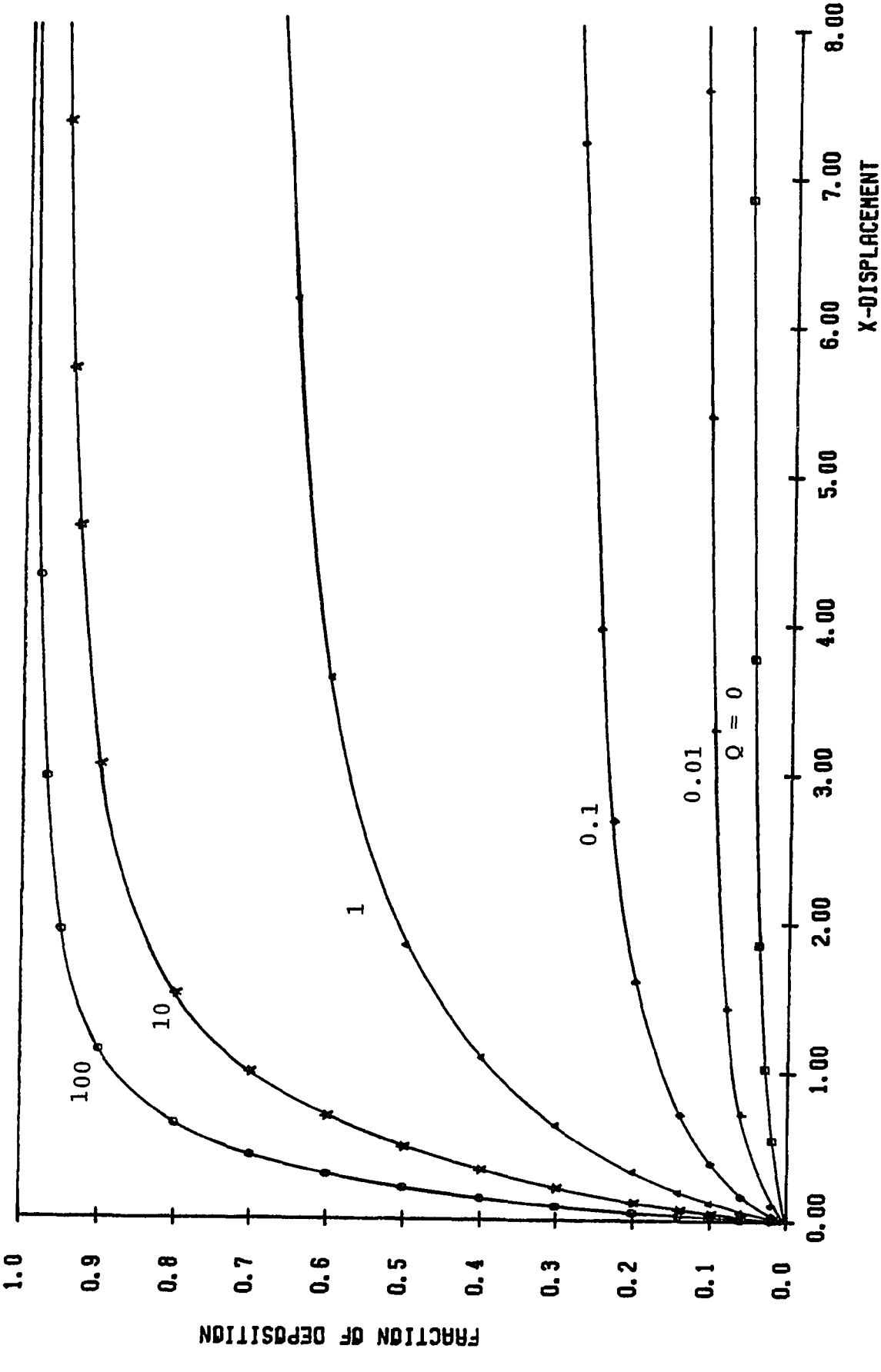

Fig. 5.32 Effect of Charge Parameter Q on Deposition for Uniform Flow in a Convergent Channel; $\theta = 2.5°$, $L = 18.3$, $St = 1$

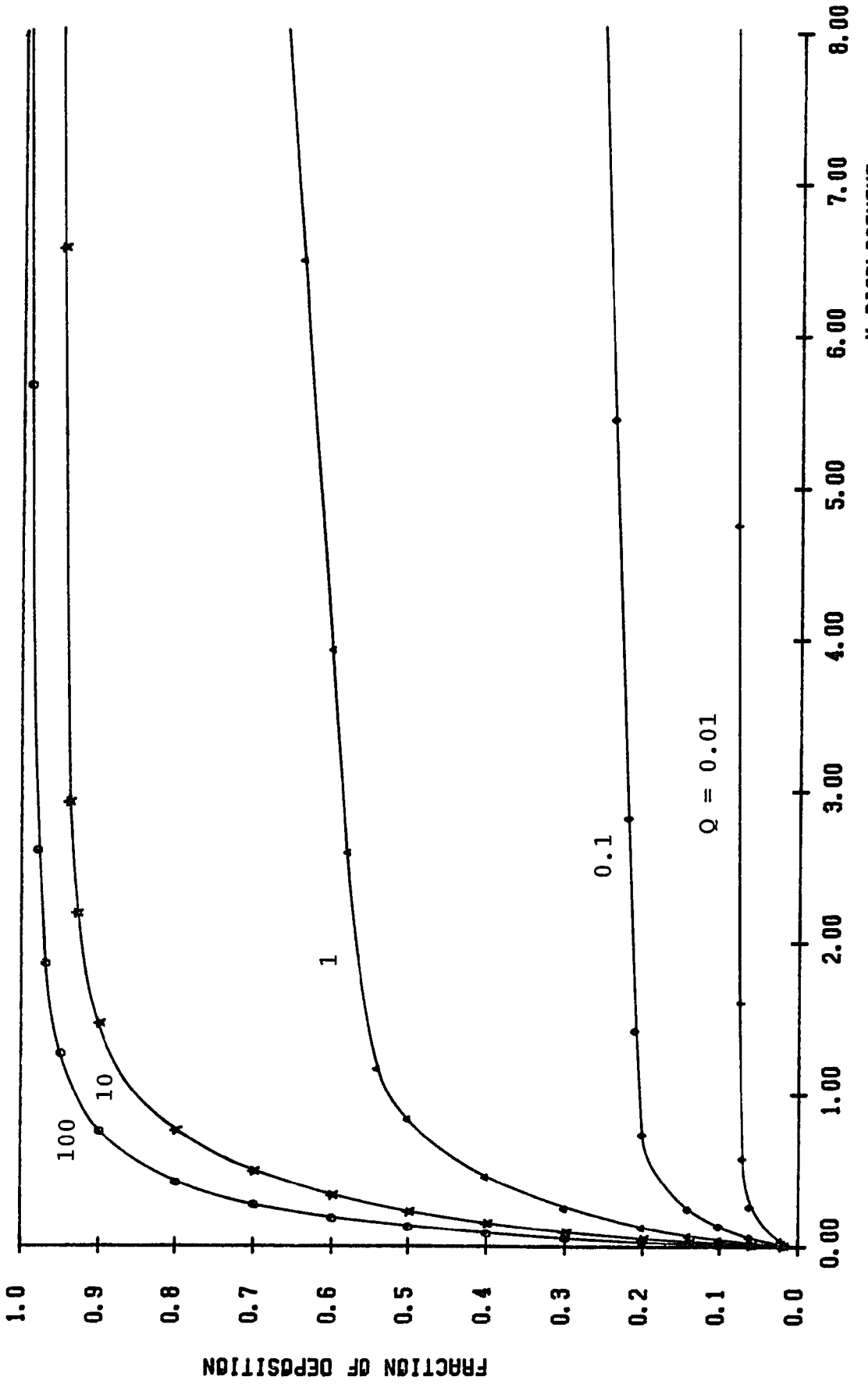

Fig. 5.33 Effect of Charge Parameter Q on Deposition for Uniform Flow in a Convergent Channel; $\theta = 2.5^{\circ}$, $L = 18.3$, $St = 0.1$

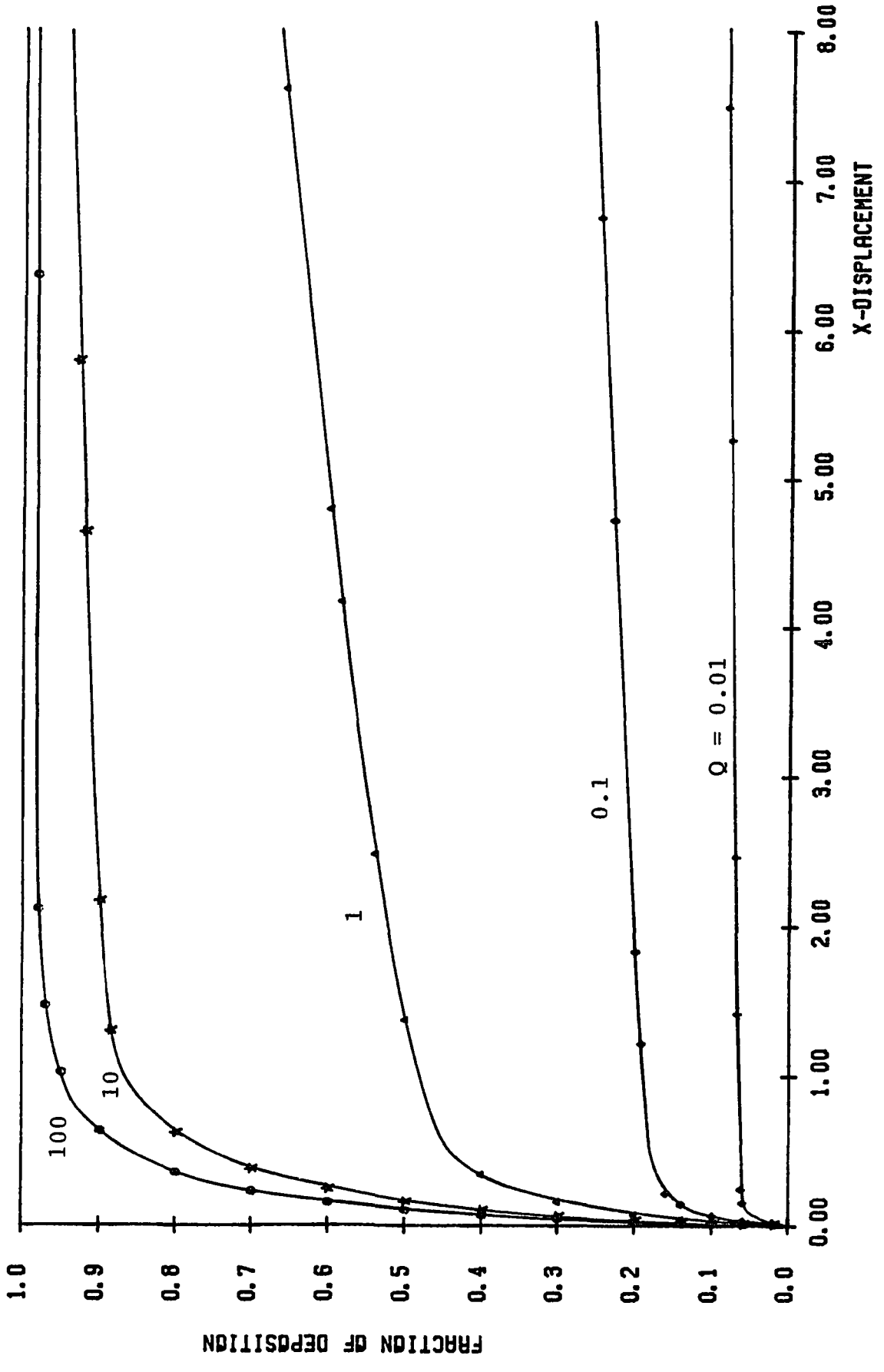

Fig. 5.34 Effect of Charge Parameter Q on Deposition for Uniform Flow in a Convergent Channel; $\theta = 2.5^{\circ}$, L = 18.3, St = 0.01

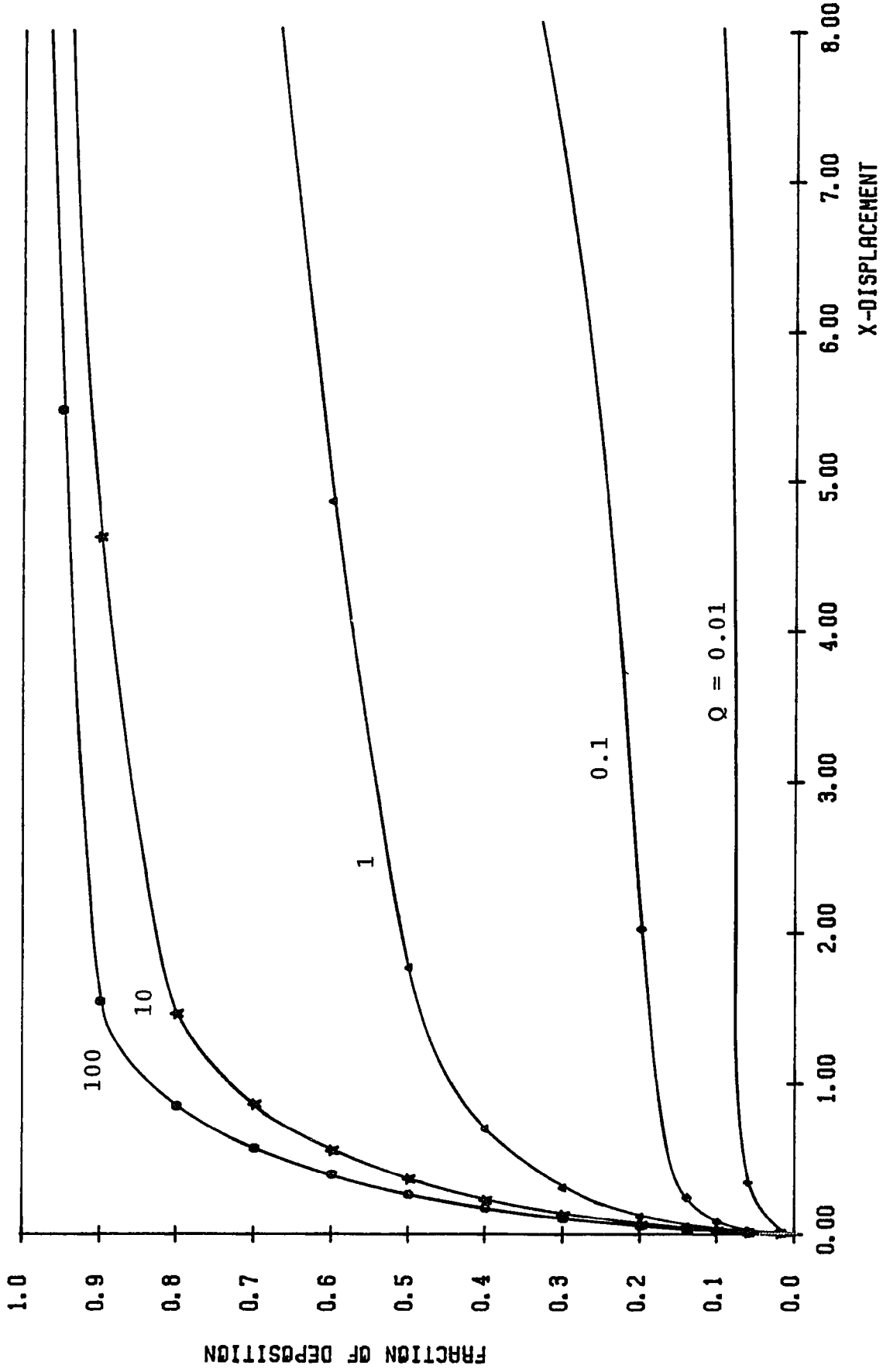

Fig. 5.35 Effect of Charge Parameter Q on Deposition for Uniform Flow in a Convergent Channel; $\theta = 2.5°$, $L = 18.3$, $St = 0$

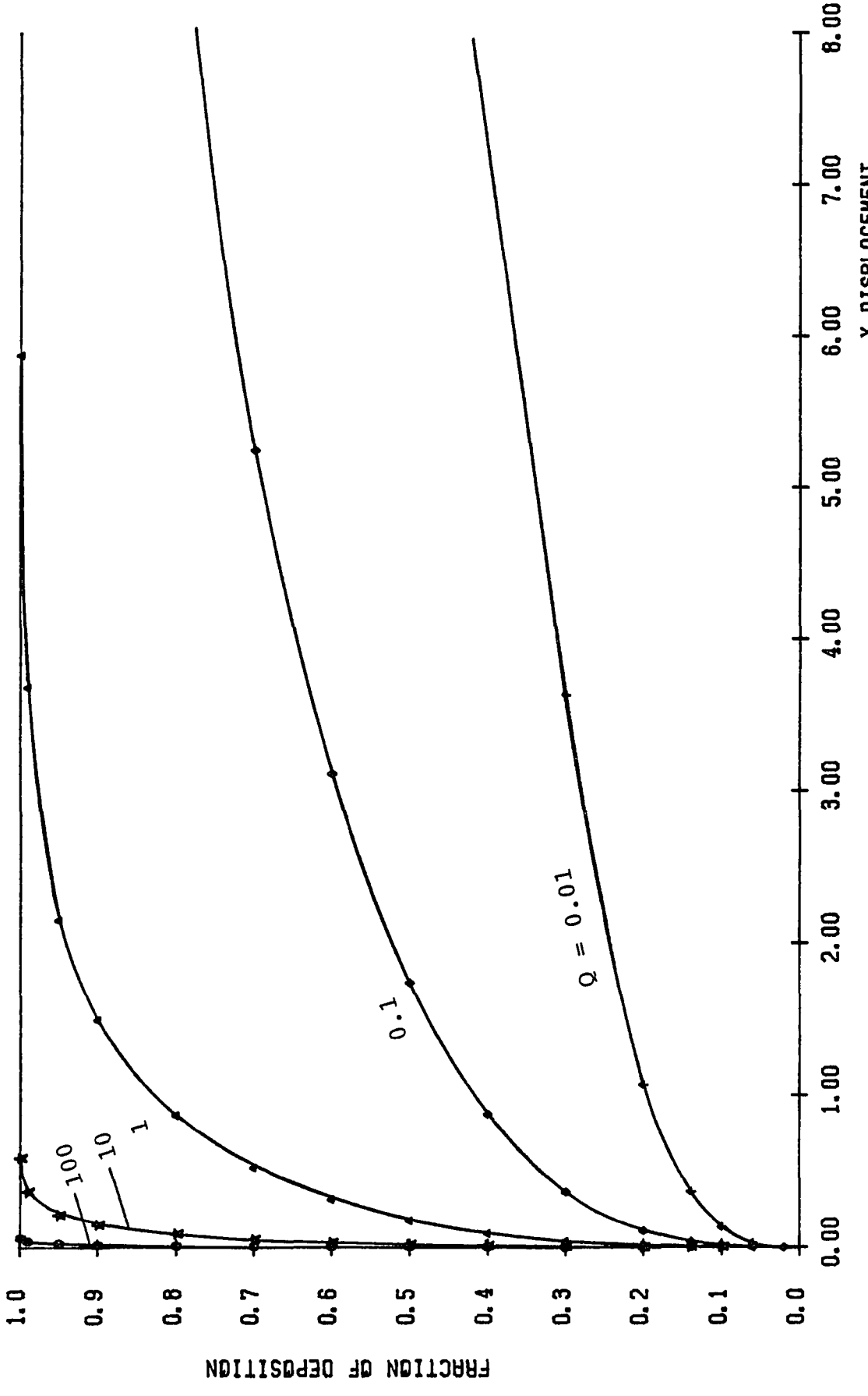

Fig. 5.36 Effect of Charge Parameter Q on Deposition for Uniform Flow in a Parallel Plate Channel; $\theta = 0°$, $L = 12.5$, $St = 0$

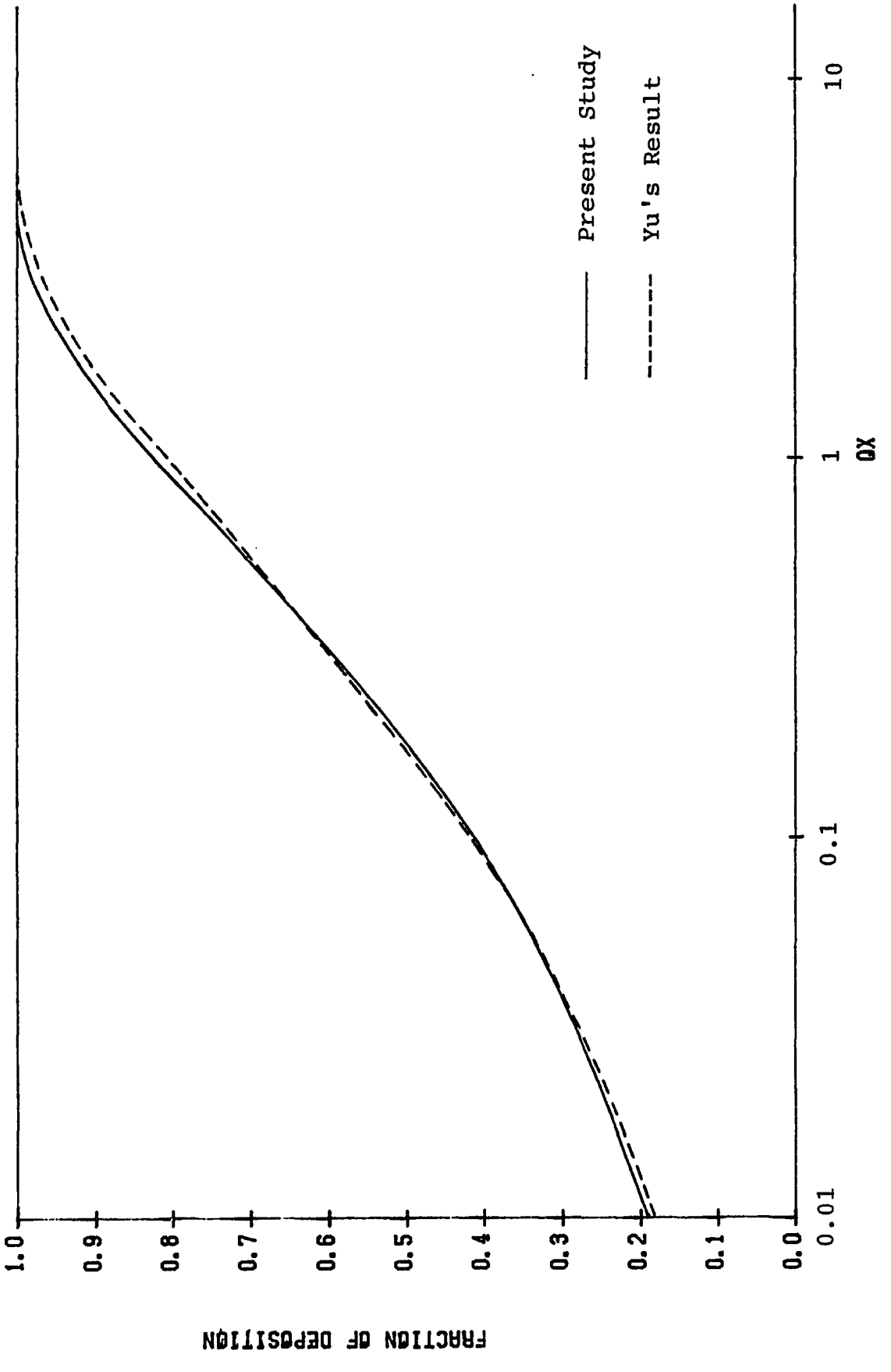

Fig. 5.37 Comparison of Deposition in a Parallel Plate Channel with Yu and Chandra's Result; $\theta = 0°$, $St = 0$

VITA

Name: HUI, Kwok Wah

Degree and Date to be conferred: D. Eng. Sci., 1986

Secondary Education: Hong Kong Pui Ching Middle School, 1969

Collegiate Institutions attended	Dates	Degree (Year)
New Jersey Institute of Technology	9/82-3/86	D.Eng.Sc.1986
Stevens Institute of Technology	9/80-6/82	M.S.M.E. 1983
Imperial College of Science and Technology University of London, England	9/73-3/75	M.S.A.E. 1975
National Cheng Kung University Tainan, Taiwan	9/69-6/73	B.S.M.E. 1973

Major: Mechanical Engineering

Minor: Aeronautical Engineering, Computer Science

Positions held:

9/84-Present	Product Engineer Borg-Warner Air-Conditioning, Inc. York, Pennsylvania, U.S.A.
9/82-8/84	Research Assistant, N.J.I.T.
6/83-8/83	Adjunct Instructor, N.J.I.T.
9/80-8/82	Research Assistant, Stevens Tech.
6/76-7/80	Assistant Research Scientist Chung Shan Institute of Science and Tech. Lung Tan, Taiwan, R.O.C.
8/75-3/76	Mechanical Designer Coronet Industries Ltd., Hong Kong

AFFILIATION:

American Society of Mechanical Engineers
American Institute of Aeronautics & Astronautics
Royal Aeronautical Society (England)

PUBLICATION:

1. "Performance Characteristics Investigation of the LTD-53 and the LTD-53 Check Compressors", Assignment number 3513, Borg-Warner Air-Conditioning, Inc., 11/1985.

2. "Performance Characteristics Investigation on the LTK-144 Compressor with Radial Vaned Diffuser", Assignment number 3443, Borg-Warner Air-Conditioning, Inc., 9/1985.

3. "Performance Characteristics Investigation of the YTH-76 Compressor", Assignment number 3513, Borg-Warner Air-Conditioning, Inc., 9/1985.

4. "Performance Characteristics Investigation on the City-Hall Annex LTD-108 Compressor", Assignment number 3517, Borg-Warner Air-Conditioning, Inc., 4/1985.

5. "Performance Characteristics Based on the LTK-131 Flange to Flange Test Data", Assignment number 3443, Borg-Warner Air-Conditioning, Inc. 3/1985.

6. "Inspection of the T-131 Impeller Casting from the Morris Bean Company", Assignment no. 3443, Borg-Warner Air-Conditioning, Inc., 10/1984.

7. "Design and Flight Test Analysis of B3-5 CF-02 Angle of Attack Sensor", Chung Shan Institute Technical Report CSITR-68B-29, 8/1979.

8. "Aerodynamic and Ballistic Conceptual Design of a Guided Glide Plane", CSITR-68B-12A, 6/1979.

9. "Design and Flight Test Analysis of B3-5 CF-01 Pitot-static Tube", CSITR-67B-83, 4/1978.

10. "Aerodynamic Design of a Subsonic Wind-tunnel", CSITR-66B-71, 8/1977.

11. "Aerodynamic Analysis of various Wing-Body-Tail Configurations", CSITR-66B-31, 11/1976.

12. "Trailing Vortex Measurements in a Wind-tunnel" Master Thesis, Imperial College of Science and Technology, England, 1974.